MASTERARBEIT | MASTER'S THESIS

Titel | Title

α-Synuclein Modulation of Monoamine Transporters in Parkinson's Disease

verfasst von | submitted by

Samuel Moser BSc

angestrebter akademischer Grad | in partial fulfilment of the requirements for the degree of

Magister pharmaciae (Mag. pharm.)

Wien | Vienna, 2025

Studienkennzahl lt. Studienblatt | Degree programme code as it appears on the student record sheet:	UA 066 605
Studienrichtung lt. Studienblatt | Degree programme as it appears on the student record sheet:	Masterstudium Pharmazie
Betreut von | Supervisor:	Mag. Thomas Steinkellner PhD

In loving memory of my father.

Zusammenfassung

Morbus Parkinson (PD) ist eine progressive neurodegenerative Erkrankung, die durch den Verlust dopaminerger Neuronen und die Akkumulation von α-Synuclein (ASYN) in Lewy-Körperchen gekennzeichnet ist. Obwohl ASYN eine zentrale Rolle in der Pathogenese von PD spielt, sind seine physiologischen und pathologischen Funktionen bislang nur unzureichend verstanden. Ziel dieser Arbeit war es, zu untersuchen, wie die Überexpression von Wildtyp-(WT-)ASYN sowie der familiären A53T-Mutante die Funktion von Monoamin-Transportern, insbesondere des humanen Serotonintransporters (hSERT) und des Dopamintransporters (hDAT), beeinflusst. Hierfür wurden Substrat-Aufnahmeassays in transfizierten HEK293- und CAD-Zellen durchgeführt und kinetische Parameter bestimmt. In beiden Zelllinien führte die Expression von WT-ASYN und A53T-ASYN zu einer erhöhten Substrataufnahme durch SERT und DAT, was mit einer gesteigerten Expression der Transporter im Immunoblot korrelierte. Obwohl die Zellviabilitätsassays keine statistisch signifikante Reduktion bei WT-ASYN Überexpression zeigten, deuteten die Daten auf eine tendenziell niedrigere Viabilität in der WT-Bedingung hin. Zudem konnte kein Unterschied in der Empfindlichkeit gegenüber MPP^+ zwischen der Kontroll- und der WT-ASYN-Bedingung festgestellt werden. Diese Ergebnisse stützen eine modulatorische Rolle von ASYN bei der Regulation von Monoamin-Transportern und legen nahe, dass neben erhöhter Transporterexpression zusätzliche Mechanismen zur dopaminergen Vulnerabilität bei PD beitragen.

Abstract

Parkinson's disease (PD) is a progressive neurodegenerative disorder characterized by the loss of dopaminergic neurons and the accumulation of α-synuclein (ASYN) in Lewy bodies. Although ASYN is considered central to PD pathology, its physiological and pathological roles remain incompletely understood. This thesis aimed to investigate how overexpression of wild-type (WT) ASYN and the familial A53T mutant affect the function of the human transporters for serotonin (hSERT) and dopamine (hDAT). To this end, uptake saturation assays were performed in transfected HEK293 and CAD cells, and kinetic parameters were determined. In both cell lines, WT-ASYN and A53T-ASYN expression led to an increase in substrate uptake, which correlated with higher transporter protein levels as demonstrated by immunoblotting. Although cell viability assays did not reveal a statistically significant reduction upon WT-ASYN overexpression, the data indicated a tendency toward lower viability in the WT condition. Moreover, no difference in MPP^+ sensitivity was observed between the control and WT-ASYN overexpression, suggesting that mechanisms other than increased DAT expression contribute to dopaminergic neurodegeneration in PD. These findings support a modulatory role of ASYN in monoamine transporter regulation and suggest that additional mechanisms beyond transporter overexpression contribute to dopaminergic vulnerability in PD.

Acknowledgements

First and foremost, I would like to express my sincere gratitude to my supervisor, Ass. Prof. Priv. Doz. Thomas Steinkellner, PhD for his continuous support, valuable feedback, and insightful guidance throughout the development of this thesis. His expertise and encouragement greatly contributed to the quality of this work.

I would also like to thank the faculty and staff of the Center for Physiology and Pharmacology at the Medical University of Vienna for providing a stimulating academic environment and the necessary resources during my project.

Last but not least, I am deeply grateful to my family for their unwavering support throughout my academic journey, especially to my late father who recently passed away. He gave me the opportunity to make the best out of myself academically, without asking anything in return. I will forever be thankful for the sacrifices he made for me.

Contents

1 Introduction 1
1.1 Parkinson's Disease 1
1.1.1 Symptoms 1
1.1.2 Diagnostic criteria 2
1.1.3 Environmental and genetic factors 2
1.1.4 Progression of PD 5
1.1.5 Pathophysiology of PD 6
1.1.5.1 Neuroinflammation 7
1.1.6 Familial Forms of PD: Monogenic Mutations 8
1.2 Role of α-Synuclein 9
1.2.1 Patho- and physiological role of alpha-synuclein 10
1.2.1.1 Regulation of Synaptic Vesicle Dynamics 10
1.2.1.2 SNARE Complex Assembly 11
1.2.1.3 Lipid Binding and Membrane Curvature Sensing 12
1.2.1.4 Mitochondrial Function 12
1.2.1.5 Regulation of Dopaminergic Neurons 13
1.2.1.5.1 Dopamine biosynthesis 13
1.2.1.5.2 Dopamine transport 13
1.2.1.6 Nuclear Functions 14
1.2.2 A53T ASYN 14
1.2.3 Structure of ASYN 15
1.2.3.1 Pathophysiological conformation/misfolding 17
1.2.3.1.1 Prion-like properties of ASYN 17
1.2.3.1.2 ASYN-Fibril formation 18
1.2.3.1.3 Propagation of ASYN-fibrils 18
1.3 Monoamine transporters 19
1.3.1 Structure of Monoamine transporters 20

1.3.2 DAT 22
1.3.2.1 Regulation of activity..... 22
1.3.3 SERT 22
1.3.3.1 Regulation of activity..... 22
1.4 ASYN and its interaction with monoamine transporters (SERT, DAT).... 23
1.4.1 Important discoveries of ASYN in the last decades 23
1.4.2 Recent discoveries of ASYN-interactions with monoamine transporters 24
2 Materials and Methods..... 26
2.1 Cell Culture 26
2.2 Protocol for transient transfection of cell lines 26
2.2.1 jetPrime Transfection..... 26
2.2.2 Lipofectamine 2000..... 26
2.2.3 PEI transfection 27
2.3 Uptake saturation assay..... 27
2.3.1 Protocol..... 28
2.4 Immunoblotting analysis..... 33
2.4.1 Protocol..... 34
2.5 AquaBluer™ Cell Viability Assay 38
2.5.1 Protocol..... 38
2.6 Data Analysis 42
3 Results 44
3.1 Aim of the thesis..... 44
3.2 Cellular Assays..... 44
3.2.1 CAD cells - Does ASYN affect SERT function in CAD cells?..... 45
3.2.1.1 Uptake Saturation Assay with Western Blots 45
3.2.2 HEK293 cells - Is the effect of ASYN on SERT conserved in HEK cells? 49

3.2.2.1 Uptake Saturation Assay with Western Blots 49
3.2.2.1.1 SERT 49
3.2.2.1.2 DAT - Does ASYN also affect DAT function?..... 53
3.2.2.2 AquaBluer Cell Viability Assay 57
4 Discussion 62
5 References 68
6 Appendix 79

Table of figures

Figure 1 Cellular mechanism that are contributors of the pathogenesis of PD. 4
Figure 2 Risk factors for PD. 5
Figure 3 Progression of PD. 6
Figure 4 Genetics of PD..... 9
Figure 5 Monomeric and aggregated structure of ASYN. 17
Figure 6 Physiological conformation of ASYN.....19
Figure 7 Schematic representation of the conformational states the transporters must shuttle between to move substrate from the extracellular space to the cytoplasm. 20
Figure 8 Transmembrane topology of SLC6 transporters, illustrated via the hSERT. 21
Figure 9 Schematic illustration of the PEI transfection. 27
Figure 10 Plasmid maps of (A) pcDNA-eYFP-hSERT (B) pcDNA-eYFP-hDAT showcasing the transgene. 29
Figure 11 Plasmid maps of (A) pAAV hSyn1 DIO hASYN cre off (B) pAAV hSyn1 DIO hASYN A53T cre off, showcasing the transgene. 30
Figure 12 Schematic illustration of the [^{3}H]-radioligand uptake assay. 32
Figure 13 Example of a standard concentration curve for the BCA assay. 35
Figure 14 Workflow of the BCA assay 35
Figure 15 Western Blot cassette assembly. 38
Figure 16 Schematic illustration of the workflow for the AquaBluer cell viability assay. 41
Figure 17 Schematic illustration of the seeded 96-well plate for the AquaBluer assay. 42
Figure 18 [^{3}H]5-HT uptake in CAD-SERT cells. 46
Figure 19 Western Blot image (A) and densitometric quantification of the images of ASYN and SERT from transfected CAD cells for the [^{3}H]5-HT SERT uptakes. 48
Figure 20 Cell counts expressed as Million cells/well of CAD-SERT cultures used in uptake assays. 49
Figure 21 [^{3}H]5-HT uptake in HEK-SERT cells. 50
Figure 22 Western Blot image (A) and densitometric quantification of the images of ASYN and SERT from transfected HEK cells for the [^{3}H]5-HT SERT uptakes. 52
Figure 23 Cell counts expressed as Million cells/well of HEK-SERT cultures used in uptake assays. 53
Figure 24 [^{3}H]DA uptake in HEK-DAT cells. 54
Figure 25 Western Blot image (A) and densitometric quantification of the image of ASYN and DAT from transfected HEK cells for the [^{3}H]DA DAT uptakes. 56
Figure 26 Cell counts expressed as Million cells/well of HEK-SERT cultures used in uptake assays. 57
Figure 27 AquaBluer cell viability assay, comparing the different vulnerability of two conditions (control and WT ASYN) to two parkinsonian toxins (rotenone, MPP+). 58
Figure 28 Comparison of IC50 of the AquaBluer Cell viability assays. 59
Figure 29 Comparison of the RFUs of the NC with different conditions. 61
Figure 30 Hypothesis of the ASYN-induced neurodegeneration in the SNc. 66

List of Tables

Table 1 Overview of the conditions for [^{3}H]5HT specific uptake. 33

Table 2 Overview of the conditions for [^{3}H]DA specific uptake. 33

Table 3 Overview of MPP+ conditions. Concentrations were adapted after failing to calculate the IC50. 39

Table 4 Overview of MPP+ conditions after adaptions. 40

Table 5 Overview of rotenone conditions for the AquaBluer Assay. 40

Table 6 Summary of kinetic parameters (V_{max} and K_m) for [^{3}H]5HT uptake in CAD SERT cells transfected with only SERT (1:0), 1:3 WT α-synuclein, or 1:3 A53T α-synuclein. 79

Table 7 Summary of statistical analysis of kinetic parameters of [^{3}H]5HT uptake in CAD SERT cells. 79

Table 8 Numeric summary of the densitometric quantification of Western Blot image from the [^{3}H]5HT CAD SERT uptake. 80

Table 9 Numeric summary of the statistical analysis for the densitometric quantification of the Western Blot image from the [^{3}H]5HT CAD SERT uptake. 81

Table 10. Summary of kinetic parameters (V_{max} and K_m) for [^{3}H]5HT uptake in HEK- SERT cells transfected with only SERT (1:0), 1:3 WT α-synuclein, or 1:3 A53T α-synuclein. 81

Table 11 Summary of statistical analysis of kinetic parameters of [^{3}H]5HT uptake in HEK SERT cells. 82

Table 12 Numeric summary of the densitometric quantification of the Western Blot image from the [^{3}H]5HT HEK SERT uptake. 82

Table 13 Numeric summary of the statistical analysis for the densitometric quantification of the Western Blot image from the [^{3}H]5HT HEK SERT uptake 83

Table 14. Summary of kinetic parameters (V_{max} and K_m) for [^{3}H]DA uptake in HEK-DAT cells transfected with only SERT (1:0), 1:3 WT α-synuclein, or 1:3A53T α-synuclein. 83

Table 15 Summary of statistical analysis of kinetic parameters of [^{3}H]DA uptake in HEK DAT cells. 84

Table 16 Numeric summary of the densitometric quantification of the Western Blot image from the [^{3}H]DA HEK DAT uptake. 84

Table 17 Numeric summary of the statistical analysis for the densitometric quantification of the Western Blot image from the [^{3}H]DAT HEK DAT uptake 85

Table 18 Numeric summary of the IC50 calculation from the AquaBluer cell viability assay. 85

Table 19 Numeric summary of the statistical analysis for the IC50 calculation for the AquaBluer cell viability assay (unpaired, two-tailed student's t-test). 85

Table 20 Numeric summary of the RFUs from Figure 28. 86

Table 21 Summary of statistical analysis of Figure 28. 87

List of abbreviations

AA	amino acid
ASO	antisense oligonucleotide
ASYN	α-synuclein
AU	arbitrary units
BCA	bicinchoninic acid
CAD cells	Cath.a-differentiated cells
CD	cluster of differentiation
β-CFT	2β-carbomethoxy-3β-(4-fluorophenyl) tropane
CMA	chaperone-mediated autophagy
CNS	central nervous system
cpm	counts per minute
CSPα	cysteine string protein α
DA	dopamine
DAMP	damage-associated molecular patterns
(h)DAT	(human) dopamine transporter
DMEM	Dulbecco's Modified Eagle's Medium
DMSO	Dimethylsulfoxide
DMV	dorsal motor nucleus of the vagus nerve
DNA	deoxyribonucleic acid
DOPAL	3,4-Dihydroxyphenylacetaldehyde
ENS	enteric nervous system
EL	extracellular loop
eQTL	expression quantitative trait loci
ER	endoplasmic reticulum
FBS	fetal bovine serum
GAPDH	glyceraldehyde 3-phosphate dehydrogenase
GBA	glucocerebrosidase
GFP	green fluorescent protein
HEK293	human embryonic kidney 293 cells
5-HT	5-hydroxytryptamine
IC50	half maximal inhibitory concentration

IL	interleukin
JAK	Janus kinase
K_m	concentration of half-maximal velocity; Michaelis-Menten constant
KHB	Krebs-Henseleit buffer
LB	Lewy Body
LBD	Lewy Body Dementia
LBP	Lewy body pathology
LC	Locus coeruleus
LeuT	Leucine transporter
LRRK2	leucine-rich repeat kinase 2
MAO	monoamine oxidase
MPTP	1-methyl-4-phenyl-1,2,3,6-tetrahydropyridine
MPP+	1-methyl-4-phenylpyridinium
MQ water	Milli-Q water
MSA	multiple system atrophy
MTS	mitochondrial targeting signal
MyD88	myeloid differentiation primary response 88
NAC	non-β-amyloid component
NC	negative control
NET	noradrenaline transporter
NF-κB	nuclear factor kappa-light-chain-enhancer of activated B cells
NLRP	Nucleotide-binding oligomerization domain, Leucine rich Repeat and Pyrin domain containing
NMS	non-motor symptoms
NSS	neurotransmitter sodium transporter
NSU	non-specific uptake
OH	orthostatic hypotension
p38 MAPK	p38 mitogen-activated protein kinase
PAMP	pathogen-associated molecular patterns
PARK2	parkin
PBS	phosphate buffered saline

PC	positive control
PEI	polyethyleneimine
PD	Parkinson’s disease
PDL	poly D-lysine
PFA	paraformaldehyde
PFF	α-synuclein preformed fibrils
PINK1	PTEN-induced putative kinase 1
PKC	protein kinase C
PKG	cGMP-dependent protein kinase
PP2A	protein phosphatase 2A
PPMI	Parkinson’s Progression Markers Initiative
PRR	Pattern-recognition receptors
PrP^{C}	cellular prion protein
PrP^{Sc}	scrapie isoform of the prion protein
PS	penicillin/streptomycin
RIPA	radioimmunoprecipitation assay
ROS	reactive oxygen species
RCF	relative centrifugal force
RFU	relative fluorescence units
RT	room temperature
SAA	seed amplification assays
SDS	sodium dodecyl sulfate
SDS-PAGE	SDS-polyacrylamide gel electrophoresis
SEM	standard error of mean
(h)SERT	(human) serotonin transporter
SLC	solute carrier transporter
SNAP	soluble N-ethylmaleimide-sensitive factor attachment protein
SNARE	soluble N-ethylmaleimide-sensitive factor attachment protein receptor
SNc	substantia nigra pars compacta
SNCA	α-synuclein
SU	specific uptake

STAT	signal transducer and activator of transcription proteins
SV	synaptic vesicle
syb2	synaptobrevin-2
TBS-(T)	Tris-buffered saline (Tween)
TH	tyrosine hydroxylase
TIM	translocase of the inner membrane
TOM	translocase of the outer membrane
TLR	toll-like receptor
TM	transmembrane
TNF-α	Tumor necrosis factor-α
TRAP	tremor, rigidity, akinesia, postural instability
TSA201	temperature sensitive A201 cells
VAMP	vesicle associated membrane protein
VMAT	vesicular monoamine transporter
V_{max}	maximal transporting velocity
VPS-35	vacuolar protein sorting-associated protein 35
WT	wild-type
YFP	yellow fluorescent protein

1 Introduction

1.1 Parkinson's Disease

Parkinson's disease (PD) is the second most common neurodegenerative disorder, characterised by the progressive degeneration of dopaminergic neurons in the midbrain, which leads to the manifestation of both motor and non-motor symptoms (Beitz 2014).

PD is a typical age-related sickness: Most of the patients are more than 60 years old, and the incidence primarily increases with age. According to estimations, around 3% of the population over 80 years suffer from the disease (Hayes 2019). This may also partially explain why mice with their limited lifespan of about 2 years don't develop PD on their own; mice have to be artificially altered by administering toxins or by applying transgenic methods (Mat Taib and Mustapha 2020). Besides age being the most important risk factor for PD, sex also seems to play an integral role: men are more prone for the disease than women with an approximate prevalence ratio of 3:2 (Brakedal et al. 2022). Genetics also play a certain role in the development of PD, with currently at least 20 genes for the familial form and over 90 genetic risk loci found for the idiopathic form of PD (Blauwendraat et al. 2020). In addition, external factors such as environmental (e.g. toxicants such as pesticides) and behavioural influences (e.g. coffee, tobacco) have been suggested to play causal or modifying roles in PD pathogenesis. Nonetheless, the exact mechanism, by which PD is caused, remains unknown, and no cure or preventive therapy has been developed yet (Tolosa et al. 2021).

1.1.1 Symptoms

James Parkinson, after which the disease was later named, first described the clinical symptoms of the disease in 1817 in his essay "An essay on the shaking palsy". More than 200 years later many pathophysiological factors are still unknown (Jankovic 2008).

The four cardinal symptoms of PD are akinesia (or bradykinesia), muscle rigidity, resting tremor, and postural instability. Furthermore, flexed posture and freezing (motor blocks) have been added to the classical features of parkinsonism, with PD

as the most frequent form (Jankovic 2008). Parkinsonism is a clinical syndrome that is seen in many neurodegenerative diseases. Even though PD makes up 80% of parkinsonism cases, parkinsonism can also arise with other neurodegenerative diseases, specific brain lesions, head trauma, medications (such as antipsychotics or reserpine), metabolic conditions, and exposure to toxins (such as manganese) (Shrimanker et al. 2025). It is essential to note that PD is not only just a neurodegenerative disorder with motor symptoms, but rather a multi-systemic disorder with both motor and non-motor symptoms (NMS). The NMS of PD consist of different cognitive, neuropsychiatric, sleep, autonomic and sensory dysfunctions. In a neuroanatomical sense, NMS can be subdivided into cortical manifestations (psychosis and cognitive impairment), basal ganglia symptoms (impulse control disorders, apathy, and restlessness or akathisia), brainstem symptoms (depression, anxiety, and sleep disorders), and the peripheral nervous system disturbances (orthostatic hypotension (OH), constipation, pain, and sensory disturbances) (Lee and Koh 2015).

1.1.2 Diagnostic criteria

The Movement Disorder Society Clinical Diagnostic Criteria for Parkinson's Disease describes the first essential criterion as parkinsonism which entails bradykinesia in combination with at least one additional cardinal motor symptom such as e.g. resting tremor or rigidity. After diagnosing parkinsonism, to give the diagnosis of clinically established PD the patient must show no absolute exclusion criteria (e.g. cerebellar gait), at least two supportive criteria (e.g. response to dopaminergic therapy) and no red flags (e.g. rapid progression of gait impairment). For the diagnosis of clinically probable PD, the patient must show no exclusion criteria and potential red flags must be counterbalanced with supportive criteria. A definite diagnosis of PD however can only be made postmortem (Postuma et al. 2015).

1.1.3 Environmental and genetic factors

Environmental exposure of certain risk factors possibly contributes to the initiation and progression of PD. A meta-analysis (Noyce et al. 2012) that examined 30 different potential risk factors found 11 environmental factors that significantly changed the risk for PD. The factors that increased risk (in decreasing order of strength of association) were pesticide exposure, prior head injury, rural living, β-

blocker use, agricultural occupation, and well-water drinking. Factors associated with a decreased risk to develop PD (in decreasing order of strength of association) include tobacco smoking, coffee drinking, use of non-steroidal anti-inflammatory drugs, calcium channel blocker use (mainly from the flunarizine and cinnarizine type), and alcohol consumption (Kalia and Lang 2015; Shin and Chung 2012) (see **Figure 2**). A meta-analysis of several epidemiological studies (Priyadarshi et al. 2001) has found that people who live in rural areas are at significantly higher risk to develop PD. This might be due to higher exposure to potential neurotoxins such as pesticides, contaminated well or spring water. Interestingly, the infamous PD-inducing neurotoxicant MPTP (1-methyl-4-phenyl-1,2,3,6-tetrahydropyridine) is structurally very similar to several agricultural chemicals such as paraquat, diquat or ethylparaquat. However, while MPP+, the active neurotoxin of MPTP, blocks complex I of the mitochondrial respiratory chain, paraquat and analogues seem to act primarily via generation of H_2O_2 and oxidative stress (Elmorsy et al. 2023). Notably, complex I is reduced in neurons and platelets of PD patients (Priyadarshi et al. 2001). Specific pesticides such as paraquat, rotenone, maneb and dieldrin were linked epidemiologically and experimentally to dopaminergic neuron loss in both humans and animal models (Gao and Hong 2011). **Figure 1** illustrates the genes that are mainly responsible for the cellular pathways implicated with PD (protein aggregation, protein/membrane trafficking, neurite structure, prion-like transmission, ubiquitin–proteasome function, mitochondrial function/mitophagy, lysosome–autophagy, and synaptic dopamine signaling) (see also **1.1.6**). ASYN is associated with protein aggregation, prion-like transmission and influences on synaptic dopamine signaling.

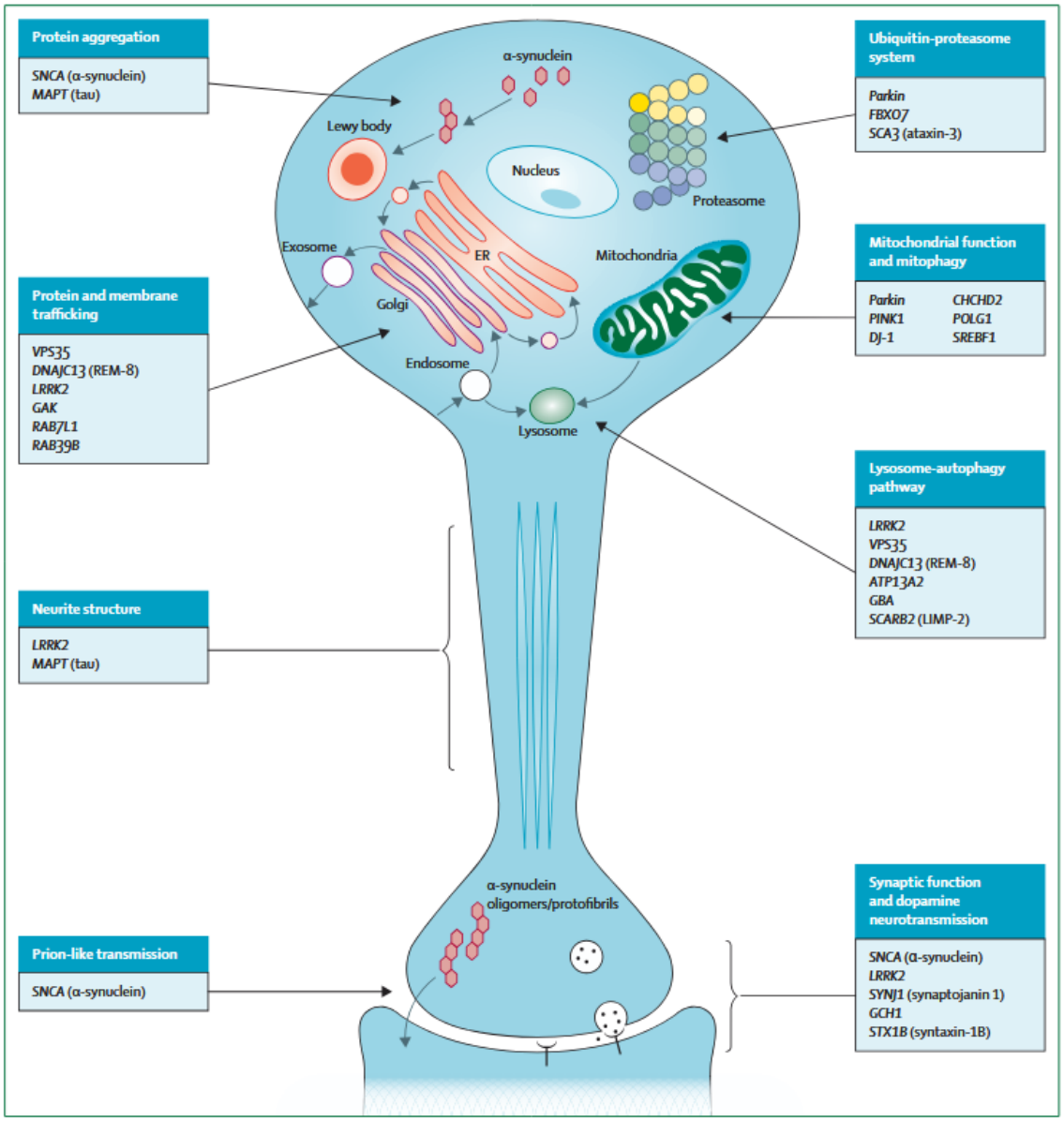

Figure 1 Cellular mechanism that are contributors of the pathogenesis of PD. Reproduced with permission from (Kalia and Lang 2015), License number: 6057760109169.

Figure 2 illustrates the potential protective and risk factors of PD, both from environmental and genetic origin (see also **1.1.6**)

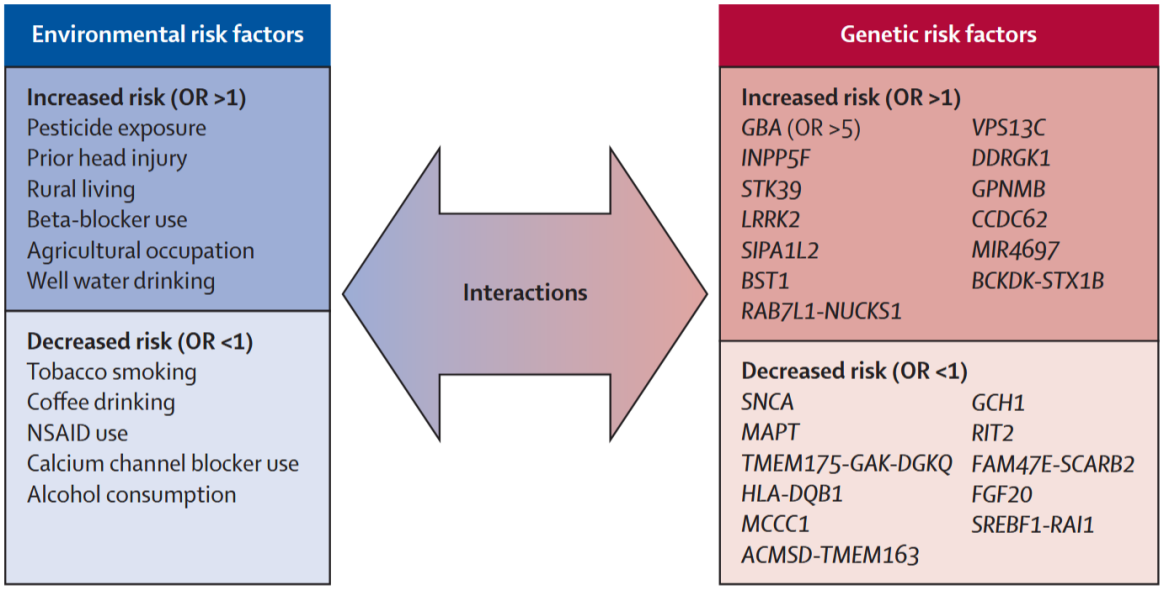

Figure 2 *Risk factors for PD. Reproduced with permission from (Kalia and Lang 2015) License number: 6057760109169.*

1.1.4 Progression of PD

Braak et al proposed a neuropathological staging scheme of PD in accordance with the presence of LBs in the brain (Braak and Del Tredici 2017). According to this model, PD begins in the olfactory bulb and/or the autonomic enteric nervous system (ENS), with a gradual caudo-rostral (retrograde) spread of Lewy body pathology (LBP), finally reaching the substantia nigra *pars compacta* (SNc). Because of that, LBs are typically seen as markers for disease progression, whilst neurodegeneration correlates with the manifestation of clinical PD symptoms. Braak et al proposed six different stages of PD that mirror the spread of LBP from the dorsal motor nucleus of the vagus nerve (DMV) (Braak stage 1) to the locus coeruleus (LC) (Braak stage 2), SNc and amygdala (Braak stage 3) and finally reaching cortical areas (Braak stage 4-6). In the first stages of the disease, primarily non-motor symptoms manifest, whilst characteristic PD motor symptoms typically emerge in stages ≥ 3, and cognitive symptoms only start when LBP progressed to the cortex in Braak stages 5 and 6 (see **Figure 3)** (Braak and Del Tredici 2017; Koeglsperger et al. 2023).

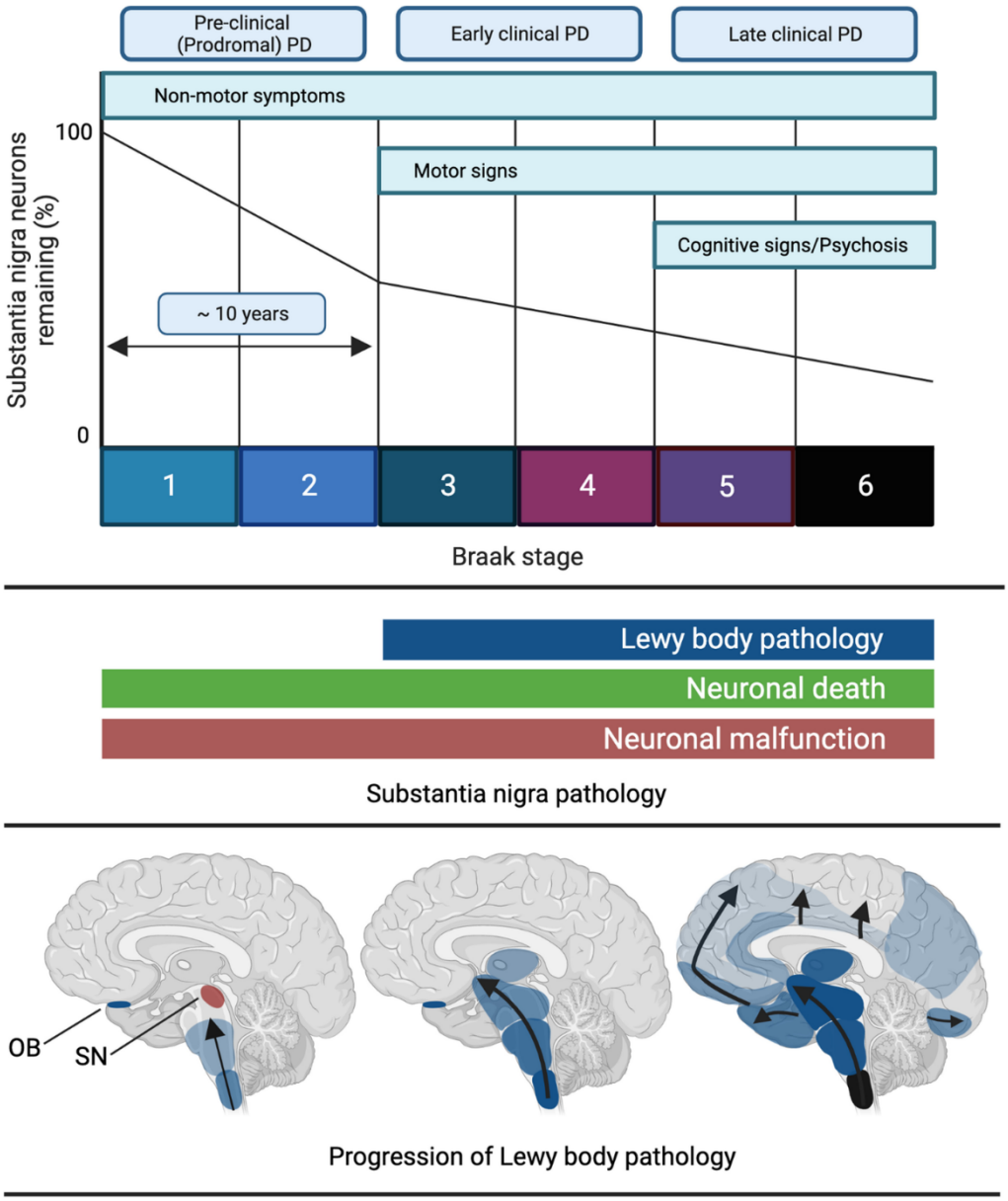

Figure 3 *Progression of PD. Demonstrating the progression from the preclinical phase of PD to the late clinical phase, including the associated clinical symptoms, SNc pathology and progression of Lewy body pathology in accordance to Braak's staging model. Figure adapted from (Koeglsperger et al. 2023), licensed under CC BY 4.0.*

1.1.5 Pathophysiology of PD

As many other diseases, the pathogenesis of PD is multifactorial and largely elusive, but the main hallmark of PD lies in the loss of dopaminergic neurons in the SNc, a region that is important in modulating basal ganglia function. Another important part for the diagnosis of PD consists of the accumulation of insoluble cytoplasmatic protein inclusions, which are referred to as either Lewy bodies (in neuronal cell bodies) or Lewy neurites (in neuronal processes) respectively. Lewy bodies and Lewy neurites also occur in other neurodegenerative diseases such as Lewy body

dementia (LBD) and multiple system atrophy (MSA) (Rocha et al. 2018). The exact pathogenesis of PD includes multiple mechanisms such as ASYN aggregation, neuroinflammation, mitochondrial dysfunction, lysosomal autophagy dysfunction, abnormal vesicle transport and gut microbiome dysbiosis (Wang et al. 2022).

Aggregation of abnormally folded proteins seems to be a common denominator in the genesis of not only PD but many other neurodegenerative diseases including for instance Alzheimer's or Huntington's disease. Protein aggregates can be categorised by those proteins found abundantly in the inclusions. In PD's case, α-synuclein was identified as the first protein component of Lewy bodies and Lewy neurites. ASYN is a small protein that can form insoluble oligomers that can aggregate into neuronal inclusions in different brain areas (Kalia and Lang 2015). PD is therefore also classified as a synucleinopathy. Similar to prion's disease, a key mechanism of PD's progression seems to be misfolding and prion like cell-to-cell propagation (Tolosa et al. 2021).

1.1.5.1 Neuroinflammation

The exact role that neuroinflammation plays in the pathogenesis of PD, as with a lot of aspects with the disease, remains poorly understood. There still is no unambiguous evidence what exactly causes neuroinflammation in PD (Wang et al. 2022). Neuroinflammation is a protective measure of the immune system against foreign, pathogenic stimuli with the main goal of maintaining CNS (Central Nervous System) parenchyma and promoting tissue repair. While short-term immune activation can help maintain cellular homeostasis, persistent neuroinflammatory activity can exacerbate neuronal cell death and lead to blood-brain barrier disruption, as well as a chronic inflammation and tissue damage. The neuroinflammatory aspect of PD entails a complex interaction between several immune cells, such as microglia and astrocytes, as well as the role of ASYN in the pathogenesis and progression of PD in a neuroimmunological context (Araújo et al. 2022). Misfolded ASYN can cause pathogen-associated molecular pathogen- or damage-associated molecular patterns (DAMP)-mediated dysregulation of microglial toll-like receptor (TLR)2 or TLR4-mediated signalling pathway, which subsequently activates myeloid differentiation primary response 88 (MyD88) and nuclear factor kappa B (NFκB), leading to tumour necrosis factor alpha (TNF-α) and interleukin-1β (IL-1β) production (Liu et al. 2022). Microglia are part of the innate immune system that

mainly protect and maintain the cellular homeostasis of the central nervous system by triggering phagocytosis and inflammatory responses. Overactivated microglia by misfolded, aggregated ASYN can lead to the activation of other innate immune components of the CNS and a subsequent peripheral adaptive immune response, which results in major damage to neurons. In summary, misfolded ASYN can trigger the following inflammatory responses in microglia: activating membrane receptors such as TLR2, TLR4 and CD36 (cluster of differentiation 36), increasing the content of STAT3 (signal transducer and activator of transcription 3) and thereby activating the intracellular JAK (Janus kinase)/STAT pathway as well as the inflammasome pathway where ASYN can activate the NLRP3 (Nucleotide-binding oligomerization domain, Leucine rich Repeat and Pyrin domain containing) inflammasome through the Fyn pathway (Wang et al. 2022). These findings suggest that ASYN oligomers act similarly to ligands of PRRs (pattern recognition receptors); a better understanding of the interaction of PRRs and ASYN might bring more elucidation on how neuroinflammation influences the pathogenesis of neurodegenerative diseases (Kim et al. 2013).

1.1.6 Familial Forms of PD: Monogenic Mutations

Genetic studies of familial PD have made it possible to determine monogenic forms of the disease, meaning the identification of disease-causing mutations in single genes. PD-causing mutations have been identified in the genes encoding α-synuclein (SNCA), leucine-rich repeat kinase 2 (LRRK2), vacuolar protein sorting-associated protein 35 (VPS-35), parkin (PARK2), PTEN-induced putative kinase 1 (PINK1), DJ1 (PARK7), and glucocerebrosidase (GBA). Even though those mutations are rare and only make up fewer than 10% of all PD cases, they have given key insights into potential mechanisms of PD etiology. ASYN-containing Lewy bodies, for example, are present in both familial and idiopathic PD cases; even though ASYN-mutations are predominantly responsible for monogenic PD cases, common genetic variants in SNCA are linked to a higher risk of developing idiopathic PD. In 90% of PD cases, there is no monogenic inheritance pattern, and the disease is classified as idiopathic. Therefore, in most PD cases, the pathogenesis presumably is a complex interplay between environmental and genetic factors. Meta-analyses of several different genome-wide association studies (International Parkinson's Disease Genomics Consortium (IPDGC) et al. 2014; Chang et al. 2017)

have determined 41 PD risk loci, each standing for common genetic variants that entail an increased risk of causing PD, see **Figure 4** (Translational Neurogenetics Unit, Wallenberg Neuroscience Center, Lund University, Lund, Sweden et al. 2018).

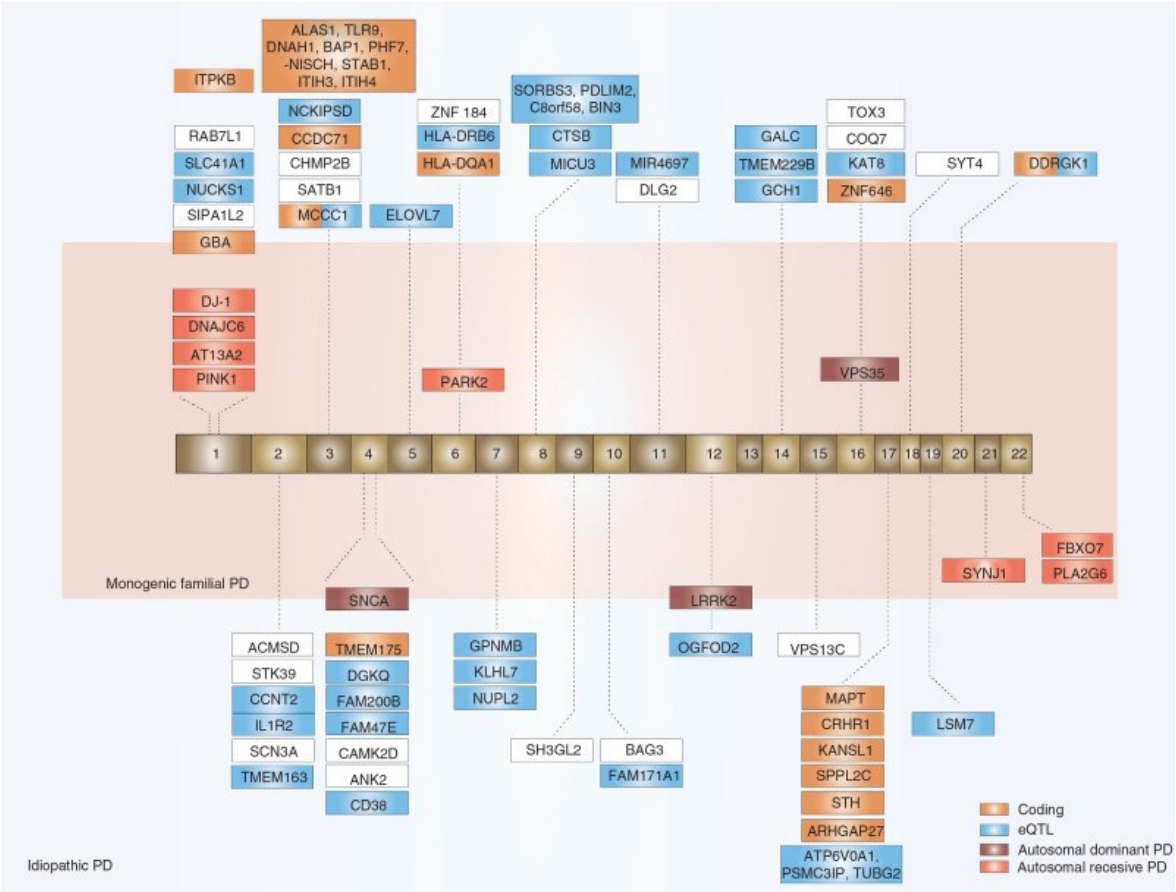

Figure 4 *Genetics of PD. Each region has identified candidate genes that have been significantly associated with PD. Some regions have multiple candidate genes. eQTL = expression quantitative trait loci (regulatory gene elements). Figure adapted from (Translational Neurogenetics Unit, Wallenberg Neuroscience Center, Lund University, Lund, Sweden et al. 2018), licensed under CC BY 4.0.*

1.2 Role of α-Synuclein

ASYN is a small protein consisting of 140 amino acids with a molecular weight of around 15 kD. It is part of the synuclein family, alongside β- and γ-synuclein, both of which are homologous to ASYN. ASYN is encoded by the SNCA gene, that is located on the long arm of chromosome 4 in humans (4q21.3-q22) (Benskey et al. 2016). ASYN is abundantly expressed in the CNS, but there are also other sites of expression, such as glia and blood cells for example. α- and β-synuclein can predominantly be found in neuronal presynaptic terminals, nevertheless, after a certain age, ASYN redistributes to the neuronal soma with a reduction of presynaptic levels (Barba et al. 2022). In immature neurons, ASYN is first localised in the soma, in the process of synaptogenesis the concentration of ASYN increases in

presynaptic terminals (Burré et al. 2018). ASYN plays an important role in the development of the CNS by promoting synaptogenesis and maturation of neuronal precursors (Barba et al. 2022). ASYN's targeting to synaptic terminals might be mediated by its affinity to synaptic vesicle (SV) membranes and/or by binding to the vesicular SNARE (Soluble N-ethylmaleimide-sensitive factor attachment protein (SNAP) receptor) protein synaptobrevin-2 (Burré et al. 2018). ASYN's biochemical properties are similar to those of protein chaperones, since it can bind to other proteins. In a dissolved state, ASYN takes a random open, rather than globular conformation, which is similar to the conformation of a chaperone (Ostrerova et al. 1999).

1.2.1 Patho- and physiological role of alpha-synuclein

1.2.1.1 Regulation of Synaptic Vesicle Dynamics

Due to its presynaptic localisation and its affinity to membranes, it is strongly implied that ASYN plays a role in neurotransmitter release. There still seems to be a dissent of the physiological functions of ASYN; some publications reported that ASYN promoted release, while other suggested an inhibitory function (Bendor et al. 2013). Nonetheless, the synuclein proteins do not seem to play an essential role in neurotransmitter release: There were no homologs found in invertebrates and triple knockout of synucleins in mice only caused minor changes in synaptic function and transmitter release (Chandra et al. 2004). ASYN- (and triple) knockout mice essentially had normal physiological function and a normal lifespan, though triple knockouts started to get neurodegeneration (Greten-Harrison et al. 2010). The involvement of ASYN in synaptic vesicle dynamics, however, should not be overlooked: overexpression and knockout studies underlined the involvement of ASYN in different steps of synaptic vesicle cycle such as control of the fusion pore, regulation of SNARE proteins, involvement in SV recycling and in the regulation of axonal transport of SVs (Brodin et al. 2022). During neurotransmitter exocytosis, synaptic vesicles form a fusion pore that enlarges before total collapse into the plasma membrane. Nevertheless, the pore can also close to immediately regenerate the vesicle, in a so-called kiss-and-run event. Both the endogenous and overexpressed ASYN promoted the dilation of the fusion pore by accelerating the release event, reducing the time to peak fluorescence (pore dilation), speeding fluorescence decay (peptide release) and preventing pore closure in murine

chromaffin cells transduced with the wild-type (WT)-ASYN and a fluorescent-dyed marker (Logan et al. 2017). Although the A30P and A53T mutations in α-synuclein did not interfere with its ability to inhibit exocytosis upon overexpression, they both abolished its capacity to promote fusion pore dilation—indicating that the regulatory effects on exocytosis and on fusion pore dynamics are mechanistically distinct (Logan et al. 2017; Huang et al. 2019). The preserved effect of both overexpressed mutant and wild-type ASYN to inhibit exocytosis might be necessary to produce neurodegeneration (Logan et al. 2017). Overexpressed ASYN inhibited synaptic vesicle exocytosis by reducing releasable and recycling synaptic vesicle pools (Nemani et al. 2010).

1.2.1.2 SNARE Complex Assembly

SNARE proteins are essential mediators of eukaryotic cell membrane fusion. The SNARE proteins syntaxin, synaptobrevin (also known as vesicle associated membrane proteins (VAMP)) and SNAP-25 were found in early biochemical studies, in which several different essential proteins at neuronal synapses and on synaptic vesicles, as well as their binding partners were discovered (Yoon and Munson 2018). Several different studies such as *in vitro* reconstitution, cell based-studies, ensemble and single-molecule studies showed that ASYN mediates membrane fusion by cross-linking v-SNARE proteins such as synaptobrevin-2 (syb2) with acidic, negatively charged phospholipids (Burré 2015; Nellikka et al. 2021). Overexpression of ASYN resulted in reduced neurotransmitter release in hippocampal neurons by affecting the re-clustering of synaptic vesicles after endocytosis (Nemani et al. 2010). According to an *in vitro* lipid mixing assay it was also suggested that ASYN inhibits vesicular fusion by directly interacting with lipid bilayers (Choi et al. 2013). Nonetheless, overexpressed ASYN was also found to promote fusion pore dilation and cargo discharge, whilst total knockouts boosted pore closure in neurons and adrenal chromaffin cells (Nellikka et al. 2021).

ASYN promoted SNARE complex assembly, therefore protecting against neurodegeneration. For instance, overexpressed ASYN could rescue neurodegeneration that was triggered by deleting CSPα (cysteine string protein α), a chaperone for the SNARE protein SNAP-25 (Chandra et al. 2005). Structurally, both the phospholipid binding mediated by the α-helices of ASYN and synaptobrevin-2 binding mediated by the C-terminal ASYN sequence were

necessary for SNARE complex assembly (Burré et al. 2010; 2012). Interestingly, only the A30P mutant of ASYN impaired the SNARE complex assembly, whilst other point mutations that partially impair phospholipid binding such as A53T and E46K did not (Burré et al. 2012).

1.2.1.3 Lipid Binding and Membrane Curvature Sensing

Since it was found that ASYN shares several different class A2 amphipathic α-helices in its sequence, it was suggested that ASYN shares similarities with plasma apolipoproteins (Davidson et al. 1998). Although sequence analyses suggested that α-synuclein shares amphipathic class A2 helices with apolipoproteins, subsequent experimental studies demonstrated that α-synuclein does not exhibit the critical lipid-binding and exchange properties of apolipoproteins. Instead, the predicted helices support a weaker but physiologically relevant association with acidic phospholipid membranes (Davidson et al. 1998; Jensen et al. 1998; Bussell and Eliezer 2004). After incubating small unilamellar vesicles of various phospholipid constitution with ASYN and subsequent gel filtration chromatography, it could be shown that ASYN preferably associates with acidic phospholipids such as phosphatidylinositol and phosphatidylserine (Davidson et al. 1998). It was also determined that ASYN rather binds to smaller vesicles with higher curvatures than with larger particles but is still able to associate with more planar surfaces if negatively charged phospholipids are present (Middleton and Rhoades 2010). There was also data collected how lipid binding affects the secondary structure of ASYN: lipid-free ASYN is intrinsically disordered in solution, upon lipid-binding however, ASYN's conformation changed to a more α-helical character (Davidson et al. 1998). Lipid raft association is necessary for ASYN to localize to synapses; the A30P mutant that is associated with PD blocks this interaction, implying an important physiological role of rafts for ASYN. Interestingly, the A53T did not block this interaction, implying a different mechanism for the neurodegeneration in PD (Fortin et al. 2004).

1.2.1.4 Mitochondrial Function

Even though the mitochondria possess their own genome, they only encode 13 proteins, which means that they must import nuclear-encoded proteins for their physiological functions. One of the best understood mechanisms by which mitochondria import proteins is the TIM-/TOM-complex system: nuclear-encoded

matrix-targeted proteins that have a mitochondrial targeting signal (MTS) are recognized by the translocase of the outer membrane (TOM) receptors and translocated through the outer membrane to the translocase of the inner membrane (TIM) and then into the matrix (Chacinska et al. 2009). In the matrix, the MTS is removed to finalize the maturation of the imported protein (Neupert and Herrmann 2007). Pathological forms of ASYN (including oligomeric and Ser129-phosphorylated species) can form amphipathic α-helices that mimic MTS. Di Maio et al. (2016) demonstrated that ASYN binds directly to the TOM20 receptor, thereby disrupting its interaction with TOM22 and competitively blocking recognition of authentic precursor proteins. This resulted in impaired mitochondrial protein import, reduced oxidative phosphorylation efficiency, decreased ATP production, and increased reactive oxygen species (ROS). Importantly, overexpression of TOM20 or addition of MTS peptides rescued TOM20 function, restoring protein import and mitochondrial respiration (Di Maio et al. 2016).

1.2.1.5 Regulation of Dopaminergic Neurons

1.2.1.5.1 Dopamine biosynthesis

ASYN has a homologous sequence to the chaperone molecule 14-3-3, which can bind to and activate tyrosine hydroxylase (TH) (Ostrerova et al. 1999). TH is the rate-limiting enzyme of dopamine (DA) synthesis. It could be shown that ASYN interacts with TH in brain as well as in a dopaminergic cell line, that ASYN inhibited TH activity in a cell-free assay, and that overexpressed ASYN in a cell line highly reduced TH activity, TH phosphorylation and DA synthesis (Perez et al. 2002). ASYN seemed to decrease TH activity by dephosphorylation of Ser40 in the N-terminal regulatory domain through promoting the phosphatase activity of PP2A (Peng et al. 2005).

1.2.1.5.2 Dopamine transport

ASYN regulates dopamine reuptake due to its presynaptic location in nerve terminals of the SNc. There is contradictory data on how exactly ASYN modulates the activity of monoamine transporters. Some data have shown that cell lines co-transfected with ASYN and the dopamine transporter (DAT) decreased the extracellular dopamine reuptake (Wersinger and Sidhu 2003). Sidhu et al also discovered that the decrease of DAT activity by ASYN could be reversed into increased activity when cell adhesion was disrupted (Sidhu et al. 2004).

Once taken up by dopaminergic neurons via the DAT, dopamine is transported in synaptic vesicles by the vesicular monoamine transporter-2 (VMAT2). VMAT2 exploits a proton gradient across vesicular membranes to store monoamines in vesicles. ASYN decreased the uptake of dopamine by VMAT2 in VMAT2-transfected cell lines (Guo et al. 2008; Mosharov et al. 2009). According to Guo et al, this would lead to an decreased uptake of dopamine into presynaptic vesicles *in vivo*, which increases intracellular dopamine concentration which in turn can auto oxidize resulting in the production of cytotoxic reactive oxygen species (Guo et al. 2008).

1.2.1.6 Nuclear Functions

It is still unclear, whether ASYN appears physiologically in the nucleus and if it acts as a transcriptional modulator. Pinho et al showed that WT-ASYN transfected cell lines promoted the deregulation of several genes (Pinho et al. 2019). Oxidized, chromatin-associated α-synuclein induced DNA strand breaks in neuronal genomes, and this damaging activity is synergistically enhanced by iron and singlet oxygen ($^1O_2$) - demonstrating a chemical nuclease-like function of pathological α-synuclein (Vasquez et al. 2017) . The positively charged N-terminal region of ASYN probably binds to the negatively charged DNA, consistent with the fact that the N-terminal region can form helix-turn-helix type of motif which is commonly present in classical DNA-binding proteins (Vasquez et al. 2017).

1.2.2 A53T ASYN

Polymeropolous et al first reported the Alanine substitution to Threonine at position 53 (A53T) of ASYN in Italian-Greek families with autosomal-dominant PD, as the first genetic cause of familial PD (Polymeropoulos et al. 1997). Patients with A53T mutant developed early-onset PD (Polymeropoulos et al. 1997). In the same year, Spillantini et al. have identified ASYN as a major component of Lewy Bodies (Spillantini et al. 1997). Both discoveries instigated further research related to ASYN and how the A53T mutant affects the pathogenesis of PD. This work also led to the discovery of other mutations such as A30P, E46K or G51D and others (Krüger et al. 1998; Zarranz et al. 2004; Lesage et al. 2013). Conway et al have discovered that A53T mutant accelerated the oligomerisation and therefore the toxic fibril formation (Conway et al. 2000). Some years later, Giasson et al reported that A53T transgenic mice developed severe motor and pathological features that were similar to PD. A53T also blocked protein clearance in the cell, leading to toxic accumulation of

ASYN and other chaperone-mediated autophagy (CMA) substrate proteins inside the cell (Cuervo et al. 2004).

A53T severely accelerated lipid-induced aggregation and secondary nucleation, especially at lower pH levels, significantly more than WT-ASYN, thereby promoting *de novo* fibril formation (Flagmeier et al. 2016). In neuroblastoma cells, the A53T mutant aggregated intracellularly in the presence of iron or oxidative stress, significantly more than the WT or the A30P mutant (Ostrerova-Golts et al. 2000). There has been circumstantial evidence that oxidative factors, particularly iron, play an important role in the etiology and pathogenesis of PD (Ostrerova-Golts et al. 2000). The expression of A53T in neuronal cells resulted in CMA dysfunction, and as a compensatory reaction, macroautophagy was induced. By blocking these lysosomal effects, A53T caused the buildup of autophagosomes and therefore neurotoxicity (Xilouri et al. 2009). A53T was able to disrupt multiple components of the endomembrane system: Golgi dilation, ER-to-Golgi delays, lysosomal/autophagosomal accumulation and exosome mediated seeding – all factors that can impair protein clearance and lead to accumulation of ASYN (Stykel et al. 2021). Transgenic mice that were transduced with a virus to deliver human A53T ASYN developed progressive motor impairment, neurodegeneration, and accumulation of detergent insoluble ASYN aggregates, whilst the WT and the A30P mice did not (Lee et al. 2002). These mice also showed non-motor prodromal symptoms such as anxiety, loss of olfaction and constipation, which is linked to disrupted PP2A and TH activity, implying synaptic and catecholamine dysregulation (Farrell et al. 2014).

Interestingly, most New World monkeys and almost every other vertebrate, including mice, express ASYN naturally with a threonine in the 53rd position, in contrast to humans, apes and Old World primates which express Alanine (Vermilyea and Emborg 2015).

1.2.3 Structure of ASYN

ASYN can have different functions depending on its cellular location since it can either be in an α-helical structure when associated with phospholipids or an unfolded conformation when dissolved in the cytosol (Davidson et al. 1998). Essentially, ASYN is an acidic protein with a small molecular weight, whose structure can be

categorized into three domains: a N-terminal lipid binding α-helix, an amyloid binding central domain (Non Amyloid-β Component (NAC)) and a C-terminal acidic tail (Emamzadeh 2016). The N-terminal region of ASYN consists of seven 11 residue repeats (KTKEGV) that are highly conserved, across species and among the three isoforms. In addition, the motif is also very distinctive, with no similar sequence found in other protein families (Bendor et al. 2013; Dułak et al. 2020). Each 11-residue repeat consists of the KTKEGV hexameric motif, which also can be found in the α-helical domain of apolipoproteins. Those repeats mediate the α-helical conformation of ASYN, which gives ASYN the ability to disrupt lipid bilayers (see **Figure 5**) (Emamzadeh 2016). Micelle-bound ASYN takes the form of two curved α-helices, termed helix-N (Val^{3}-Val^{37}) and helix-C (Lys^{45}-Thr^{92}), connected by a short linker in an antiparallel matter, with a consecutive short extended region (Gly^{93}-Lys^{97}) and a primarily unstructured mobile tail (Asp^{98}-Ala^{140}; Fig. 7) (Ulmer et al. 2005).

The NAC domain of ASYN, originally described to be deposited with amyloid-β in the brains of patients with Alzheimer's disease, also called the core region (residues 61-95) is a contributor in fibril formation and aggregation by forming cross β-structures (Rodriguez et al. 2015; Emamzadeh 2016). The residues 68-78, also known as NACore, is the fibril-forming core of the NAC domain; it is therefore essential for both the aggregation and cytotoxicity of ASYN (see **Figure 5**). The A53T mutation of ASYN can promote its transition into the amyloid state, thereby causing early onset PD (Rodriguez et al. 2015).

The residues 96-140 form the C-terminal domain which is an acidic tail of 43-AA residues, containing 10 Glu and 5 Asp residues. Due to its low hydrophobicity and high net negative charge, the C-terminal domain usually is in a random coil conformation. By lowering the pH, the negative charges of the C-terminal domain could be neutralised which triggers the aggregation of ASYN (see **Figure 5**) (Emamzadeh 2016).

There have been some reports that ASYN forms an aggregation-resistant tetrameric state physiologically, before the onset of the disease, the tetramer disassembles to an aggregation-prone monomer. However, the actual existence of such a physiological tetramer has proven to be highly controversial (see **Figure 5**) (Li et al. 2022).

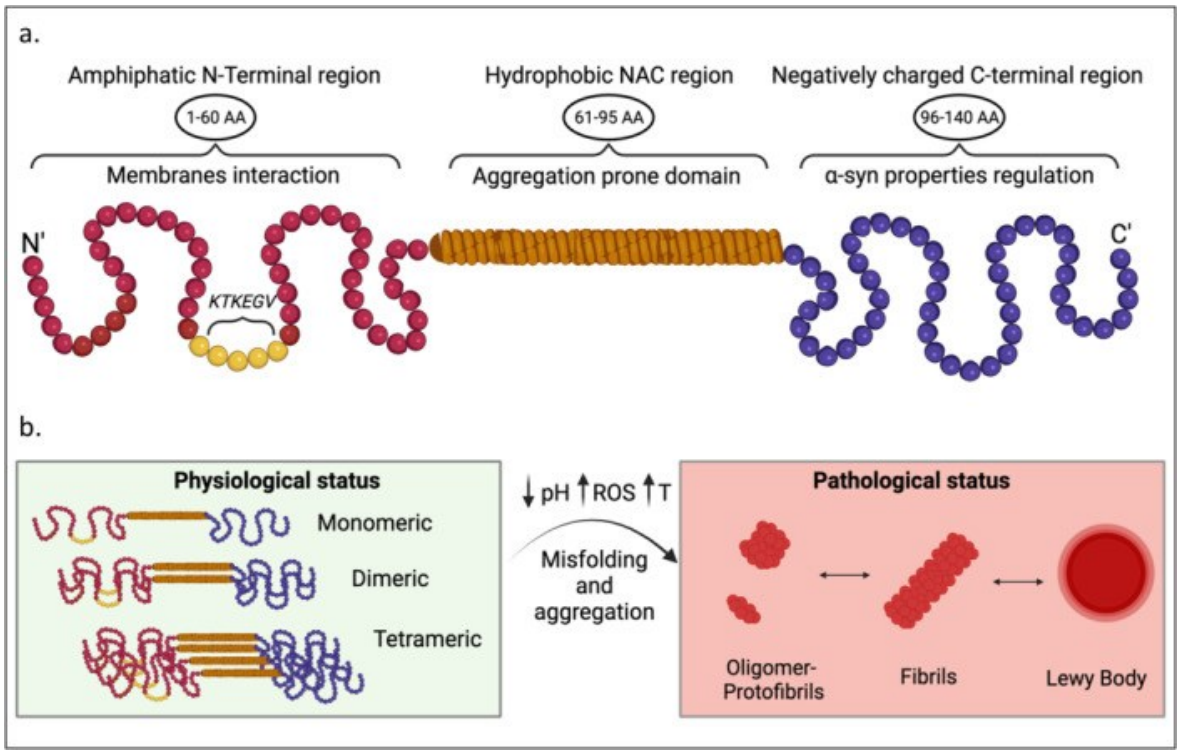

Figure 5 *Monomeric and aggregated structure of ASYN.* ***(a)*** *primary structure of ASYN.* ***(b)*** *Physiologocially (green) ASYN occurs as unstructured soluble monomeric and tetrameric forms, whilst pathologically (red) ASYN misfolds and aggregates into oligomer-protofibrils and fibrils, leading to the formation of Lewy Bodies. Abbreviations: AA, amino acids; α-syn, α-synunclein; T, temperature. Figure adapted from (Bellini et al. 2025), licensed under CC BY 4.0.*

1.2.3.1 Pathophysiological conformation/misfolding

1.2.3.1.1 Prion-like properties of ASYN

Prion diseases like Creutzfeld-Jakob in humans or scrapie in sheep showcase that seeded aggregation is not only a critical feature of neurodegeneration, but the cause of it (Prusiner 1982; 1998; Colby and Prusiner 2011). The infectious prion (PrP^{Sc}) propagates by turning the normal prion protein PrP^{C} (cellular prion protein) into the pathological PrP^{Sc} (scrapie isoform of prion protein)-containing aggregates, thereby inducing a pathological conformation of the native endogenous protein. This naturally occurring process can be replicated in vitro by using a small number of "seeds", ergo aggregated PrP^{Sc}, and an excess of natively folded prion protein. Thought to be only a mechanism exclusive for prion-like diseases, there have been emerging evidences over the years that there are also other proteins that follow this self-perpetuating seeded aggregation and cell-to-cell spreading in vitro but also in vivo in animal models, such as ASYN (Polymenidou and Cleveland 2012). There is substantial evidence that ASYN causes synucleinopathies through a prion-like mechanism; Prusiner et al. showed for example that inoculation of transgenic mice

expressing human ASYN with brain homogenate from MSA patients was enough to transmit the disease (Li et al. 2022; Prusiner et al. 2015). Furthermore, Virginia Lee and colleagues demonstrated that a single inoculation of recombinant ASYN preformed fibrils (PFF) in vitro and in a non-transgenic mouse model resulted in the spread of ASYN pathology (Volpicelli-Daley et al. 2011; Luk et al. 2012).

1.2.3.1.2 ASYN-Fibril formation

The exact mechanism how monomeric ASYN forms fibrils is poorly understood, however, there is crucial evidence, that this process precedes the generation of conformationally heterogeneous pathologic ASYN oligomers. The oligomerisation is promoted by lipid interactions leading to the formation of oligomers with variable β-sheet structure. Those resulting oligomers are inherently neurotoxic, operating by different neurotoxic mechanisms such as electrolyte disturbances and production of reactive oxygen species as well as disruption of membrane integrity. Interestingly, the truncation of the C-terminal region of ASYN increases the rate of fibril formation but decreases the rate of toxic oligomer formation. There are also physiological mechanisms to protect against pathological ASYN conformations through heat shock proteins, such as the Hsc70-based system that disassembles pathologic oligomers and short ASYN fibrils, but has only little activity against larger ASYN amyloid fibrils (Li et al. 2022).

1.2.3.1.3 Propagation of ASYN-fibrils

In living beings, ASYN fibrils might propagate from cell to cell in a prion like manner. The exact origin of ASYN spread is not known, but it is strongly suggested that ASYN may propagate in a retrograde manner via the gut-brain axis (Li et al. 2022). **Figure 6** illustrates the physiological conformation of ASYN: α-synuclein exists in equilibrium between cytosolic and membrane-bound states. In the cytosol, it is mainly unfolded (or possibly a folded tetramer), while membrane binding induces a folded conformation stabilized by two N-terminal/central α-helices. These anchors can link to a single vesicle, bridge multiple vesicles, or connect vesicles to the plasma membrane. At presynaptic sites, ASYN supports SNARE complex assembly, and higher-order multimers may be required for efficient neurotransmitter release.

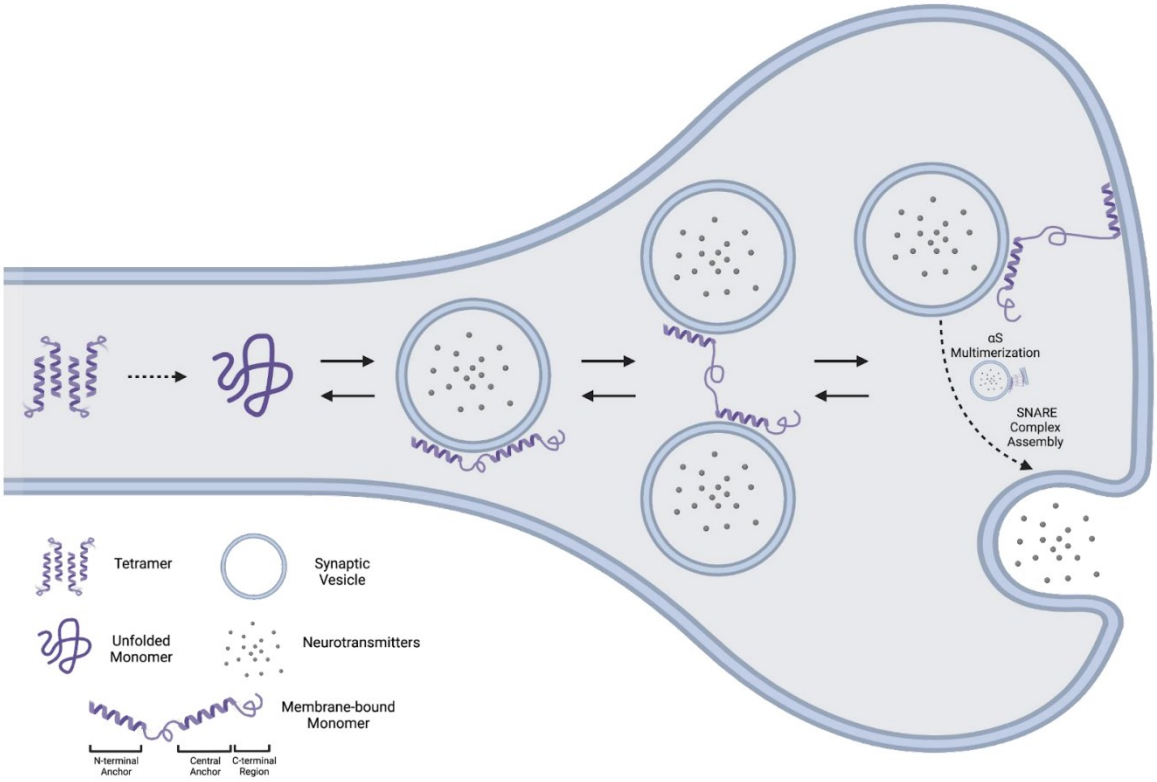

Figure 6 *Physiological conformation of ASYN. Cytosolic and membrane-associated ASYN both exist intracellularly in a steady-state balance. Cytosolic ASYN forms an unfolded monomer, or controversially, a folded tetramer (far left), whilst the membrane-bound ASYN takes a folded structure. Two α-helical anchors on the N-terminal and central region of the protein stabilise the membrane association. ASYN's anchors can be associated with either the same vesicle (middle left), two distinct vesicles, promoting vesicle clustering (middle right) or a vesicle and the plasma membrane, bringing vesicles to the membrane sites (far right, at the top). At the presynaptic membrane, ASYN helps with the SNARE complex assembly; ASYN's self-assembly in higher order multimers might be required for SNARE-mediated neurotransmitter release. Figure adapted from (Li et al. 2022), licensed under CC BY 4.0.*

1.3 Monoamine transporters

Molecular cloning studies have shown that plasma membrane transporters for monoamines such as norepinephrine, serotonin and dopamine are part of a large family of Na^+/Cl^--dependent transporters that also entails transporters from other neurotransmitter and substrates such as GABA, proline and glycine (Chen et al. 2004). The monoamine transporters are members of the neurotransmitter sodium symporter (NSS) family of transporters, which in turn belongs to the larger family of solute carrier 6 (SLC6) transporters (Kristensen et al. 2011). Characteristic for these kinds of transporters is the inward cotransport of the substrate with sodium ions, which provides the energetic driving force for accumulation within the cell (see **Figure 7**) (Rudnick and Clark 1993). Further kinetic studies have shown that other ions such K^+ and Cl^--ions are also contributors in the substrate transport. Potassium ions promote the return of the transporter to the extracellular facing conformation,

resulting in the unbinding of the substrate and ions within the cytoplasm. This applies for the SERT; the DAT, however, does not depend on potassium antiport. Instead, DAT relies on the membrane potential to drive the return step (Rudnick and Nelson 1978; Erreger et al. 2008). Another specific group of transporters mediate the translocation of monoamines from the cytoplasm into secretory and synaptic vesicles. These vesicular monoamine transporters (VMATs) couple substrate translocation to the proton electrochemical gradient across the vesicular membrane — typically exchanging one monoamine for two protons — providing the driving force for vesicular accumulation (Amara 1995; Yaffe et al. 2018; Srivastava et al. 2024).

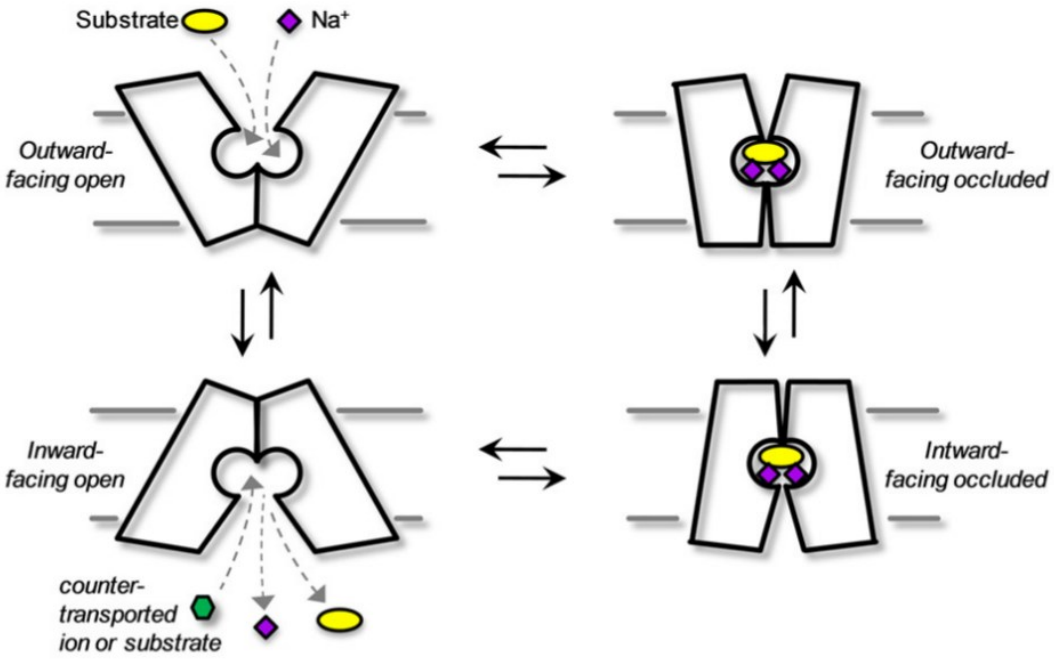

Figure 7 *Schematic representation of the conformational states the transporters must shuttle between to move substrate from the extracellular space to the cytoplasm. Figure adapted from (Kristensen et al. 2011), License number: 6091260780859.*

1.3.1 Structure of Monoamine transporters

A conserved characteristic structure for the SLC6 transporters is the canonical LeuT fold, where the transmembrane helices TM1-5 are related to the TM6-10 by a pseudo two-fold axis of symmetry, which is aligned approximately parallel to the membrane (Srivastava et al. 2024). One of the key features of transporters with the LeuT fold are 12 transmembrane helices that are organised into two inverted repeats of 5 TM (TM1-5 and TM6-10), which are structurally similar (see **Figure 8**) (Yamashita et al. 2005). The inverted symmetry is crucial for alternating access

mechanism, making it possible for the transporter to switch between outward-facing and inward-facing conformation, thereby exposing the central binding site to either side of the membrane. The transport of the substrate is often coupled with sodium ions, which contribute to the transport through an electrochemical gradient (Forrest et al. 2008). According to the rocking bundle model, where the major conformational change in the outward-open and inward-open transition is the relative motion of the bundle of core TM1, TM2, TM6 and TM7 with respect to the hash motif consisting of TM3, TM4, TM8 and TM9 (see **Figure 8**) (Jeschke 2013). The central ligand binding site, also known as the S1 site, is mainly for binding the substrate and sodium ions, whereas the secondary substrate-binding site, also called S2 or extracellular vestibular binding site, is mainly for binding second substrates or inhibitors (Nyola et al. 2010). The C-terminal "latch", which borders the cytoplasmatic side of the membrane, is the most expansive cytoplasmatic motif observed to date in an NSS. It consists of three short C-terminal helices (CT1, CT2 and CT3) that cover the cytoplasmatic termini of TM3, TM10 and TM12, which results in a greater stabilisation of the closed conformation of the cytoplasmatic gate (Srivastava et al. 2024).

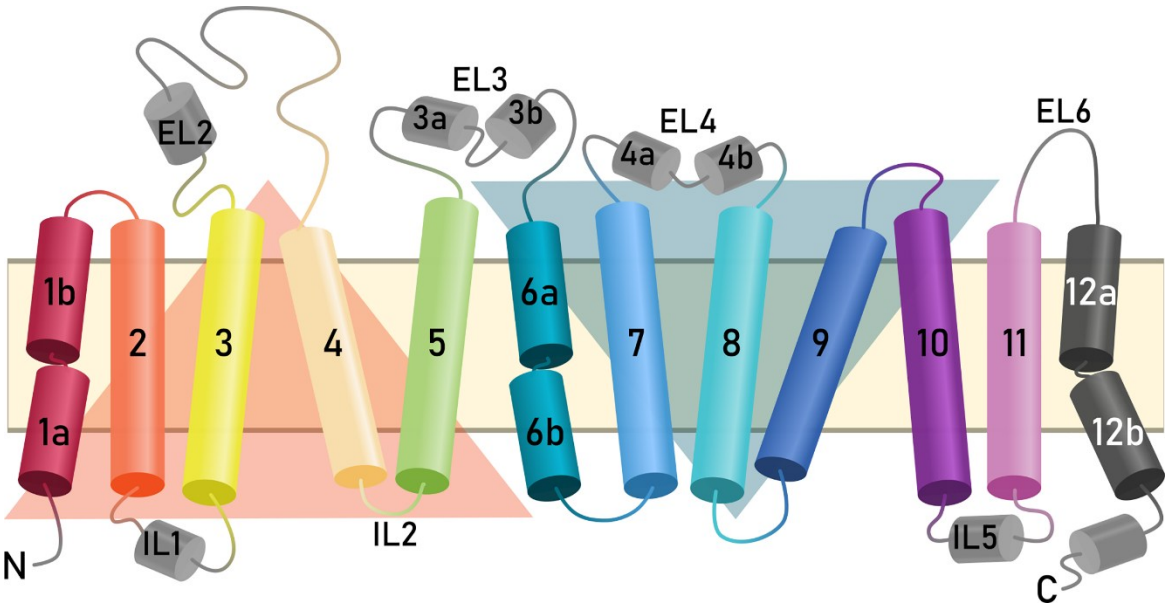

Figure 8 *Transmembrane topology of SLC6 transporters, illustrated via the hSERT. 12 TM helices are linked by intra- and extracellular loops (ILs, Els). The pseudo two-fold axis of symmetry is highlighted by orange (TM1-5) and blue (TM6-10) triangles. The "rocking bundle" consists of TM1, TM2, TM6 and TM7. Figure adapted from (Hellsberg et al. 2019), licensed under CC BY 4.0.*

1.3.2 DAT

The DAT is part of the Na^+/Cl^--dependent membrane transporter protein family and possesses twelve transmembrane α-helical domains, cytoplasmic N and C termini as well as a large glycosylated extracellular loop (Giros et al. 1992; Giros and Caron 1993; Kristensen et al. 2011). Psychostimulants such as cocaine and amphetamine can bind to the DAT and prevent DA reuptake. The neurotoxin 1-methyl-4-phenylpyridinium (MPP+) is transported into dopaminergic neurons via the DA transporter, thus causing parkinsonism (Langston et al. 1983; Javitch et al. 1985). The activity of the human dopamine transporter (hDAT) is different in comparison to its biogenic amine transporter relatives, in that transport activity is inhibited by physiologically related levels of Zn^{2+}, which is co-released with neurotransmitters, as well as synthetic small molecules that target allosteric sites (Srivastava et al. 2024).

1.3.2.1 Regulation of activity

Psychostimulant drugs regulate the DAT in opposite ways: amphetamine promotes rapid internalization and decreased surface availability of DAT, while cocaine tends to increase DAT surface expression, often by blocking internalization or stimulating reinsertion - a dynamic that significantly influences dopamine clearance and signaling (Saunders et al. 2000; Zahniser and Sorkin 2009; Richardson et al. 2016; Saenz et al. 2023).

1.3.3 SERT

The human SERT (hSERT) consists of 630 amino acids. The hSERT possesses 12 transmembrane helices with cytoplasmatic N- and C-termini, a common trait of SLC6 transporters. Transmembrane domains 3 and 4 are separated by a big, hydrophilic loop which possesses two canonical sites for N-linked glycosylation. The hSERT forms homo-multimeric complexes and possesses potential phosphorylation sites for multiple kinases (Ramamoorthy et al. 2011).

1.3.3.1 Regulation of activity

SERT's regulation is mediated by multiple signal transduction pathways including protein kinase C (PKC), p38 mitogen-activated protein kinase (p38 MAPK) cAMP, cGMP and calmodulin (Zhang and Rudnick 2011).

1.4 ASYN and its interaction with monoamine transporters (SERT, DAT)

1.4.1 Important discoveries of ASYN in the last decades

Over the past 25 years, ASYN has emerged as a central protein in the pathogenesis of PD and related synucleinopathies, especially after the discovery of the disease-causing A53T mutation in the SNCA gene (Polymeropoulos et al. 1997). The causal role of ASYN was further cemented through the discovery of SNCA gene multiplications, where duplications and triplications were shown to produce dose-dependent familial PD (Singleton et al. 2003). Besides gene multiplication being a driving factor, post-translational modifications of ASYN attracted significant attention as well, with phosphorylation at Ser129 identified as the predominant modification in Lewy pathology (Fujiwara et al. 2002; Anderson et al. 2006). While initially considered a driver of aggregation, subsequent evidence indicated that phosphorylation at Ser129 is more likely a downstream consequence of fibrillization. It was proposed that the Ser129-hyperphosphorylation of ASYN aggregates was the consequence of failing to remove said degradation-resistant aggregates (Arawaka et al. 2017).

Advances in the structural visualization of proteins have also contributed to a better understanding of ASYN aggregation. Cryo-electron microscopy revealed fibril structures on an atomic level (Guerrero-Ferreira et al. 2018) and demonstrated the existence of multiple polymorphs with distinct protofilament folds (Li et al. 2018). At the same time, ultrastructural analyses (electron microscopy analyses) of human brain tissue discovered that Lewy bodies are not homogeneous fibrillar deposits but rather organelle- and membrane-rich inclusions containing ASYN filaments (Shahmoradian et al. 2019).

Experimental models have illustrated that ASYN aggregates propagate in a prion-like manner. Pre-formed fibril models demonstrated that exogenous ASYN fibrils seed endogenous misfolding in neurons (Volpicelli-Daley et al. 2011), resulting in Lewy body-like inclusions, dopaminergic neurodegeneration, and motor impairments in wild-type animals (Luk et al. 2012). At the same time, studies further elucidated the physiological role of ASYN at the presynapse, where it functions as a SNARE-complex chaperone that supports vesicle docking and fusion. Consistent

with this role, triple knockout mice lacking all synucleins developed age-progressive neurodegeneration and synaptic dysfunction (Burré et al. 2010).

In recent years, seed amplification assays (SAAs) have been optimized to detect misfolded ASYN with high sensitivity and specificity in cerebrospinal fluid. These assays can differentiate PD patients from controls and divide prodromal individuals into subgroups in large long-term studies such as Parkinson's Progression Markers Initiative (PPMI) (Siderowf et al. 2023).

1.4.2 Recent discoveries of ASYN-interactions with monoamine transporters

While most of the research has focused on ASYN's interaction with DAT, a growing amount of work demonstrated that ASYN also regulates SERT. The first mechanistic study reported that ASYN directly interacts with SERT, reducing its activity by decreasing transporter surface expression (Wersinger, Rusnak, et al. 2006; Oaks and Sidhu 2011). Comparative studies showed that γ-synuclein exerts only partial regulation, while ASYN strongly inhibits SERT (Wersinger and Sidhu 2009).

Contrary to *in vitro* assays, *in vivo* studies implied that ASYN does not only act as a strict inhibitor of SERT: Viral-mediated or antisense oligonucleotide (ASO)-driven knockdown of ASYN in monoaminergic neurons increased extracellular 5-HT (and dopamine), whereas overexpression of ASYN in dorsal raphe 5-HT neurons reduced forebrain serotonergic release and induced depressive-like phenotypes. These phenotypes could be reversed by targeted ASYN reduction (Alarcón-Arís et al. 2018; Miquel-Rio et al. 2022).

The first reports about the interaction between ASYN and DAT demonstrated that ASYN binds directly to the C-terminus of DAT and alters its function by increasing dopamine uptake (Lee et al. 2001). In contrast to that, this interaction was described in subsequent studies to result in a reduction of DAT-mediated dopamine uptake, primarily by lowering transporter surface expression (Wersinger and Sidhu 2003). Following studies showed that ASYN can exert context-dependent effects, either attenuating or facilitating transporter function depending on oxidative stress and cell adhesion states (Wersinger and Sidhu 2005).

Mechanistic studies have shown that ASYN can regulate DAT trafficking by reducing its surface expression, an effect that could be reversed by proteolytic treatment (e.g., trypsin), indicating that ASYN sequestered DAT into intracellular compartments (Wersinger et al. 2004). In addition, it has been demonstrated that the inhibitory impact of ASYN on DAT depends upon intact microtubule interactions, as microtubule disruption (via vinblastine, colchicine, or nocodazole) restored DAT surface localization and dopamine uptake (Wersinger and Sidhu 2005). Additional cellular studies showed that intracellular ASYN could evoke DAT-dependent ionic currents of chloride (Swant et al. 2011). More recent work revealed that DAT activation itself could recruit ASYN to cholesterol-rich microdomains, where it stabilizes efflux-prone transporter states (Butler et al. 2015). In vivo, ASYN has been demonstrated to enhance DAT function in a cholesterol-dependent manner (Threlfell et al. 2021).

In PD mouse models, ASYN–DAT complexes redistributed in affected striatal regions (Bellucci et al. 2012) and post-mortem human studies showed altered ASYN–DAT complexes in PD striatum (Longhena et al. 2018). Furthermore, parkin has been shown to disrupt the ASYN–DAT interaction, thereby causing dopamine toxicity and linking transporter regulation to genetic forms of PD (Moszczynska et al. 2007).

These recent studies indicate that ASYN modulates SERT and DAT trafficking and surface expression in a complex, context-dependent manner, exerting either inhibitory or promoting effects depending on the cellular environment and aggregation state.

2 Materials and Methods

2.1 Cell Culture

Human embryonic kidney (HEK) 293 cells were cultured in Dulbecco's modified Eagle's medium (DMEM, Capricorn Scientific, DMEM-HA) with added 10% fetal bovine serum (FBS) and 1% penicillin/streptomycin (PS). Cath.-a-differentiated (CAD) cells were cultured in DMEM/Ham's F-12 (Capricorn Scientific, DMEM-12-A) with added 10% FBS and 1% PS. All cell lines were grown in a humidified 5% CO_2 atmosphere at 37°C.

2.2 Protocol for transient transfection of cell lines

For optimal transfection efficiency, cells should be 60% to 80% confluent. The day after transfection, transfection efficiency was checked by brightfield microscopy.

2.2.1 jetPrime Transfection

First, 500 µL of jetPRIME buffer (Polyplus, #2000003) was added to the Eppendorf tube of the respective condition (the amount of buffer depends on the size of the cell culture dish, for 10 cm petri dishes it is 500 µL). Afterwards, 10 µg of Plasmid-DNA was added to the Eppendorf tubes with a subsequent 10 second vortex and spinning down. Then, jetPRIME transfection reagent (Polyplus, #0000002970) (in a ratio 1:2 (DNA/jetPRIME reagent) was added to the tubes. After one second vortex and spinning down, the Eppendorf tubes were incubated for 10 minutes at room temperature. The transfection mixture was then added to a dish. After 4h incubation time, the media was replaced with a fresh one.

2.2.2 Lipofectamine 2000

Two mixtures were prepared separately: For mixture I, 25 µL of Lipofectamine 2000 (Invitrogen by Thermo Fisher Scientific, #13778-150) was added to 1mL of Opti-MEM media (Gibco, #11058-021), vortexed and spun down. For mixture II, a total of 20 µg of Plasmid-DNA was added to 1ml of Opti-MEM media, vortexed and spun down. Both mixtures were incubated for 5 minutes at room temperature. After the incubation time, equal amounts of mixture I was put into mixture II and incubated for 20 minutes at room temperature. After that, the transfection mix was added to the cells.

2.2.3 PEI transfection

500 µL of serum-free DMEM was added to Eppendorf tubes. At first, 10 µg of Plasmid-DNA was added to the tube. In a ratio of 1:3 (DNA:PEI), polyethyleneimine (PEI, Polyscience Europe GmbH, #23966) was added to the tube. After vortexing and spinning down, it was incubated for 20 minutes at room temperature. As a final step, the transfection mix was added to the cells and incubated overnight (for visual illustration see **Figure 9**).

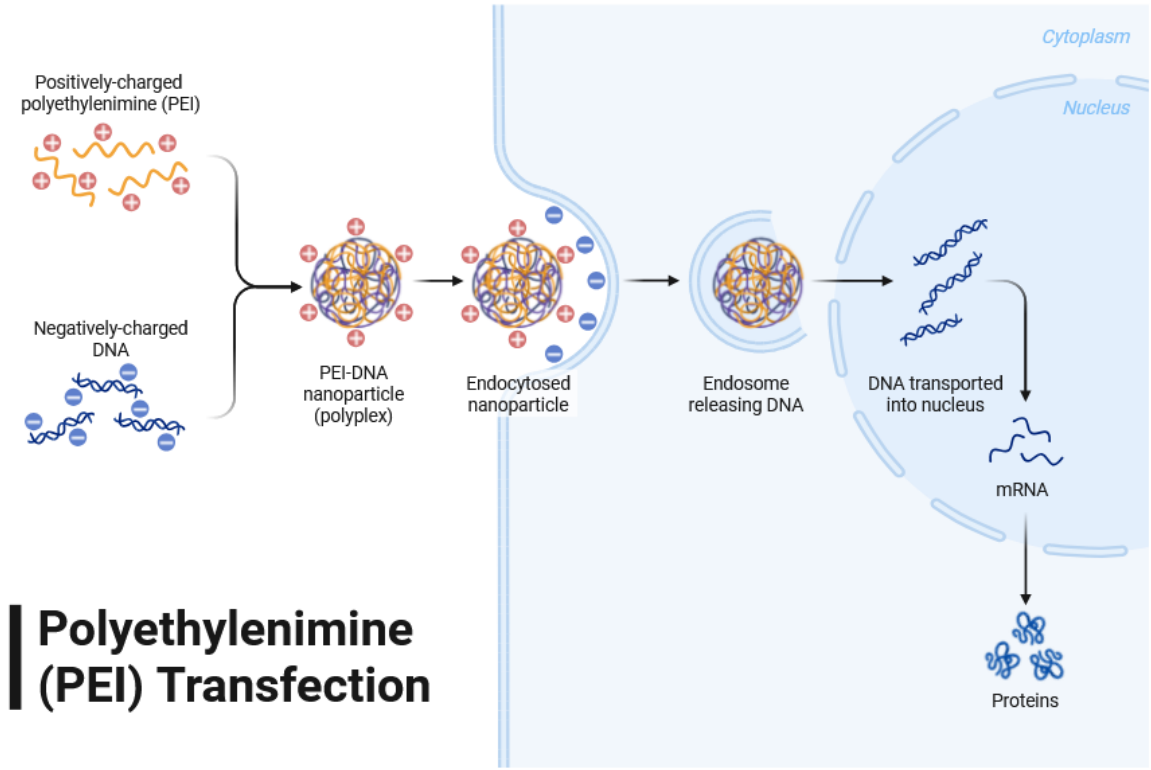

Figure 9 *Schematic illustration of the PEI transfection. Positively charged PEI forms a nanoparticle with negatively charged DNA, which is subsequently endocytosed by the cell. Intracellularly, the DNA gets released and is expressed into the respective protein. Image created with BioRender.*

2.3 Uptake saturation assay

Kinetic assays are employed to characterize the rate of an enzymatic reaction under varying substrate concentrations and conditions. In contrast to endpoint assays, which only measure product accumulation after a fixed period, kinetic assays follow the reaction continuously over time, thereby allowing determination of reaction velocity. By plotting initial reaction rates against substrate concentration, it is possible to derive key kinetic parameters using Michaelis–Menten analysis. These include the Michaelis-Menten constant (K_m), which reflects the apparent substrate affinity of the enzyme, and the maximum velocity (V_{max}), which represents the

catalytic capacity of the enzyme under saturating substrate concentrations. Such kinetic assays therefore provide fundamental insights into enzyme efficiency, substrate specificity, and potential regulation by inhibitors or activators (Segel 1975).

The changes of kinetic parameters of monoamine transporters due to overexpressed WT-ASYN and A53T ASYN was measured by conducting such saturation assay. Radioligand uptake assays are vastly used to quantitatively measure the substrate uptake via the plasma membrane or other compartments like vesicles or synaptosomes. By using radiolabelled ligands, it is possible to quantitatively measure the substrate uptake with a scintillation spectrophotometer. By conducting a radioisotope dilution, adding non-radiolabelled substrate to the radiolabelled one at different concentrations to the cells, the reaction rate and the affinity of the transporter towards the substrate can be determined, i.e. Michaelis-Menten kinetics (Dvorak et al. 2021).

After being confronted with detecting variable effects of ASYN in HEK293 cells, the uptake saturation assay was also conducted with CAD cells, derived from murine neuroblastoma cells (Cevallos et al. 2025).

2.3.1 Protocol

Three 10 cm dishes were seeded with HEK293 or CAD cells so that on the next day there would be a confluency from 60-80%, which is optimal for transfection. On the next day, the cells were transfected according to the jetPRIME protocol (see above **2.2.1**). Some experiments were also transfected according to the Lipofectamine 2000 Protocol from Invitrogen/Thermo Fisher Scientific (see above **2.2.2**) or by PEI transfection (see above **2.2.3**). For the used plasmid maps see **Figure 10** and **Figure 11**.

A

B

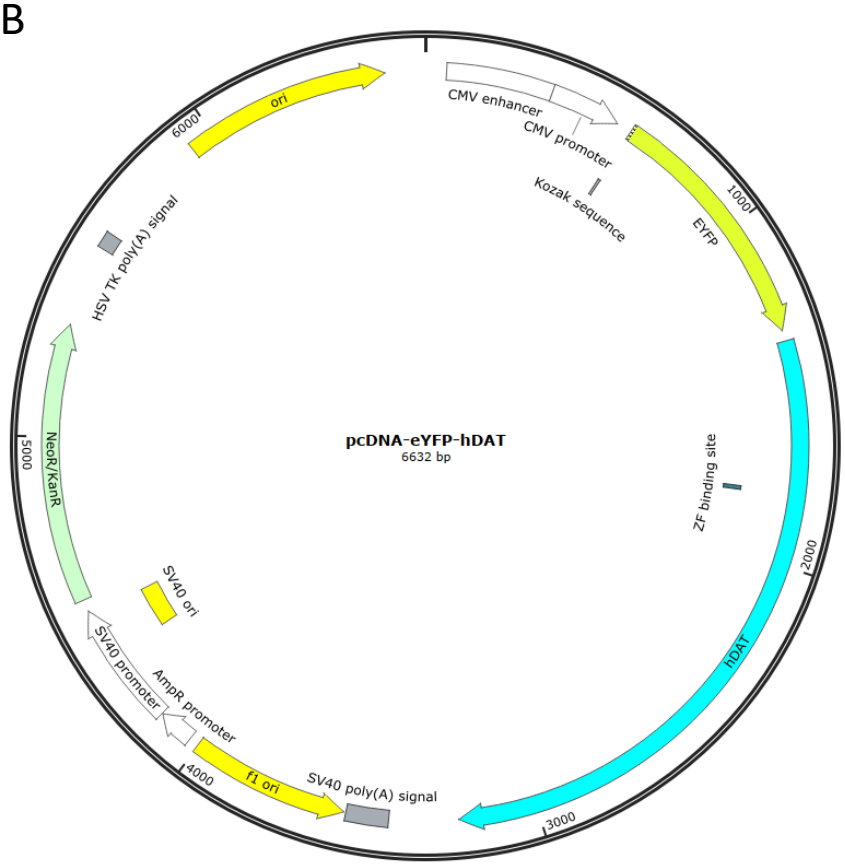

Figure 10 *Plasmid maps of* ***(A)*** *pcDNA-eYFP-hSERT* ***(B)*** *pcDNA-eYFP-hDAT showcasing the transgene. Images from SnapGene Viewer.*

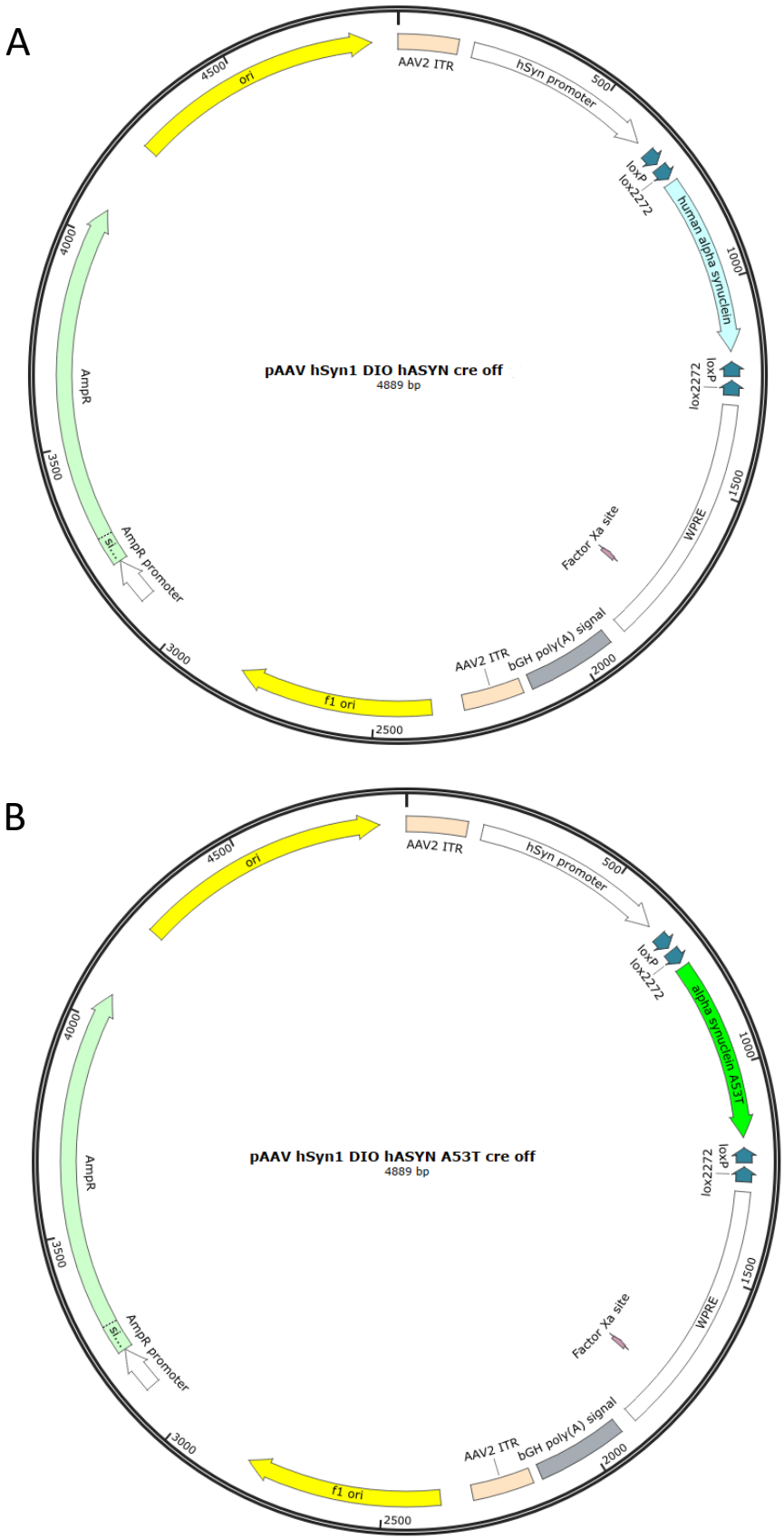

Figure 11 *Plasmid maps of* ***(A)*** *pAAV hSyn1 DIO hASYN cre off* ***(B)*** *pAAV hSyn1 DIO hASYN A53T cre off, showcasing the transgene. "Cre off" is referring to flanking loxP sites at the transgene, recognition sequences for the Cre-recombinase. If Cre-recombinase is present in the cell, it recombines the DNA between the loxP sites and deletes the gene. Since there is no Cre-recombinase present in CAD or HEK cells, the gene of interest was expressed accordingly. Images from SnapGene Viewer.*

Each plate received the same amount of monoamine transporter plasmid (either hSERT or hDAT), but different amounts of ASYN or empty vector (pcDNA3.1; control). The 1:0 condition included 2.5 µg transporter plasmid DNA and 7.5 µg pcDNA3.1; 1:3 WT was 2.5 µg transporter plasmid DNA and 7.5 µg pAAV hSyn1 DIO hASYN cre off and 1:3 A53T was 2.5 µg transporter plasmid DNA and 7.5 µg pAAV hSyn1 DIO hASYN A53T cre off. The following day, expression levels were determined via fluorescence microscopy by looking at YFP-tagged monoamine transporter expression. Cells were then seeded into PDL (poly D lysine, 1 mg/ml)-coated 48 well-plates according to **Figure 12**. Remaining cells (ca. 50 % of the cells grown in a 10 cm dish) were put back into the dish to lyse them the next day for Western Blotting. About 48 hours after transfection, the actual radioligand uptake assay was conducted: The assay was performed in triplicates, with 8 conditions in each transfection conditions. The first six columns were reserved for different concentrations of the substrate (either [^{3}H]5-HT or [^{3}H]DA + additional amounts of unlabeled substrates to reach a certain final concentration), the 7th column was for measuring non-specific uptake and the 8th column was reserved for cell counting (required for normalization). At first, a solution of Krebs-HEPES buffer (KHB) (10mM HEPES, 120mM NaCl, 3mM KCl, 2mM $CaCl_2.2H_2O$, 2mM $MgCl_2.6H_2O$, 20mM D-(+)-glucose-monohydrate, pH 7.3) containing the respective radioligand was produced and then put equal amounts into 7 Eppendorf tubes. For SERT, a concentration of 0.1 µM of [^{3}H]5-HT ([^{3}H]5-hydroxytryptamine (=serotonin), Revvity, NET498001MC, specific activity: 32.79 Ci/mmol) was used; for DAT a concentration of 0.1 µM of [^{3}H]DA (Revvity, NET673001MC, specific activity: 32 Ci/mmol) respectively. Subsequently, a dilution series of the non-radiolabeled (“cold”) ligand was made: 10 mM -> 1 mM -> 100 µM of either serotonin hydrochloride or dopamine hydrobromide. The cold ligand was added to the Eppendorf tubes to get the following final concentrations: 0.1 µM, 1 µM, 3 µM, 10 µM, 15 µM and 30 (SERT) or 20 (DAT) µM. For unspecific uptake, a specific antagonist of either SERT or DAT was added to the KHB containing 0.1 µM radioligand. For SERT I used 10 µM paroxetine, a selective-serotonin-reuptake inhibitor, whereas I used 10 µM mazindol for DAT. In each case, preincubation with just the inhibitor (but no radioligand) was done prior (ca. 5-10 min) to incubation with radioligand containing the inhibitor to maximize saturation of transporters with the respective inhibitor.

After all the solutions are prepared, the actual uptake assay was started. First the media from the 48-well plate in rows 1 to 7 were removed and washed with KHB (room temperature: approximately 22 °C). Each well was then incubated for exactly 1 minute with the solutions. To do so, KHB was removed from the wells and then 100 µL of the radioligand was added to each well (I chose to do 10 sec intervals between the different wells). After the end of the incubation time, the reaction was stopped by washing the wells with ice-cold KHB three times. For non-specific uptake, the wells were incubated with the non-radiolabeled transporter inhibitor for at least 5 minutes and then the uptake assay was conducted the same way as with the radioligand but with the radiolabeled transporter inhibitor.

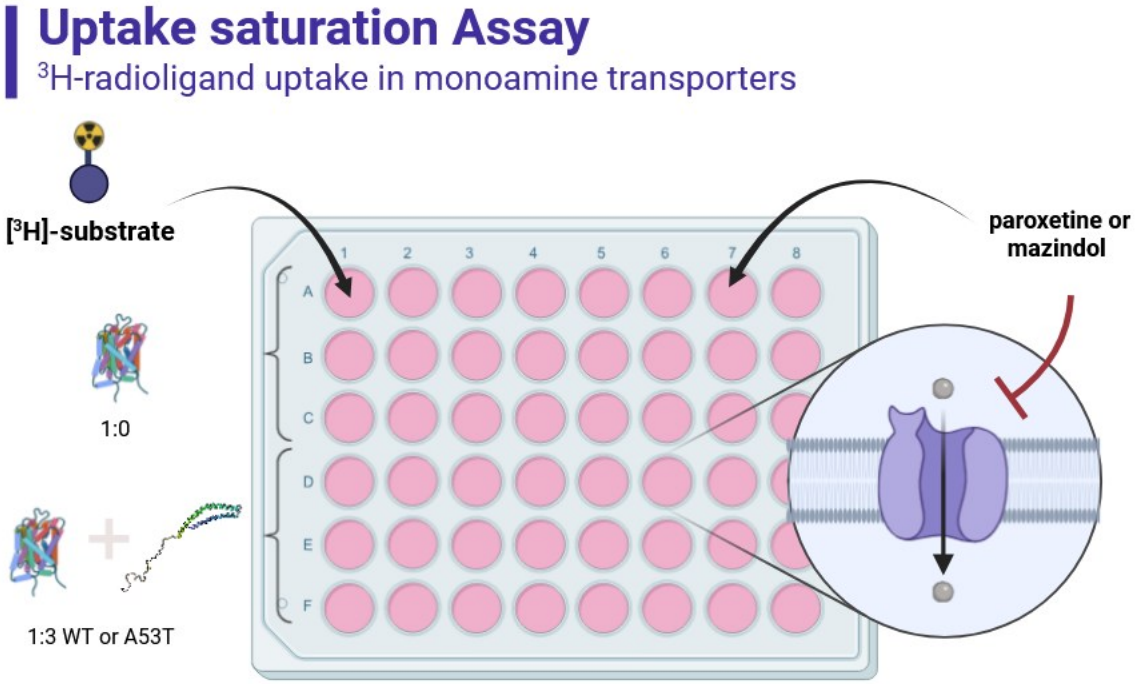

Figure 12 *Schematic illustration of the [^{3}H]-radioligand uptake assay. Image created with BioRender.*

Finally, the cells were lysed by adding 1% sodium dodecyl sulfate (SDS, Sigma-Aldrich, 75746) to the wells. After cell lysis, the lysates were transferred to scintillation vials, that have been pre-filled with 2 mL of scintillation cocktail (Carl Roth, 1P1A.2) before. To measure the total activity of the radioligand solution, 10 µL of the solution was added per vial (measured in triplicates). Subsequently, the vials were thoroughly mixed and then measured (counts per minute; cpm) using a scintillation spectrophotometer (Tri-Carb 4910TR Liquid Scintillation Counter, Revvity). Cells in the 8th column were washed three times with KHB and then

detached with 10% trypsin (v/v). After homogenization, the cells in each well were counted with a hemocytometer ('Neubauer chamber').

Table 1 *Overview of the conditions for [^{3}H]5HT specific uptake.*

Label	End concentration	Concentration of cold ligand/inhibitor	Amounts added [µL]
2	1 µM 5-HT	100 µM	8.64
3	3 µM 5-HT	1 mM	2.78
4	10 µM 5-HT	1 mM	9.5
5	15 µM 5-HT	10 mM	1.43
6	30 µM 5-HT	10 mM	2.87
Hot or cold NS	10 µM paroxetine	1 mM	9.6

Table 2 *Overview of the conditions for [^{3}H]DA specific uptake.*

Label	End concentration	Concentration of cold ligand/inhibitor	Amounts added [µL]
2	1 µM DA	100 µM	8.64
3	3 µM DA	1 mM	2.78
4	10 µM DA	1 mM	9.5
5	15 µM DA	10 mM	1.43
6	**20** µM DA	10 mM	1.91
Hot or cold NS	10 µM mazindol	1 mM	9.6

2.4 Immunoblotting analysis

To confirm the presence of the transfected ASYN and the monoamine transporters, the respective expression levels were measured through immunoblotting analysis. Cell lysates (see below **2.4.1**) were prepared and separated by gel electrophoresis. An electric current separates proteins according to their molecular weight. Subsequently, the separated protein bands were transferred to a nitrocellulose membrane via an electric current. By doing that, the membrane can easily be incubated with antibodies that bind to the protein of interest and can also be visualized. At first, the primary antibody binds directly to the protein of interest, whereas the secondary antibody binds to the primary antibody. The secondary antibody is conjugated with a fluorophore allowing fluorescence detection. The

signal intensity is proportional to the actual amounts of the protein of interest (Yang and Mahmood 2012).

2.4.1 Protocol

As described above (**2.3.1.**), for each uptake assay remaining cells of each condition were put back into the 10 cm dish, kept overnight and lysed for protein detection roughly 48 hours after transfection (i.e. at about the same time as the uptake assay). 10 cm dishes of each condition were taken out of the incubator and put on ice. The cells were washed with ice-cold PBS at least 2 times before adding the radioimmunoprecipitation assay (RIPA) lysis and extraction buffer (150 mM NaCl, 10 mM EDTA, 0,1% SDS, 1% Triton X-100, 50 mM Tris-HCl, pH=7.4), containing protease inhibitor with a concentration of 1 tablet/50 mL(cOmplete™, EDTA-free Protease Inhibitor Cocktail, Roche, 04693132001). The amount of added RIPA buffer was dependent on the cell confluency (the higher the confluency, the higher was the added amount); it ranged from 200 to 400 µL. Then using a cell scraper, that has been disinfected with 70% ethanol, the bottom of the petri dish was scrubbed thoroughly to ensure that cells were detached. Suspensions were then transferred to plastic tubes (1.5 mL Eppendorf) and rotated at 4°C for 30 minutes to lyse cells. The samples were then centrifuged at 4°C for 10 minutes with 16000 x g. The supernatant was then transferred to new tubes and frozen at -20°C.

Protein concentrations were determined with the bicinchoninic acid (BCA) assay. First, a standard curve of using albumin was prepared, with 2 mg/ml being the highest concentration and 0.025 mg/ml being the lowest. Then reagent A and reagent B were mixed in a ratio of 50:1. 200 µL of this solution was added to the wells of a 96-well plate. Each sample was measured in triplicates. After adding 25 µL Milli-Q (MQ) water and 5 µL sample to each well, the plate was incubated at 37°C for 30 minutes. Afterwards, the absorption was measured at 544 nm wavelength by a Perkin Elmer VICTOR3V Multilabel Plate Reader (see **Figure 14**). The protein concentration of the samples could then be calculated with the help of the standard concentration curve (see **Figure 13**).

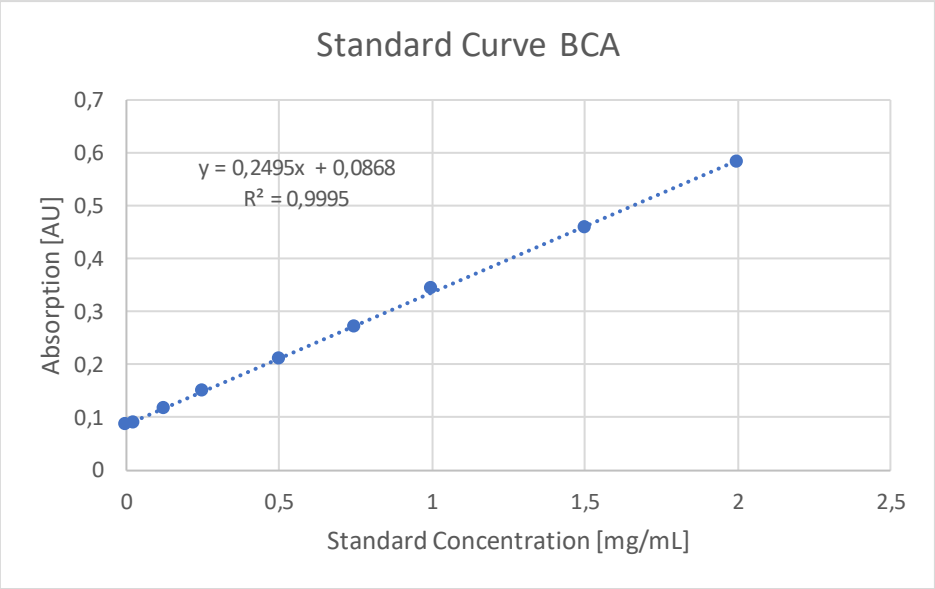

Figure 13 *Example of a standard concentration curve for the BCA assay.*

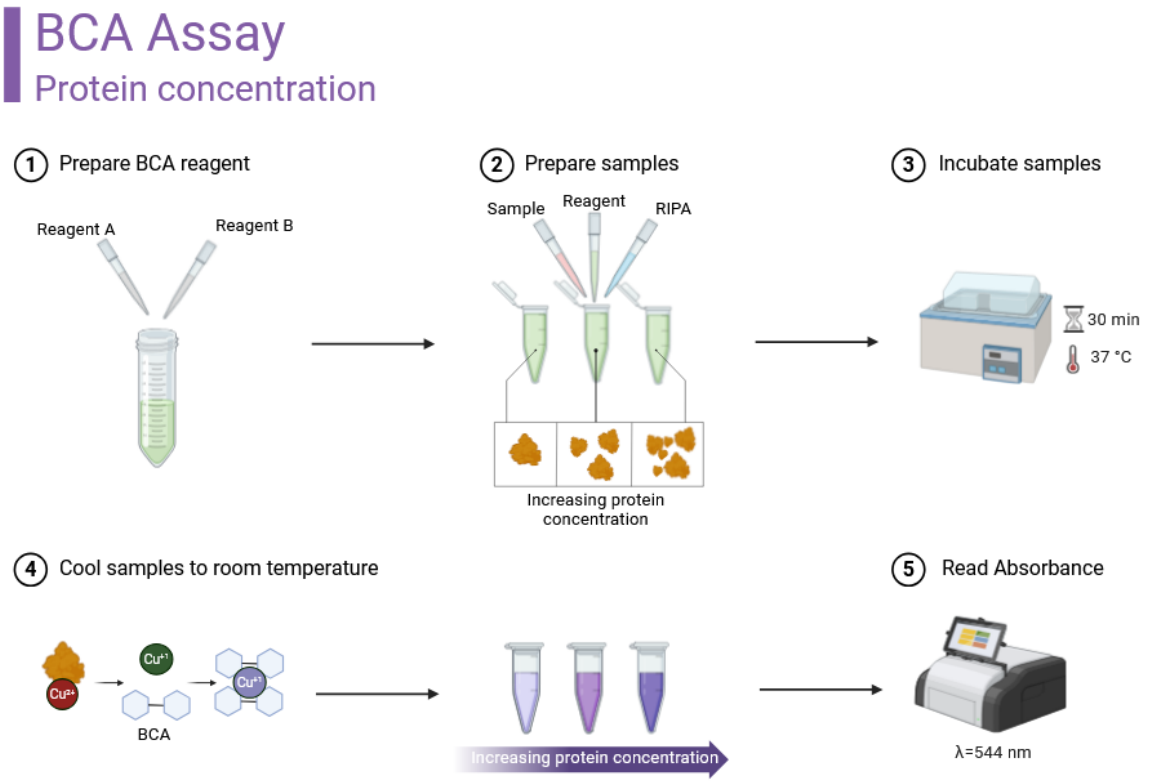

Figure 14 *Workflow of the BCA assay*

Samples were diluted with RIPA buffer to get a total amount of 30 µg of protein per sample. After adding the Laemmli sample buffer (0.0625M Tris-HCl pH 6.8, 2% SDS, 10% glycerol, 0.01% bromophenol blue, 5% β-mercaptoethanol) the samples were either boiled for 5 minutes at 95°C or heated up for 30 minutes at 37°C. Importantly, high temperatures promote protein denaturation and the separation of disulfide

bonds; this is optimal for soluble proteins. Nevertheless, for membrane proteins like DAT or SERT that contain large hydrophobic parts higher temperatures promote aggregation. Therefore, I performed slow denaturation at lower temperatures to avoid getting aggregates. Depending on which proteins should be detected, either 10% (for DAT and SERT; MW of ca. 60 kD) or 12% (ASYN; MW of ca. 15 kD) gels were used for the protein separation. To prepare the resolving and stacking gel, I first made a 10% (w/v) ammonium persulfate (APS) solution in Milli-Q water. The gel mixture for the resolving gel consisted of 2.5 ml Tris-HCl (1.5 M, pH 8.8), 0.1 ml of 10% (w/v) SDS, 3.96/3.29 ml MQ water (for 10%/12% gel), 3.33/4.0 ml 30% (w/v) Acrylamide/Bis Solution (SERVA, 10688.01), and 0.1 ml 10% APS. I did not shake the mixture to avoid bubble formation caused by SDS. I added 0.01 ml TEMED last as the radical initiator and worked quickly after its addition. Following this, I homogenized the solution and distributed it equally into the gel glass plates. I carefully overlaid the gel with 100% isopropanol to eliminate bubbles and allowed the gel to polymerize for 15 minutes. During this time, I checked the resolving gel solution in the Falcon tube and prepared the combs (e.g., 10 wells, 1 mm thickness), ensuring they were intact. For the stacking gel (5%), I prepared a mixture of 1.25 ml Tris-HCl (pH 6.8), 0.05 ml 10% SDS, 2.81ml MQ water, and 0.84 ml 30% (w/v) Acrylamide/Bis Solution, adding 0.05 ml 10% APS and 0.005 ml TEMED last. I removed the isopropanol from the resolving gel by pouring it off and blotting the rest with tissue. After adding APS and TEMED to the stacking gel mixture, I overfilled the space between the glass plates without introducing bubbles and inserted the combs carefully, again ensuring no bubbles were present. I then allowed the stacking gel to solidify for 10–15 minutes before proceeding. The protein separation is based on a SDS-polyacrylamide gel electrophoresis (SDS-PAGE), first applying 100V in the SDS-PAGE buffer (25 mM Tris, 192 mM Glycine, 0.1 mM EDTA.Na2, 0.175 mM SDS, pH 8.5), increasing the voltage to 150V after the proteins have passed through the stacking gel. The purpose of using different percentages of polyacrylamide gels is the resolution of protein separation: higher percentages make it harder for bigger proteins to pass through, therefore making the resolution of smaller proteins higher. In contrast, lower gel percentages have a higher resolution for bigger proteins. When the proteins reached the end of the gel, the electrophoresis was stopped and a blotting cassette as seen in **Figure 15** was assembled. The proteins were then transferred to a nitrocellulose membrane using a wet transfer system (transfer buffer:

25 mM Tris, 192 mM glycine, 10 % MeOH, pH 8.3). Unfortunately, there were difficulties detecting ASYN (especially when using HEK cells as the transfected cells) by conducting the wet transfer with constant 100V for 45 minutes. Different optimization methods were applied: changing the transfer to a constant 120 mAmp (which is equal to approximately 30V) for 75 minutes made the detection of ASYN in ASYN-transfected CAD cells possible, but not in transfected HEK cells. By decreasing the transfer to 50 minutes with constant 120 mAmp, ASYN could also be detected in transfected HEK cells, but still in a far lower intensity compared to ASYN-expressing CAD cells. After the transfer, the membranes were fixed with 0.4% PFA (paraformaldehyde) at RT for 25-30 minutes to increase the binding of monomeric ASYN to the membrane (Lee and Kamitani 2011). After fixation, the membranes were stained with Ponceau S solution (0.1% Ponceau S (w/v) in 5% acetic acid (v/v)) for approximately 1 minute to control the protein loading and the transfer efficiency. Subsequently, the membranes were blocked for 1 hour in 5% non-fat dry milk in Tris-buffered saline-Tween (TBS-T) (20 mM Tris, 150 mM NaCl, 0,1% Tween20, pH 7.5).

After blocking, membranes were incubated with the primary antibodies at 4°C overnight. The primary antibodies that were used for this project after diluting them in TBS-T were the following: for ASYN detection 1:1000 mouse anti-α-synuclein 4D6 (Biolegend, #834301); 1:100 rat anti-α-synuclein 15G7 (Enzo Life Sciences, ALX-804-258-LC05), for DAT and SERT detection of the eYFP epitope tag was done with 1:1000 rabbit anti-green-fluorescent protein (GFP) (Invitrogen, Thermo Fisher Scientific, #A11122); glyceraldehyde-3-phosphate dehydrogenase (GAPDH) detection 1:1000 rabbit GAPDH (D16H11) XP® (Cell Signaling Technologies, #5174S). After the incubation overnight, the primary antibody was removed and for future uses, sodium azide (0.01 %) was added to the primary antibody solution. The membrane was then washed three times with TBS-T for 5 minutes and then incubated with the secondary antibody as a 1:5000 dilution in the blocking buffer at RT (room temperature) for 2 hours. As a protection against bleaching of the fluorophore that is attached to the secondary antibody, the boxes of the membranes were covered with aluminum foil. The secondary antibodies used were IRDye® goat anti-rabbit 800 (#926-32211), goat anti-rabbit 680 (#926-68071), goat anti-rat 680 (#926-68076) and goat anti-mouse 680 (#926-68070) (LI-COR Biotechnology), all

applied at a 1:5000 dilution. After incubation of the secondary antibodies, the membrane was washed three times with TBS-T for 5 minutes and then with TBS for 5 minutes, before imaging the membranes by using the LI-COR Odyssey® F Imaging System. Immunoblots were analyzed as described in **Chapter 2.6**

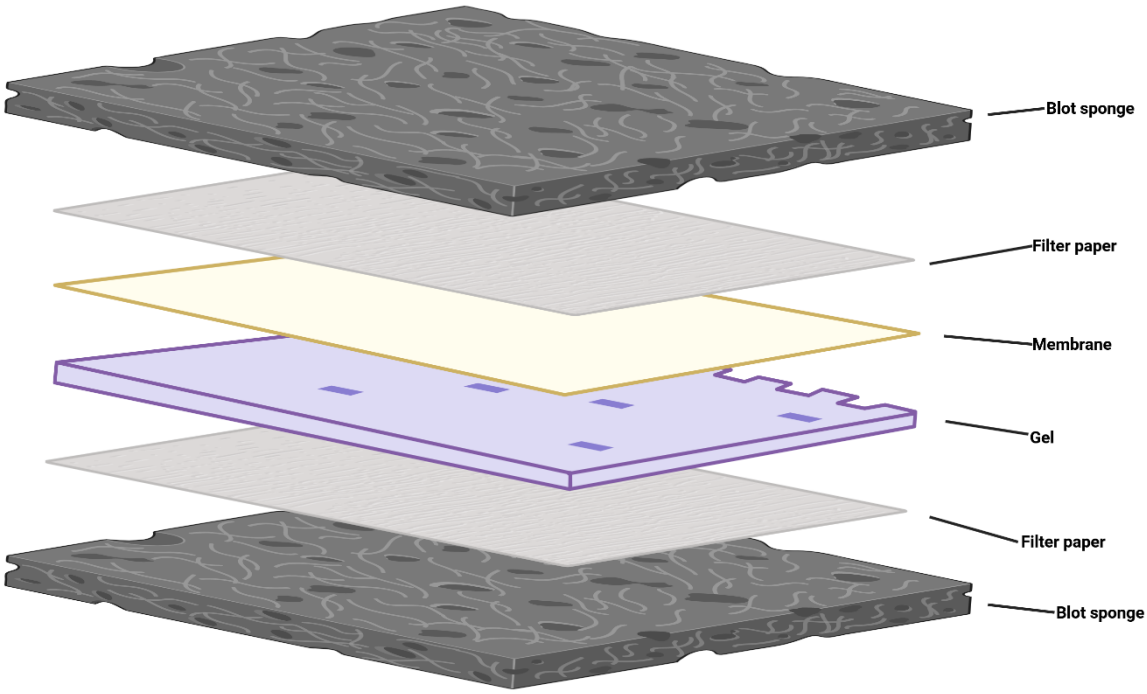

Figure 15 *Western Blot cassette assembly. The blotting sandwich is assembled in the order shown, starting on the black side of the Western blot cassette, with the clear side placed on top to close the sandwich. The assembled sandwich is then positioned in the blotting chamber so that the gel faces the cathode (−) and the membrane faces the anode (+). This orientation ensures that the negatively charged proteins migrate from the gel onto the membrane toward the positive electrode during the transfer. Image created by BioRender.*

2.5 AquaBluer™ Cell Viability Assay

A cell viability assay was performed to investigate potential toxic effects of ASYN for cell survival. The AquaBluer™ Cell Viability Assay was done according to the instructions of the manufacturer. This assay relied on the reduction of a non-fluorescent redox indicator to a fluorescent compound by metabolically active cells after incubation with the toxin. Only viable cells with intact enzymatic activity were able to catalyse this conversion; the resulting fluorescence intensity was directly proportional to the number of viable cells.

2.5.1 Protocol

The AquaBluer Cell viability assay was done in a similar manner as the uptake saturation assay. HEK293 cells were transfected with either only the hDAT and an

empty vector (1:0) or with the hDAT and WT-ASYN in a ratio 1:3. The transfected cells were then seeded in a 96-well plate with 0.018 Mio cells per well. On the following day, solutions with Parkinsonian toxicants were prepared: For one plate, the neurotoxin MPP^+ (Sigma-Aldrich, D048-1G) was dissolved in water and then diluted in DMEM to get 6 different concentrations, for the other plate, rotenone, (Sigma-Aldrich, #8875), a mitochondrial complex I inhibitor was first dissolved in dimethyl sulfoxide (DMSO) and then diluted in DMEM at different concentrations. For the exact concentrations see **Table 3, Table 4** and **Table 5**. The cells were then incubated either with MQ water (positive control), with normal growth media (negative control) or with six different concentrations of neurotoxicants. Another row without cells was incubated with water or DMSO to detect the background signal (see **Figure 17**). After a 72h incubation time, media was removed and AquaBluer Reagent in a dilution ratio of 1:100 in DMEM was added to each well. The well plates were covered with aluminium foil and then put into the incubator for 4 hours. After that, the well plates were analysed by Perkin Elmer VICTOR3V Multilabel Plate Reader to measure the relative fluorescence units (RFU) at 540 excitation/590 emission (see **Figure 16**). The measurements were then analysed as described in **Chapter 2.6.**

Table 3 *Overview of MPP+ conditions. Concentrations were adapted after failing to calculate the IC50.*

Label	End concentration (C2)	Concentration of stock (C1)	Amounts added [µL]
1	1 µM	1 mM	1.5
2	3 µM	1 mM	4.5
3	10 µM	10 mM	1.5
4	30 µM	10 mM	4.5
5	100 µM	100 mM	1.5
6	300 µM	100 mM	4.5
Negative	DMEM media		200 µL
Positive	100% H_20		200µL
Background	100% H_20		200µL

Table 4 *Overview of MPP+ conditions after adaptions.*

Label	End concentration (C2)	Concentration of stock (C1)	Amounts added [µL]
1	3 µM	1 mM	4.5
2	10 µM	10 mM	1.5
3	30 µM	10 mM	4.5
4	100 µM	100 mM	1.5
5	300 µM	100 mM	4.5
6	1 mM	100 mM	15
Negative	DMEM media		200 µL
Positive	100% H_20		200µL
Background	100% H_20		200µL

Table 5 *Overview of rotenone conditions for the AquaBluer Assay.*

Label	End concentration (C2)	Concentration of stock (C1)	Amounts added [µL]
1	1 nM	1 µM	1.5
2	10 nM	10 µM	1.5
3	100 nM	100 µM	1.5
4	1 µM	1 mM	1.5
5	10 µM	10 mM	1.5
6	30 µM	10 mM	4.5
Negative	DMEM with ≤ 1% DMSO		200 µL
Positive	100% H_20		200 µL
Background	100% DMSO		200 µL

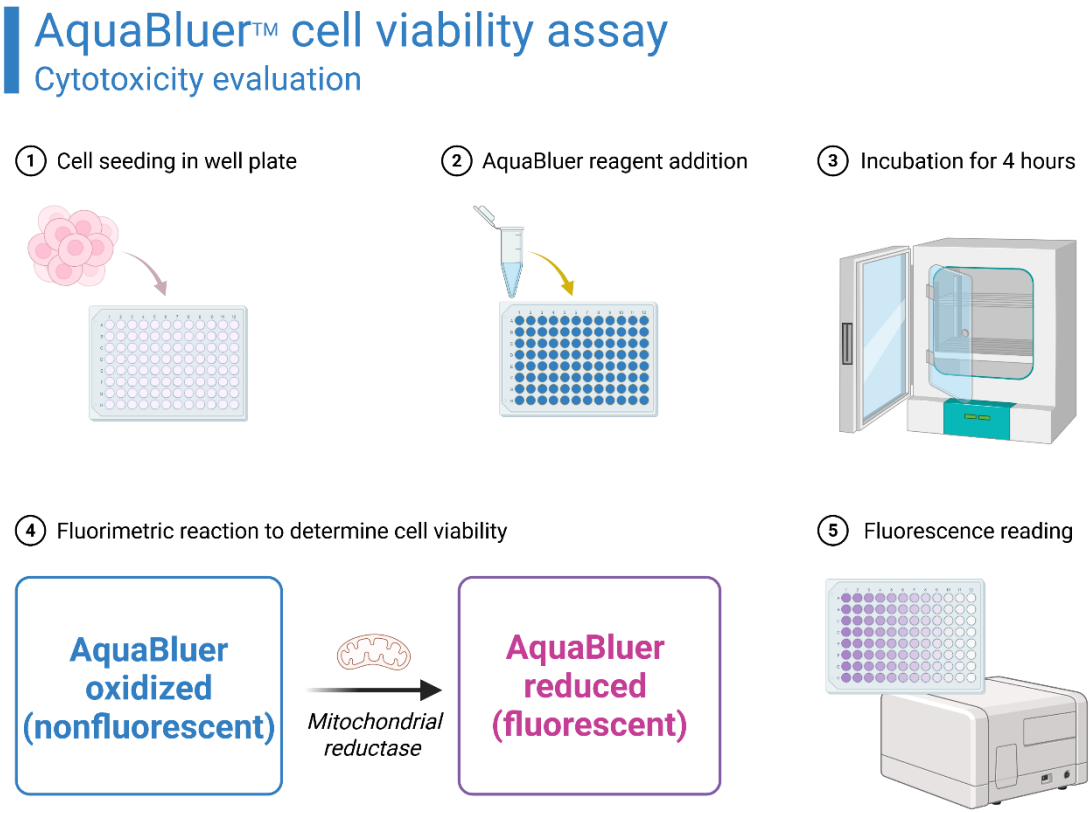

Figure 16 *Schematic illustration of the workflow for the AquaBluer cell viability assay. The non-fluorescent AquaBluer reagent gets reduced by the mitochondrial reductase of viable cells into a fluorescent product. The subsequent RFUs are proportional to the number of viable cells.*

Since the first few experiments with MPP+ have not led to more than 40 % cell loss at the highest concentration used, the protocol was adapted: the incubation time

was extended to 72 hours and the highest concentration was increased from 300 µM to 1mM (see **Table 4**).

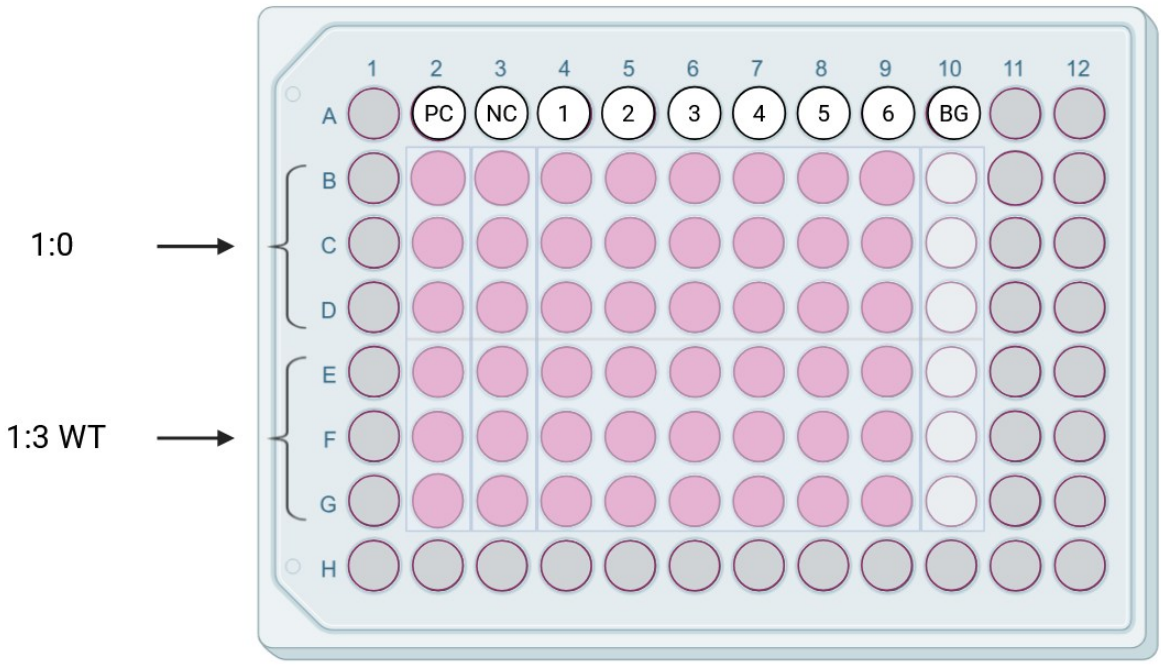

Figure 17 *Schematic illustration of the seeded 96-well plate for the AquaBluer assay. 48 wells were seeded with the 1:0 conditions and the other 48 wells with the 1:3 WT-ASYN condition. Column 2 was treated with water (positive control), column 3 was not treated (negative control) and the columns 4-9 were treated with increasing concentration of the toxin (see* ***Table 3, Table 4*** *and* ***Table 5****). Column 10 was not seeded with cells and just treated with water or DMSO. Image created with BioRender.*

2.6 Data Analysis

For the analysis of uptake assays, scintillation counts per minute (cpm) were first corrected by subtracting background signal (non-specific uptake). The resulting values were then multiplied by a concentration factor, calculated as the ratio of total substrate concentration to the radiolabelled substrate concentration. These adjusted counts were further normalized by dividing with the product of cell number, incubation time, and the total activity of the reaction. Final uptake values were expressed as pmol of [^{3}H]-substrate per million cells per minute. Calculations were performed using Microsoft Excel. Nonlinear regression analysis was conducted in GraphPad Prism by fitting the Michaelis–Menten equation to the data to determine kinetic parameters K_m and V_{max}. Statistical comparisons were made using a one-way ANOVA followed by Dunnett's and/or Tukey's multiple comparisons test with a significance level $p < 0.05$.

Western blot images were quantified using ImageJ by measuring the intensity of protein bands. GAPDH served as a loading control, and target protein signals were

normalized against GAPDH. Quantification was performed in Excel by calculating the ratio of net intensity of the protein of interest to the net intensity of the loading control. Standard deviation and standard error of mean were also calculated in Excel. Statistical analysis was performed using one-way ANOVA with Dunnett's post hoc test ($p < 0.05$) in GraphPad Prism if data showed a normal distribution. If the data did not show normal distribution, Kruska-Wallis test with Dunn's multiple comparison test were performed ($p < 0.05$) in Prism.

For the AquaBluer Toxicity Assay, at first all the RFU values were subtracted by the average RFU from the background wells. The cell viability was calculated by dividing RFU from the test substances (RFU_{test}) by the RFU from the negative control wells ($RFU_{vehicle}$) ($100*RFU_{test}/RFU_{vehicle}$). Following that, the viability values and corresponding log test compound concentration were entered into non-linear regression program of GraphPad Prism (Four Parameter Model) to obtain IC_{50} values and a dose-response curve. Statistical analysis was performed using two-tailed, unpaired student's t-test ($p < 0.05$) and a two-way ANOVA with uncorrected Fisher's LSD ($p < 0.05$) in GraphPad Prism.

3 Results

3.1 Aim of the thesis

The small protein ASYN is a key player in PD pathogenesis and a main component of Lewy pathology. The aim of the thesis was to get cellular insight into how ASYN-modulation of monoamine transporters may relate to selective vulnerability in PD. Previous studies have shown that ASYN can modulate monoamine transporters, but the effects were inconsistent and hence remain unclear. Oaks et al and Wersinger et al for example have shown that ASYN decreased the cell surface expression of monoamine transporters such as DAT, NET (noradrenaline transporter) and SERT (Wersinger, Jeannotte, et al. 2006; Oaks and Sidhu 2011), whereas Lee et al. have found that overexpressed ASYN leads to DAT clustering at the plasma membrane (Lee et al. 2001). In addition, Threlfell et al have demonstrated in an ASYN-overexpressed mouse model, that there was a higher DAT surface availability and function (but no change in total DAT) in the striatum (Threlfell et al. 2021). The goal of my thesis was to investigate how wildtype and A53T ASYN modulate the function and expression of monoamine transporters, particularly DAT and SERT, in cellular models. Using uptake assays in combination with immunoblotting and the AquaBluer™ cell viability assay, this thesis aimed to link transporter kinetics, expression levels, and potential cytotoxicity to better understand ASYN's contribution to dopaminergic neurodegeneration in Parkinson's disease.

3.2 Cellular Assays

My first experiments investigated the effects of overexpressed ASYN on monoamine transporter function (i.e. uptake activity) and on cell viability. To determine Michaelis-Menten kinetics for DAT and SERT in the presence or absence of ASYN, WT-ASYN or A53T-ASYN were overexpressed in CAD and HEK293 cell lines together with the respective transporters (DAT or SERT). The measured counts per minute (cpm) were normalised into picomole [^{3}H]-radioligand per million cell per minute (pmol/mio cell/min). The purpose of the uptake saturation assay was to find out if ASYN can potentially modulate the maximal transporting velocity (V_{max}) and the concentration

of half-maximal velocity (Michaelis-Menten constant, K_m) of monoamine transporters (SERT and DAT).

Interestingly, I noted, that cell numbers were lower in ASYN and A53T transfected cells. So I decided to further investigate this systematically using a specific cell viability assay called AquaBluer assay.

3.2.1 CAD cells - Does ASYN affect SERT function in CAD cells?

3.2.1.1 Uptake Saturation Assay with Western Blots

To determine whether ASYN modulates serotonin transporter function in CAD cells, I first conducted uptake saturation assays with [^{3}H]5HT. I found that overexpressed WT and mutant ASYN increased the V_{max} of SERT, especially in the A53T condition. In addition, I found that the K_m was higher in the WT condition compared to the control, but I did not see a significant change in the A53T condition compared to the control (see **Figure 18, Table 6** and **Table 7 (Appendix))**. I observed a statistically significant difference only between the K_m of the control and WT ASYN condition ($p = 0.0459^*$ and 0.0233^*), while other comparisons of V_{max} and K_m did not reach significance (see **Figure 18B-E)**. This is probably related to variability, which probably derives from different transfection efficiencies of each experiment replicate. Additionally, another reason for missing statistical significance could be that I was underpowered; I would have needed a number of uptake assay replicates of at least 4 to 5.

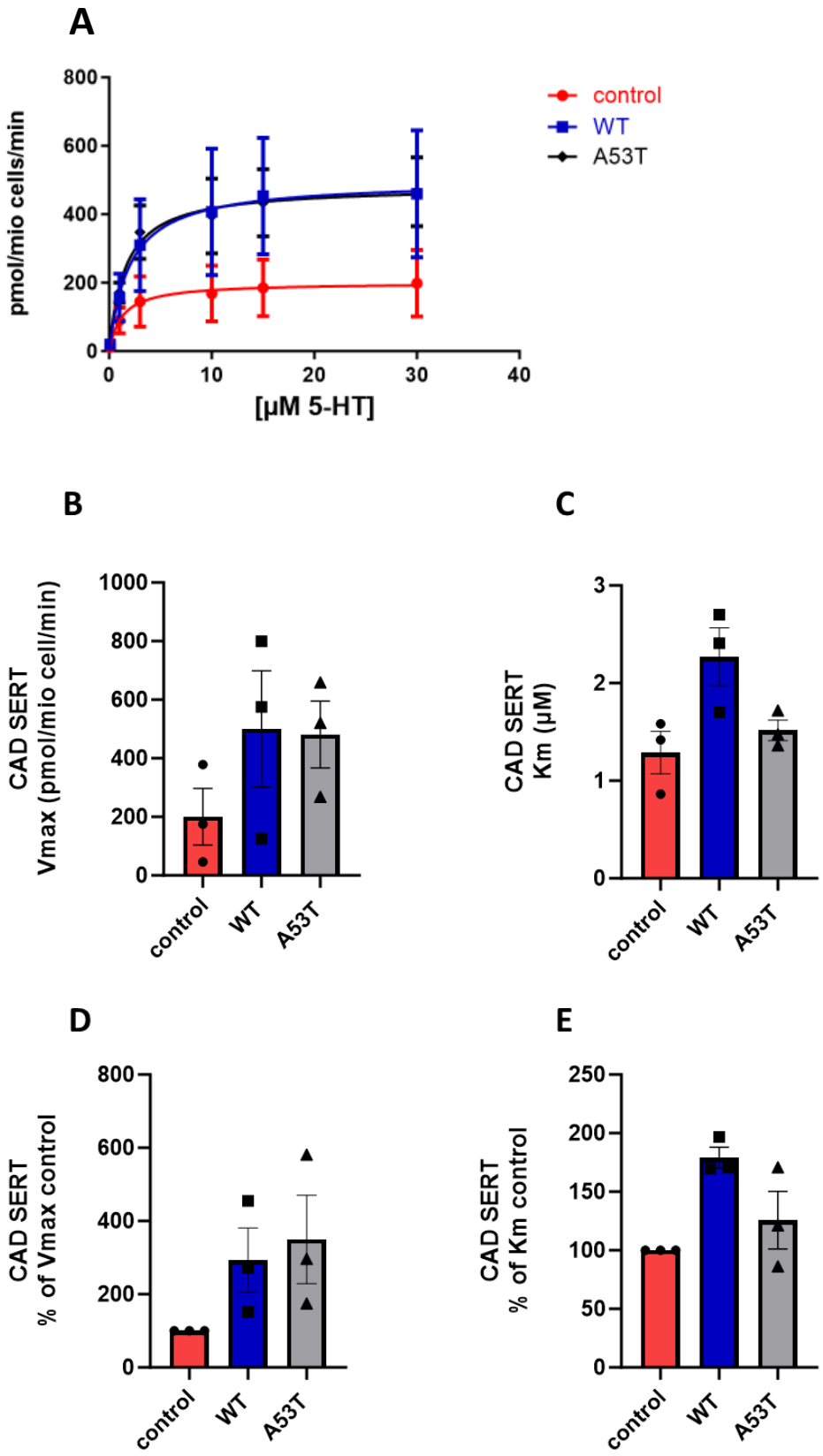

Figure 18 *[³H]5-HT uptake in CAD-SERT cells. Error bars represent mean ± SEM (n=3).* ***(A)*** *Kinetic Analysis of [³H]5-HT uptake in CAD-SERT cells.* ***(B, C)*** *Comparison of the absolute V_{max} and K_m values.* ***(D, E)*** *Comparison of V_{max} and K_m values normalised to the control condition. Statistically significant differences were observed between K_m of control and WT (one-way ANOVA and Dunnett's multiple comparison test, p-values see* ***Error! Reference source not found.****).*

Furthermore, to test whether the increase of V_{max} and K_m was due to changes in protein expression, I next analyzed SERT levels by Western blot and subsequent densitometric quantification (see **Figure 19** as well as Error! Reference source not found. and **Table 9** (**Appendix**)). Both WT and A53T conditions showed increased SERT expression relative to control (**Figure 19A**), consistent with the uptake data. I observed that the total amount of SERT as well as the core glycosylated and mature glycosylated forms of SERT were increased compared to the control, even though without statistical significance (see **Figure 19C, D, E, G, H and I**). Again, this is probably due to being underpowered. “Core” and “mature” refer to immature ER glycosylation (core) and fully processed Golgi glycosylation (mature) of SERT.

I also observed that there was statistically significantly more ASYN (p=0.0458*) in the A53T condition compared to the control condition, which is to be expected when you conduct overexpression via transfection. There is also more in the WT condition, even though it did not reach significance (see **Figure 19A, B, F**). Interestingly, I also found that there was more A53T- ASYN than WT-ASYN in the respective transfected cells, even though the same amounts of plasmid was transfected for both conditions (see **Figure 19B, F**).

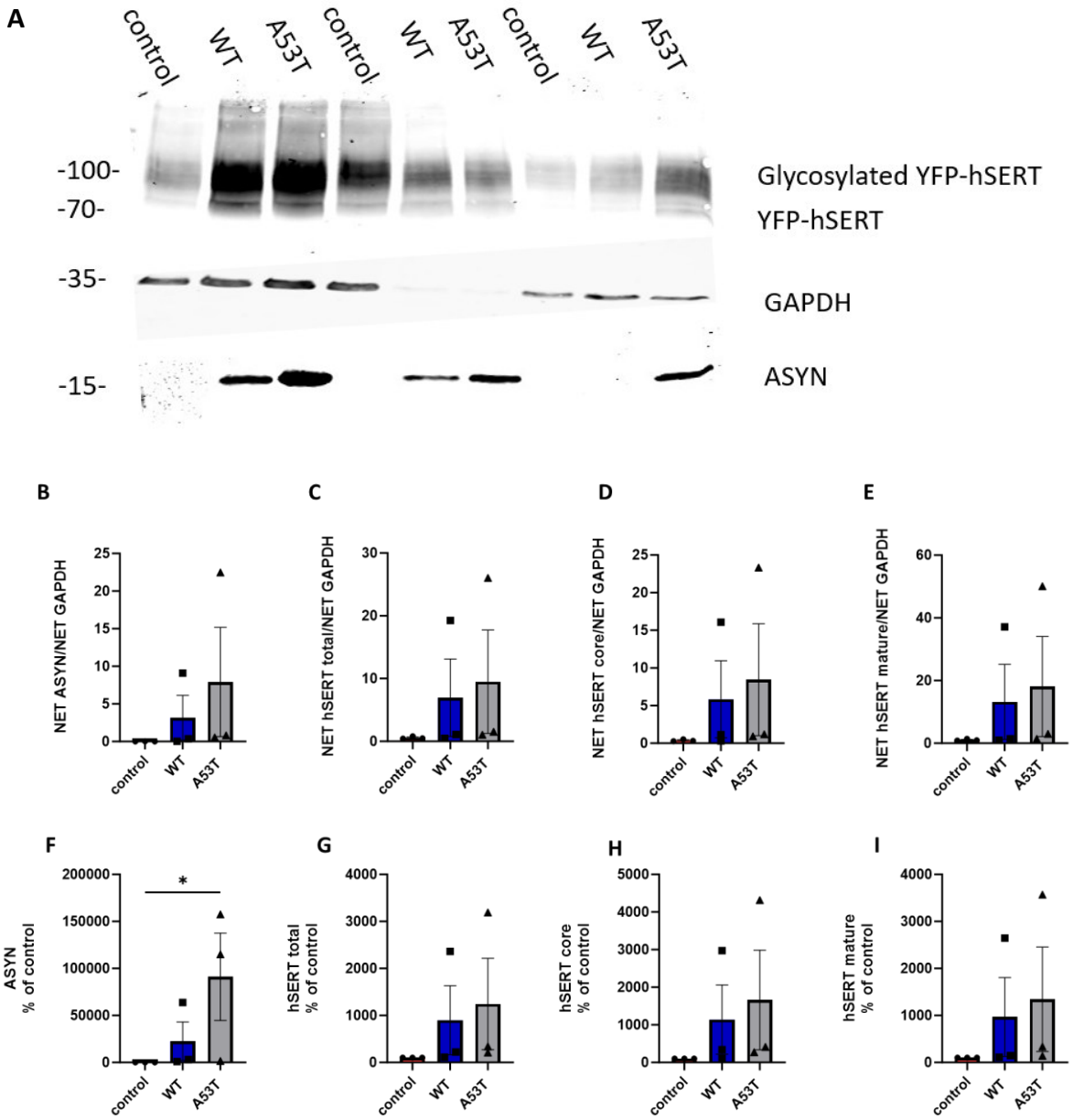

Figure 19 *Western Blot image* ***(A)*** *and densitometric quantification of the images of ASYN and SERT from transfected CAD cells for the [³H]5-HT SERT uptakes. Error bars represent mean ± SEM (n=3).* ***(B)*** *Y-axis represents the ratio of quantified net ASYN and the net loading control (GAPDH).* ***(F)*** *Y-axis shows the amount of protein relative to the control condition.* ***(B, C, D, E)*** *Y-axis represents the ratio of quantified net Protein and the net loading control (GAPDH).* ***(F, G, H, I)*** *Y-axis shows the amount of protein relative to the control condition. The statistical analysis used was Kruska-Wallis test with Dunn's multiple comparison test (p-values see* ***Table 9****).*

However, I also noticed that cell counts during uptake experiments were consistently lower in the ASYN conditions (see **Figure 20**). Cell counts showed a clear trend of being lower with the WT (p=0.0120*) and mutant (p=0.0128*) ASYN conditions. This suggested a possible effect on cell viability, which I therefore examined systematically using a viability assay in HEK cells (see **3.2.2.2** Introduction**AquaBluer Cell Viability Assay**).

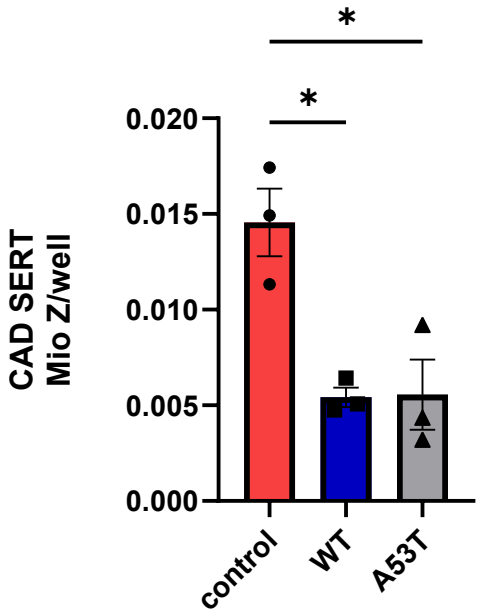

Figure 20 *Cell counts expressed as Million cells/well of CAD-SERT cultures used in uptake assays. Cells were manually counted using a haemocytometer to normalize the measured cpm: only SERT (control), WT ASYN, and A53T ASYN transfected cells. Data are presented as mean ± SEM (n = 3). Statistically significant differences were observed between control and WT (p=0.0120) as well as control and A53T (p=0.0128, one-way ANOVA).*

3.2.2 HEK293 cells - Is the effect of ASYN on SERT conserved in HEK cells?

3.2.2.1 Uptake Saturation Assay with Western Blots

3.2.2.1.1 SERT

To test whether the effects of ASYN on transporter function observed in CAD-SERT cells are conserved in HEK cells, I next performed uptake saturation assays in HEK-SERT cells with [^{3}H]5HT. Similar to the CAD SERT cells, I observed that HEK SERT cells with overexpressed WT and mutant ASYN showcase higher V_{max} of SERT. In contrast to the CAD cells, I did not see a difference of the K_m when comparing the control and WT condition. However, the A53T condition showed a higher K_m compared to the control. I also observed that the A53T condition had a higher V_{max} and K_m than the control and WT condition, although I found no statistical significance in the comparisons of the V_{max} and K_m, not even in the cell counts (see **Figure 21, Table 10** and Error! Reference source not found. **(Appendix)**). Once again, this could be due to variable transfection efficiency and due to being underpowered.

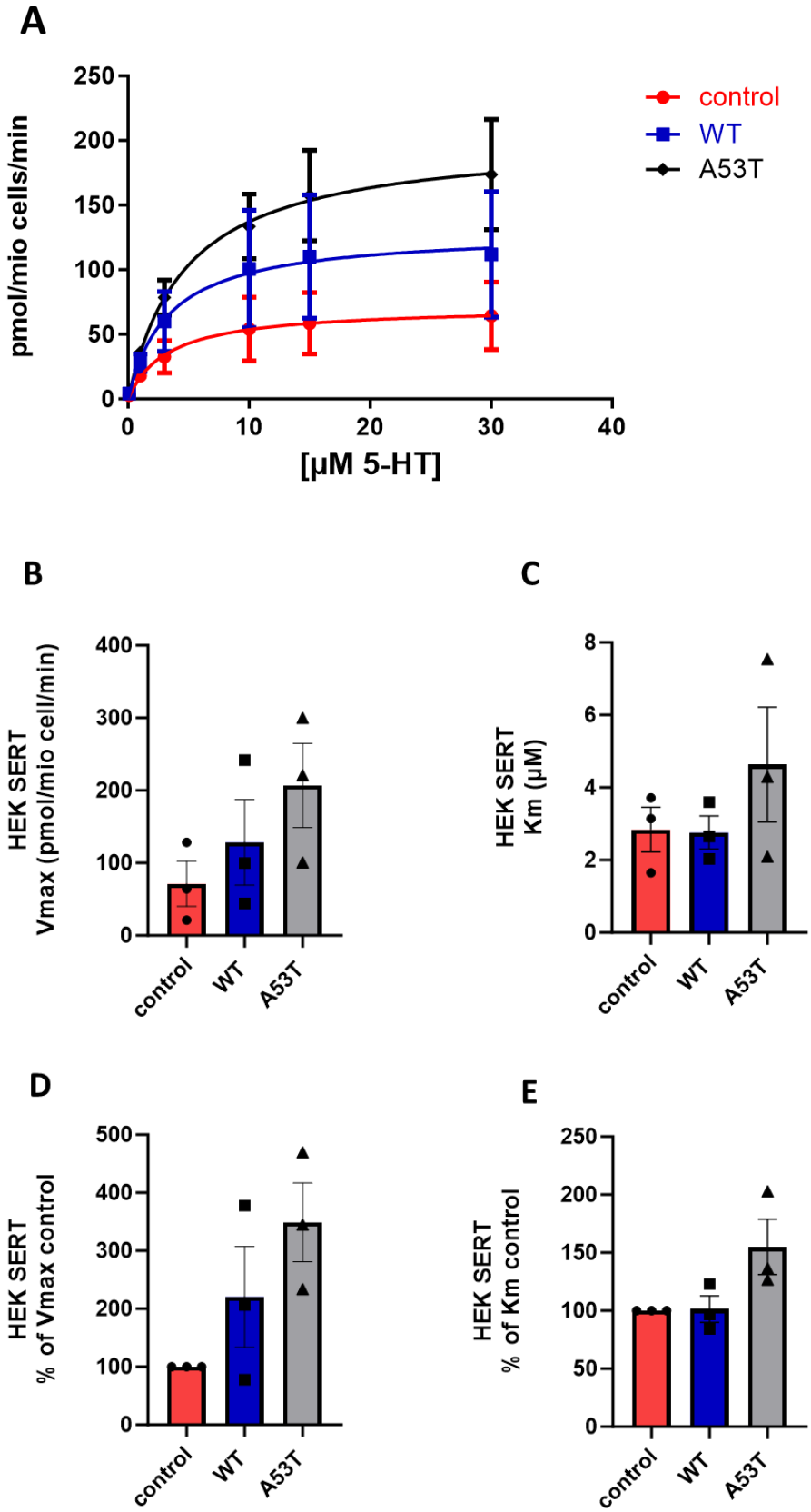

Figure 21 *[³H]5-HT uptake in HEK-SERT cells. Error bars represent mean ± SEM (n=3).* ***(A)*** *Kinetic Analysis of [³H]5-HT uptake in HEK-SERT cells.* ***(B, C)*** *Comparison of the absolute Vmax and Km values.* ***(D, E)*** *Comparison of Vmax and Km values normalised to the control condition. No statistically significant differences were observed (one-way ANOVA and Tukey's multiple comparison test).*

I performed a Western blot analysis to determine whether the uptake results reflect in the expression levels of SERT. And indeed, similar to CAD SERT cells, the total amount of protein as well as the core glycosylated and mature glycosylated forms of SERT were increased in the WT ASYN and especially in the A53T ASYN conditions (see **Figure 22A, C, D, E, G, H, I,** Error! Reference source not found. and Error! Reference source not found. **(Appendix)**). Thus, while ASYN clearly increases SERT expression in HEK cells, these changes were not reflected in uptake kinetics with statistical significance. Again “core” and “mature” refer to immature ER glycosylation (core) and fully processed Golgi glycosylation (mature) of SERT.

I also observed that there was statistically significantly more ASYN in the A53T condition compared to the control condition as well as statistically significantly less ASYN in the WT condition compared to the control and the A53T condition (see **Figure 22B, F**, Error! Reference source not found. and Error! Reference source not found. **(Appendix)**), which reflects the problem I had with detecting ASYN in HEK cells via Western Blot analysis (see **4 Discussion**).

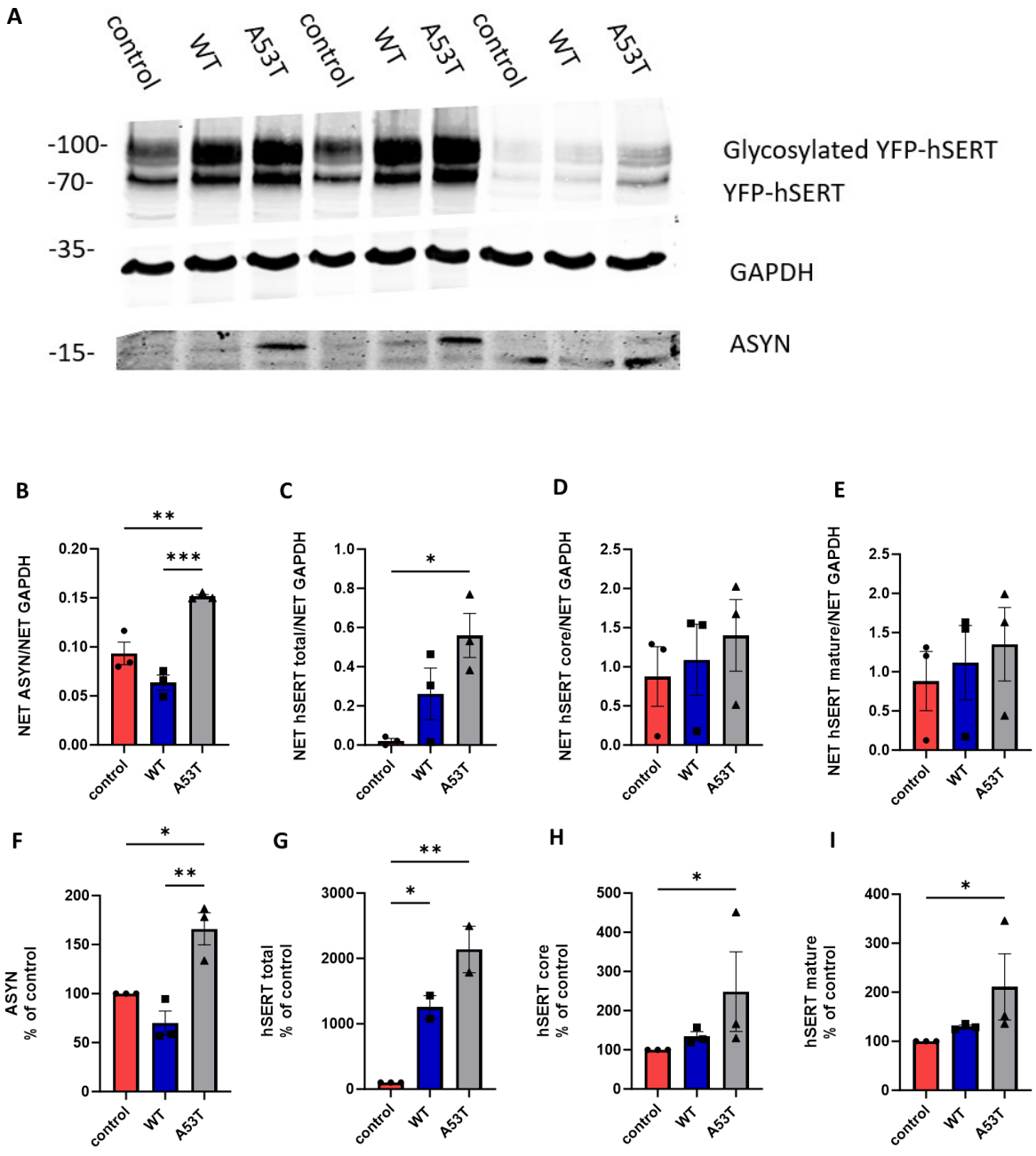

Figure 22 *Western Blot image* ***(A)*** *and densitometric quantification of the images of ASYN and SERT from transfected HEK cells for the [³H]5-HT SERT uptakes. Error bars represent mean ± SEM (n=3).* ***(B, C, D, E)*** *Y-axis represents the ratio of quantified net Protein and the net loading control (GAPDH).* ***(F, G, H, I)*** *Y-axis shows the amount of protein relative to the control condition. The statistical analysis used were one-way ANOVA with Tukey's multiple comparison test for* ***(B, C, D, E, F)*** *and Kruska-Wallis test with Dunn's multiple comparison test for* ***(G, H, I)*** *(p-values see* ***Table 13****).*

I observed once more that the cell counts obtained during the uptake assays appeared lower in ASYN-expressing conditions compared to control (**Figure 23**), although these differences did not reach statistical significance. Nevertheless, this trend raised the possibility that ASYN may influence cell number or viability. I therefore examined this more systematically by conducting the AquaBluer assay in HEK cells (see **3.2.2.2 AquaBluer Cell Viability Assay**).

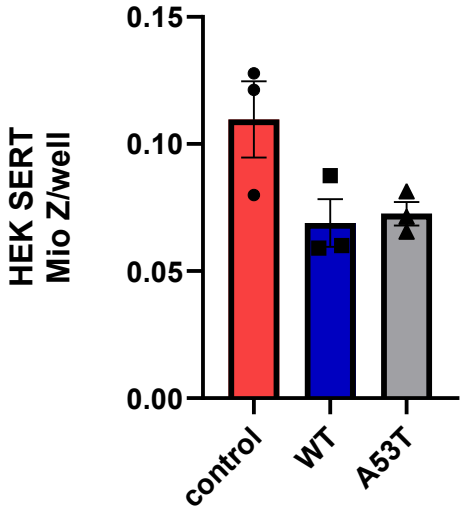

Figure 23 *Cell counts expressed as Million cells/well of HEK-SERT cultures used in uptake assays. Cells were manually counted using a haemocytometer to normalize the measured cpm: only SERT (control), WT ASYN, and A53T ASYN transfected cells. Data are presented as mean ± SEM (n = 3). No statistically significant differences were observed (one-way ANOVA, p > 0.05).*

3.2.2.1.2 DAT - Does ASYN also affect DAT function?

I next investigated whether ASYN also modulates DAT function by conducting [^{3}H]DA uptake saturation assays. Very similar to HEK SERT cells, HEK DAT cells with overexpressed WT and mutant ASYN led to a higher V_{max} of DAT, especially the A53T condition (**Figure 24B, D** and Error! Reference source not found.). I found that the A53T K_m was significantly higher than the K_m of the control and WT condition, while K_m of control and WT condition did not show a difference (**Figure 24C, E** and Error! Reference source not found.). I observed a statistically significant difference between the V_{max} of the control and A53T ASYN condition, while the K_m comparison reached significance after normalisation to the control condition (see Error! Reference source not found. (**Appendix**)). Other comparisons did not reach significance, which could be once again related to variable transfection efficiency and underpowered assays.

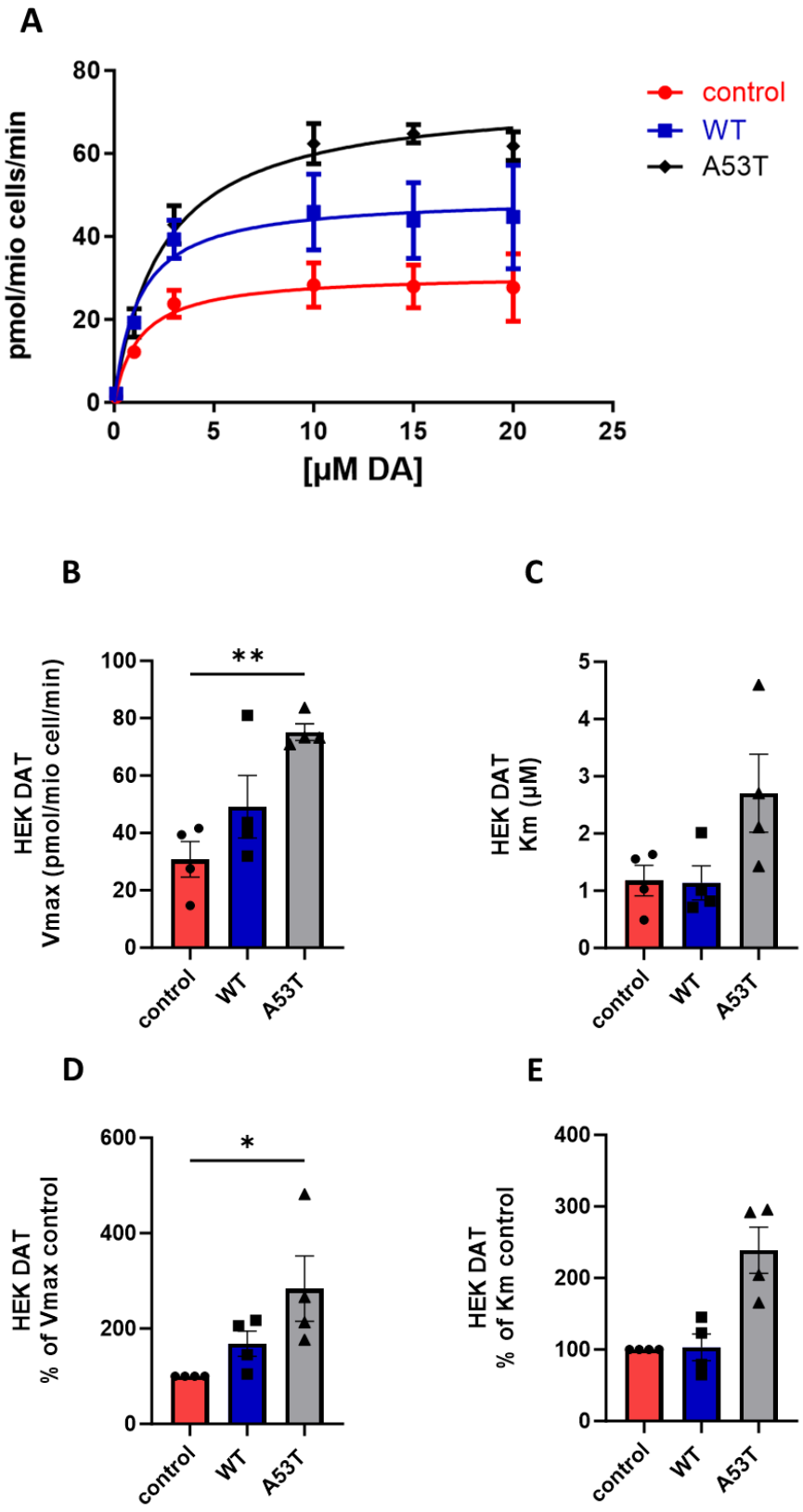

Figure 24 *[³H]DA uptake in HEK-DAT cells.Error bars represent mean ± SEM (n=4).* ***(A)*** *Kinetic Analysis of [³H]DA uptake in HEK-DAT cells.* ***(B, C)*** *Comparison of the absolute V_{max} and K_m values.* ***(D, E)*** *Comparison of V_{max} and K_m values normalised to the control condition. Statistically significant differences were observed between the V_{max} of control and A53T, K_m of control and A53T as well as the K_m of WT and A53T (one-way ANOVA and Tukey's multiple comparison test, p-values see* ***Error! Reference source not found.****).*

To test whether these changes were associated with altered protein levels, I measured DAT expression by Western blot. Similar to the CAD SERT and HEK SERT cells, I found that the total amount of the DAT as well as its core glycosylated and mature glycosylated form were increased in the ASYN conditions, especially in the A53T condition (see **Figure 25A, C, D, E, G, H, I,** Error! Reference source not found. and **Table 17 (Appendix)).** I observed statistical significance in the comparison of the A53T condition to the control condition when it comes to ASYN and DAT levels and also comparing the WT with control when it comes to the total and core glycosylated DAT (see **Figure 25B, C, D, E,** Error! Reference source not found. and **Table 17 (Appendix)**).

Similar to HEK SERT cells, I also observed that there was statistically significantly more ASYN in the A53T condition compared to the control condition as well as significantly less ASYN in the WT condition compared to the control and the A53T condition (see **Figure 25B, F, Table 16 and Table 17 (Appendix))**, which reflects

the problem I had with detecting ASYN in HEK cells via Western Blot analysis (see **4 Discussion**).

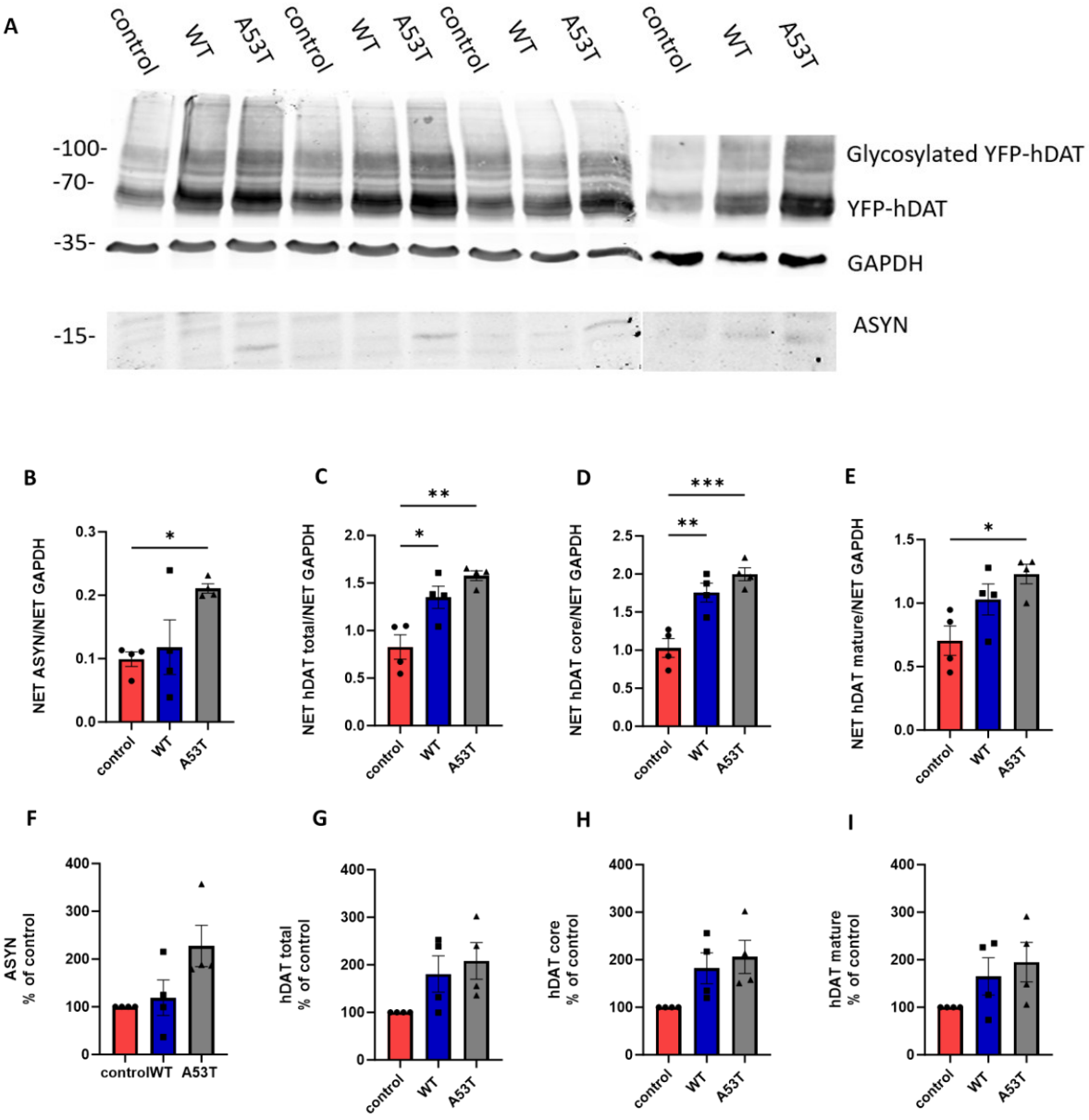

Figure 25 *Western Blot image* ***(A)*** *and densitometric quantification of the image of ASYN and DAT from transfected HEK cells for the [³H]DA DAT uptakes. Error bars represent mean ± SEM (n=4).* ***(B, C, D, E)*** *Y-axis represents the ratio of quantified net hDAT and the net loading control (GAPDH).* ***(F, G, H, I)*** *Y-axis shows the amount of protein relative to the control condition. The statistical analysis used were one-way ANOVA with Tukey's multiple comparison test for* ***(B, C, D, E, F, H)*** *and Kruska-Wallis test with Dunn's multiple comparison test for* ***(G, I)*** *(p values see* ***Table 17****).*

Similar to the experiments described above, I observed that the cell counts obtained during the uptake assays were lower in ASYN-expressing conditions relative to control (see **Figure 26**), with statistical significant differences between control and WT (p=0.0029) as well as control and A53T (p=0.0147) (see **Table 17 (Appendix)**). This observation further cemented the possibility of an effect on cell number or

viability, which I investigated more systematically with the AquaBluer assay (see **3.2.2.2 AquaBluer Cell Viability Assay**).

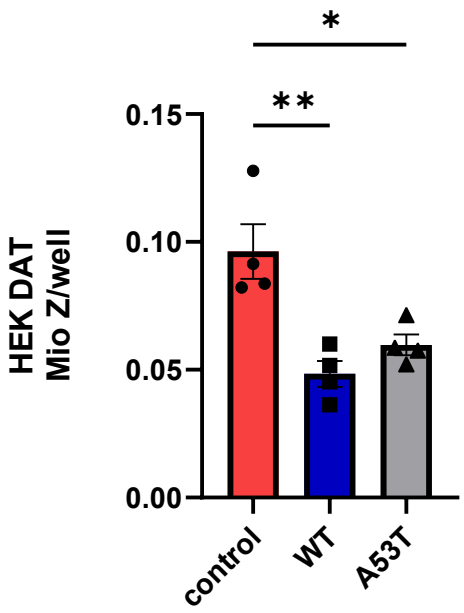

Figure 26 *Cell counts expressed as Million cells/well of HEK-SERT cultures used in uptake assays. Cells were manually counted using a haemocytometer to normalize the measured cpm: only SERT (control), WT ASYN, and A53T ASYN transfected cells. Data are presented as mean ± SEM (n = 4). Statistically significant differences were observed between control and WT (p=0.0029) as well as control and A53T (p=0.0147, one-way ANOVA).*

3.2.2.2 AquaBluer Cell Viability Assay

I conducted the AquaBluer cytotoxicity assay to find out if ASYN can potentially lead to a higher vulnerability by expressing more DAT on the plasma membrane, and as an indirect result, more parkinsonian toxins can enter the cell (such as oxidative stress inducers like dopamine and MPP+). Rotenone as a very lipophilic substance enters the cell via passive diffusion and is therefore independent of DAT transport; it served as a control. I quantified the vulnerability by IC_{50} calculation after making a nonlinear regression curve.

I discovered that the ASYN condition led to lower RFUs in general after treatment with rotenone (see **Figure 27A**). After normalisation to percentages of cell viability (**Figure 27C**), both fitted models appear very similar, but I observed that the IC_{50} of the WT condition was lower (IC_{50} = 293.3 ± 44.3 nM) than the control condition (IC_{50} = 1152.7 ± 549.8 nM) (see **Figure 28A** and **C, Table 18** and **Table 19**). After I normalised the ASYN condition to the control condition control, a statistically significant difference from the IC_{50} of the WT condition to the IC_{50} of the control

condition could be proven (p=0.0014**; unpaired student's t-test, see Error! Reference source not found.).

In contrast to rotenone, I did not see differences between the two conditions after MPP+ treatment, neither the RFUs nor relative viability (**Figure 27B** and **D**). The IC_{50} of the WT condition was slightly lower (IC_{50} = 24.3 ± 3.5 µM) than the control condition (IC_{50} = 25.9 ± 4.7 µM) but not statistically significant (p=0.1459; unpaired student's t-test, see **Error! Reference source not found.**) (**Figure 28B** and **D, Table 18** and **Table 19**).

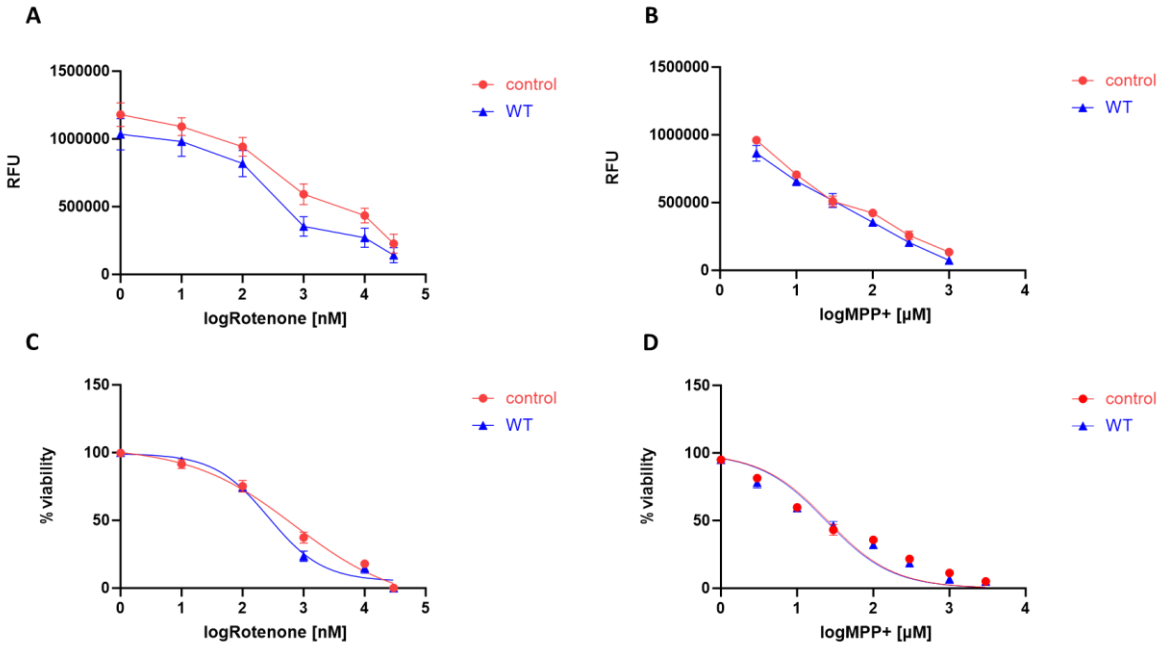

Figure 27 *AquaBluer cell viability assay, comparing the different vulnerability of two conditions (control and WT ASYN) to two parkinsonian toxins (rotenone, MPP+).* ***(A, C)*** *Cell viability after incubation of rotenone, expressed as absolute values (RFU, A) and as percentages (% viability, C) (n=6, mean ± SEM).* ***(B, D)*** *Cell viability after incubation of MPP+, expressed as absolute values* ***(RFU, A)*** *and as percentages* ***(% viability, C)*** *(n=3, mean ± SEM). Figures C and D show a fitted model after non-linear regression done in GraphPad Prism.*

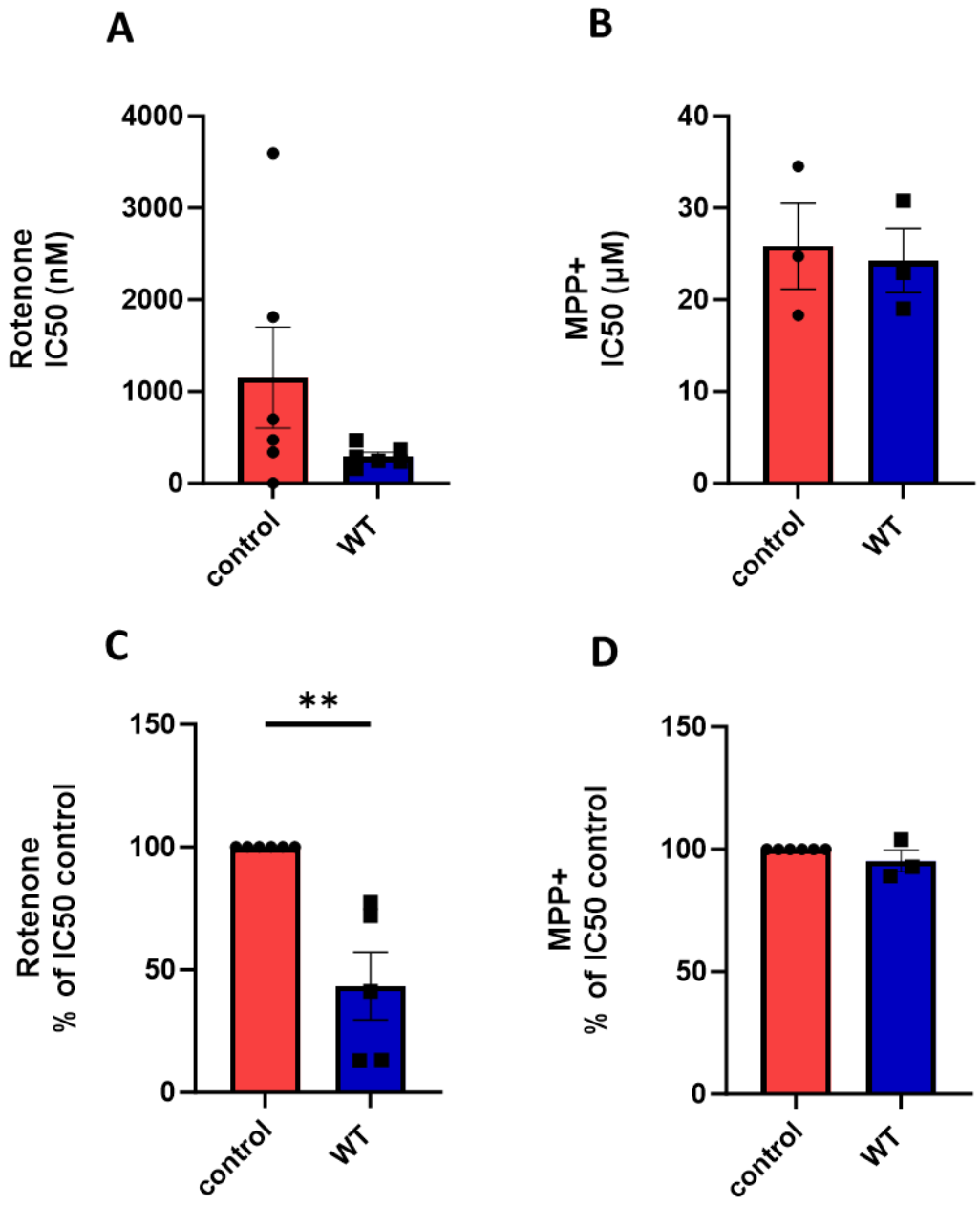

Figure 28 *Comparison of IC50 of the AquaBluer Cell viability assays.* ***(A, B)*** *Absolute values of IC50 from rotenone* ***(A)*** *and MPP+* ***(B)*** *in the control and WT condition.* ***(C, D)*** *IC50 values of WT relative to the control condition for rotenone* ***(C)*** *and MPP+* ***(D)****. Error bars represent mean ± SEM (n=6 for A, C; n=3 for B, D). Statistical analysis was done via unpaired, two-tailed Student's t-test (p=0.0014).*

To test whether cell death was caused by the toxin or by excessive cell growth after long incubation time, I compared the RFUs of the negative control with several different conditions. I observed that RFUs of the negative control were lower than RFUs of the first concentration of the control condition in the rotenone AquaBluer assays, which suggests that the cells died more from overgrowth after the incubation than with the lowest concentration of rotenone. There also were statistically lower RFU measured in the WT NC condition compared to the control 1. concentration

condition (see **Figure 29A**). In contrast, in the MPP+ AquaBluer assays I observed that the “1. concentration” condition had statistically lower RFUs than the NC condition (see **Figure 29B**). Furthermore, I was interested to see if the negative control that received DMEM with added DMSO had more cell death, but I found no statistical difference between the NC with or without DMSO (see **Figure 29C**). Next, I was interested to see if the NC was different after variable incubation times, and indeed I observed a statistical difference between the incubation time of 24h and the incubation times 48h and 72h, but not when 48h is compared to 72h (see **Figure 29D**, numerical values and p-values see **Table 20** and **Table 21**).

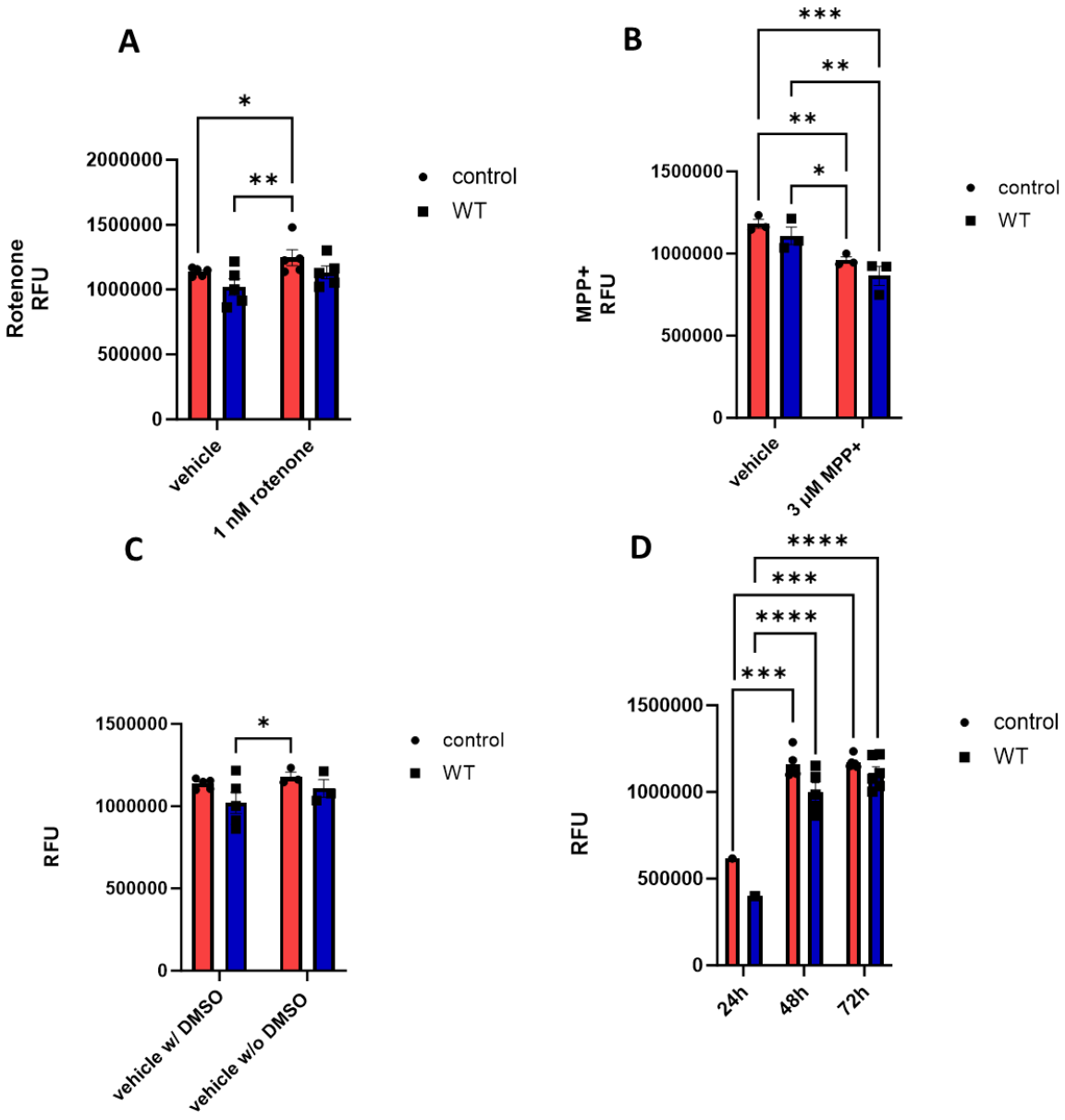

Figure 29 *Comparison of the RFUs of the NC with different conditions. Error bars represent mean ± SEM* ***(A)*** *Comparison of the RFUs from the NC with the RFUs from the 1. Concentration with rotenone as toxin (n=6)* ***(B)*** *Comparison of the RFUs from the NC with the RFUs from the 1. Concentration with MPP+ as toxin (n=3)* ***(C)*** *Comparison of the RFUs from the NC incubated with DMEM <0.1% DMSO (rotenone) and NC incubated with DMEM without any DMSO (MPP+).* ***(D)*** *Comparison of the RFUs from the NC with different incubation times (24h, 48h and 72h) during the rotenone AquaBluer assay. A two-way ANOVA with uncorrected Fisher's LSD was used for the statistical analysis (p-values see* ***Error! Reference source not found.****)*

4 Discussion

In this thesis, I explored the effects of WT-ASYN and A53T mutant ASYN on monoamine transporters, SERT and DAT. Even though SERT's role in the pathogenesis and progression of PD is rather small, the effects of ASYN on the SERT underline the lack of knowledge about the physiological and pathophysiological functions of ASYN. Early-stage PD patients report preserved SERT activity; serotonergic neurons (especially from the raphe nuclei) can compensate nigrostriatal dopamine loss by converting L-DOPA into dopamine (Pagano et al. 2018; Muñoz et al. 2020) and releasing it. SERT, which controls 5-HT uptake, could potentially indirectly modulate this process, but the exact influence is poorly understood (Strecker et al. 2011).

In my uptake saturation assays I continuously observed higher [^{3}H]5-HT uptake in HEK and CAD cells co-transfected with SERT and WT- or A53T- ASYN than in control (expressing only endogenous levels of ASYN) SERT transfected cells. This trend was supported by immunoblot experiments where I observed higher SERT protein expression in the ASYN conditions. The high variability, even after normalisation, is probably due to multiple factors related to the uptake assay: the transfection efficiency can vary depending on cell confluency, cell line passage number, different batches of [^{3}H]5HT, or differences in ambient temperature. In addition, even small differences in cell counts after uptake may explain some of the variability because this is what I normalize the uptake to in the end. As shown by previous work from the lab, there is a strong trend supporting that higher ASYN promotes uptake via SERT, possibly through effects on transporter trafficking to the plasma membrane. Additional replicates of the experiment increase the power and sensitivity of the assay and can potentially decrease some of the variability observed. Interestingly, in experiments with CAD cells there was also a statistically significant increase of the K_m in the WT condition ($p=0.0459$) implying a decrease of substrate affinity when overexpressed WT-ASYN is present. WT-ASYN could potentially change the conformation of hSERT so that the affinity to 5-HT decreases, resulting in the need of higher concentration of 5-HT for the same transporting velocity.

When it comes to PD, a higher activity of SERT could lead to higher intracellular 5-HT which is subsequently metabolised by the monoaminoxidase A (MAO-A) into 5-

hydroxyindoleacetaldehyde (5-HIAL) which leads to higher reactive oxygen species (ROS) levels. This in turn can result in oxidative stress, mitochondrial damage, cellular dysfunction and apoptosis, a very important mechanism with relevance to neurodegeneration in PD.

A frequent non-motor symptom of Parkinson's disease is depression, which has been associated with lower synaptic serotonin levels due to degeneration of serotonergic terminals in the raphe nuclei and limbic regions (Politis and Niccolini 2015). Higher uptake via increased SERT in presynaptic terminals after elevated ASYN may therefore link ASYN-modulation of SERT to depression in PD. In HEK cells, there was significantly more SERT expressed in the WT and A53T condition than in the control condition. The higher expression was especially noticeable in the A53T condition. Since both core and mature glycosylated forms were increased in the A53T condition, it likely means that there is overall more SERT expression, which aligns with my uptake findings. For example, if only the core glycosylated SERT would have been increased, it would probably mean that there is an impairment in the trafficking of the transporter, which leads to lower glycosylation and lower density of the transporter at the plasma membrane. If only the mature glycosylated form increased, it would imply that ASYN influences the ER and Golgi directly by increasing the glycosylation and as a result, the amount of surface-resident, mature transporter. Since both forms were higher, ASYN may increase the rate of SERT gene expression in the nucleus, but it could also be possible that ASYN increases both the gene expression and glycosylation of SERT in the ER/Golgi. In CAD cells, the higher expression was also noticeable.

Interestingly, the lab had difficulties detecting ASYN in HEK cells after transfection and subsequent Western Blot; something which was done multiple times before in the lab without any problems. Possible explanations could be that HEK cells, being non-neuronal, may be more prone to α-synuclein aggregation or degradation, especially under high-temperature denaturation. α-synuclein detection was robust in CAD cell lysates prepared at 95 °C. However, the same protocol failed to yield detectable levels in HEK cells. This discrepancy may reflect differences in cellular context, expression levels, and the protein's thermal stability. This could potentially explain the missing statistical significance in the comparison between the control and WT condition. Another possible explanation could be that ASYN, and

monoamine transporters interact with each other bidirectionally: ASYN increases the transporter density on the cell surface which can trigger oxidative stress with higher uptake of dopamine, which in turn can upregulate higher ASYN expression as a cellular stress response. So, more ASYN means more transporter and vice versa. This could also explain why the A53T band in the Western Blot consistently was bigger than the WT band. Another explanation for seeing generally higher uptake in the A53T condition could be that WT-ASYN has a multifaceted regulatory role when it comes to monoamine transporter trafficking to the membrane: If there is too much extracellular monoamines that get taken up by the transporter, WT-ASYN reacts by decreasing the density of the transporter on the membrane; A53T loses this physiological regulatory function and does not recycle the transporter from the plasma membrane, resulting in higher transporter density and uptake.

In DAT-transfected HEK cells, WT- or mutant ASYN promoted higher uptake of [^{3}H]DA than the control condition. Especially the A53T condition yielded a statistically significant increase of the V_{max} compared to the control condition (p=0.0056**), which is in accordance with A53T being a key factor for the pathogenesis of PD. Even though the WT-ASYN condition did not reach significance, similarly to the SERT uptakes, there still was an observable trend where ASYN conditions resulted in a higher V_{max} than the control conditions. Once again, the assay probably was underpowered to detect statistically significant effects of WT-ASYN. Western Blot analysis proved statistically that there were higher expression levels of the DAT in the WT and A53T condition, similar to the SERT-transfected cells.

Similar to SERT, higher DAT density on the plasma membrane results into increased dopamine uptake into the cytosol. Excessive dopamine spontaneously oxidises at physiological pH, which generates reactive metabolites such as dopamine-quinones and ROS, which can result in mitochondrial dysfunction by damaging macromolecules such as proteins and DNA. Monoamine oxidases break dopamine down to 3,4-dihydroxyphenylacetaldehyde (DOPAL), which is highly reactive and cytotoxic; it can promote ASYN aggregation to toxic oligomers (Burke et al. 2008), creating a vicious cycle. Dopaminergic neurons in the SNc are highly active in dopamine metabolism, making them especially vulnerable to DA-induced oxidative damage (Watanabe et al. 2024).

To further explore the higher vulnerability of SNc dopaminergic neurons due to higher ASYN-induced DAT expression, the AquaBluer Toxicity Assay with MPP+ was conducted. The idea was that elevated DAT expression at the plasma membrane facilitates excessive intracellular MPP+ accumulation, thereby inducing oxidative stress and ultimately causing cell death. Since there was no statistical difference observed between the overexpressed ASYN and control condition, neither in the absolute or relative comparison, it is implied that the higher vulnerability probably derives from ASYN oligomerisation rather than its influence in the trafficking of DAT to the plasma membrane. Further cell viability assay should be conducted to explore the effects of the A53T mutant, since in my previous experiments the mutant showed the most statistical differences to the control, especially in the cell counting of the uptake assays. Nevertheless, the normalised comparison of the IC_{50} to the control condition showed a difference when treated with rotenone, implying that ASYN promotes higher vulnerability to parkinsonian toxins, even though probably not due to higher DAT density but related to other pathomechanisms such as the formation of toxic oligomers which can disrupt membranes, cause mitochondrial dysfunction and disrupt protein degradation pathways. Another DAT-independent explanation could be that ASYN inhibits the synaptic exocytosis of dopamine since its influence on synaptic vesicle dynamics, which also leads to higher dopamine concentration in the presynapses and therefore higher oxidative stress. My proposed hypothesis of ASYN-induced neurodegeneration in the SNc is illustrated in **Figure 30**.

When comparing the RFUs of either negative control from the control and WT condition, there was no significant difference found, even though there was continuously lower RFUs detected in the WT condition. An observation which is supported by the lower cell counts in the uptake assays. Even though the effect seemed to be too small to be proven statistically, the trend of lower cell viability could still be seen in the WT condition (see **Figure 27A**). The lack of statistical significance, despite a consistent downward trend in WT viability, likely reflects biological variability and limited power rather than the absence of an effect.

When comparing the negative controls to the first concentration in the AquaBluer assays, it could be seen that the NC in general was lower than the first concentration of rotenone (1 nM), implying that the lowest concentration of rotenone used was

already having an effect on cell viability. There was no difference found in the NC with DMSO and without DMSO confirming that DMSO alone had no effect on cell viability. The assay incubation time was adapted from 24h to 48h and 72h; since there was a difference found between 24h and 48h/72h, the experiment with 24h was excluded in the analysis.

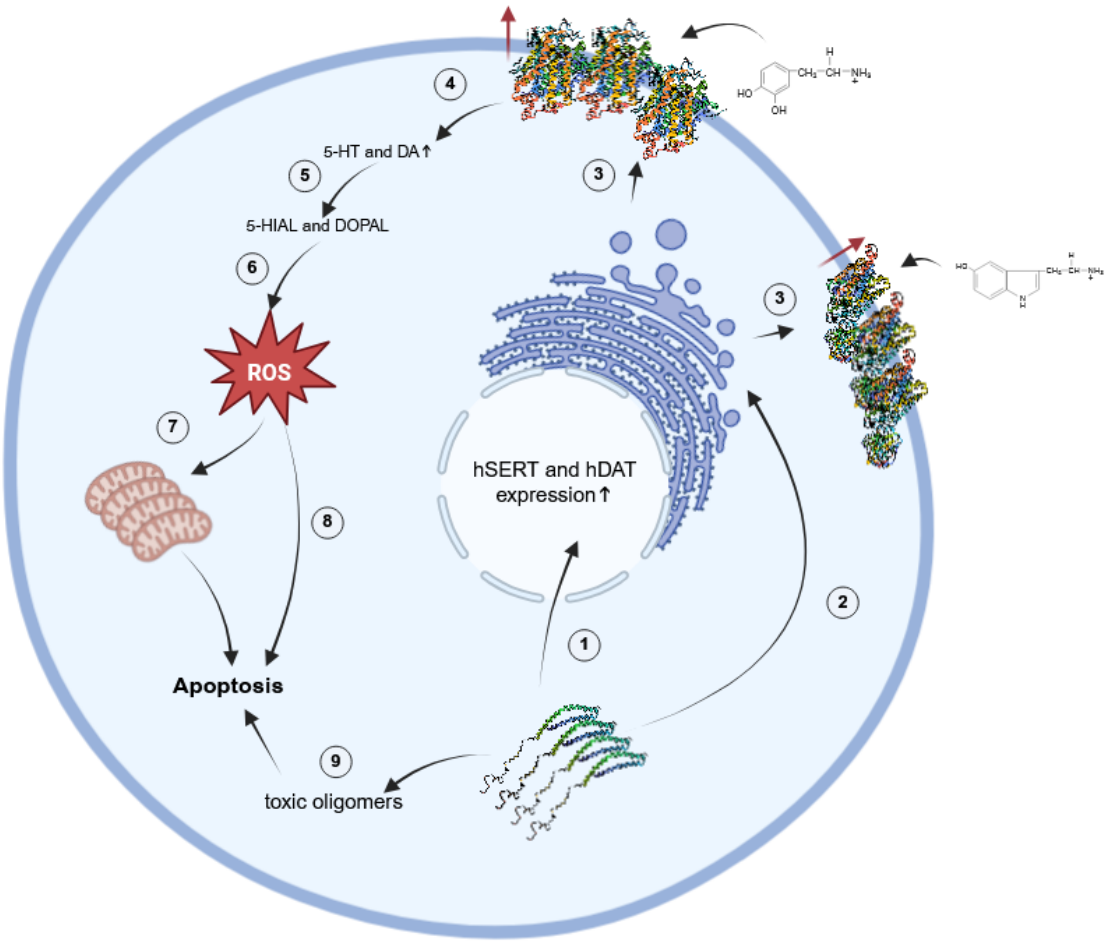

Figure 30 *Hypothesis of the ASYN-induced neurodegeneration in the SNc.* ***(1)*** *Overexpressed WT and A53T ASYN increases the expression rate of the SERT and DAT in the nucleus and* ***(2)*** *increases the transporter glycosylation in the ER and Golgi. As a result* ***(3)****, more transporter protein is transferred to the plasma membrane.* ***(4)*** *The higher intracellular levels of 5-HT and DA due to increased uptake are metabolised by* ***(5)*** *MAO-A/B into* ***(5, 6)*** *ROS-producing metabolites, 5-HIAL and DOPAL. The subsequent mitochondrial damage and/or the ROS directly can lead to cell death. In addition, ASYN can also lead to apoptosis directly by forming toxic oligomers* ***(9)*** *which can disrupt membranes, cause mitochondrial dysfunction* ***(7)*** *and disrupt protein degradation pathways* ***(8)****.*

I obtained several data with my *in vitro* experiments, so the logical implication is to see if the same effect of ASYN on monoamine transporters could be found *in vivo*. The Steinkellner lab plans to further explore that by conducting uptake assays with synaptosomes extracted from ASYN-transduced mice which can be performed cell-type specifically using a novel adeno-associated vector to overexpress ASYN generated in the lab (Garcia Moreno et al. 2024).

There is still a lot to explore about the exact function of ASYN; previous experiments as well as my own have shown that there is high variability associated with ASYN, implying its multifaceted neurobiological functions. For example, ASYN multimerization is necessary for physiological neurotransmitter release, but it could also lead to higher toxicity by forming toxic oligomers. Slight changes in experimental conditions could lead to different regulatory functions of ASYN and therefore different results. By elucidating the physiological and pathophysiological role of ASYN, it could potentially revolutionize how early PD could be diagnosed as well as potentially laying the groundwork for the development of causal therapies instead of only symptomatic therapies for PD.

5 References

Alarcón-Arís, Diana, Ariadna Recasens, Mireia Galofré, et al. 2018. 'Selective α-Synuclein Knockdown in Monoamine Neurons by Intranasal Oligonucleotide Delivery: Potential Therapy for Parkinson's Disease'. *Molecular Therapy* 26 (2): 550–67. https://doi.org/10.1016/j.ymthe.2017.11.015.

Amara, Susan G. 1995. 'Monoamine Transporters: Basic Biology with Clinical Implications'. *The Neuroscientist* 1 (5): 259–67. https://doi.org/10.1177/107385849500100503.

Anderson, John P., Donald E. Walker, Jason M. Goldstein, et al. 2006. 'Phosphorylation of Ser-129 Is the Dominant Pathological Modification of α-Synuclein in Familial and Sporadic Lewy Body Disease'. *Journal of Biological Chemistry* 281 (40): 29739–52. https://doi.org/10.1074/jbc.M600933200.

Araújo, Bruna, Rita Caridade-Silva, Carla Soares-Guedes, et al. 2022. 'Neuroinflammation and Parkinson's Disease—From Neurodegeneration to Therapeutic Opportunities'. *Cells* 11 (18): 2908. https://doi.org/10.3390/cells11182908.

Arawaka, Shigeki, Hiroyasu Sato, Asuka Sasaki, Shingo Koyama, and Takeo Kato. 2017. 'Mechanisms Underlying Extensive Ser129-Phosphorylation in α-Synuclein Aggregates'. *Acta Neuropathologica Communications* 5 (1): 48. https://doi.org/10.1186/s40478-017-0452-6.

Barba, Lorenzo, Federico Paolini Paoletti, Giovanni Bellomo, et al. 2022. 'Alpha and Beta Synucleins: From Pathophysiology to Clinical Application as Biomarkers'. *Movement Disorders* 37 (4): 669–83. https://doi.org/10.1002/mds.28941.

Beitz, Janice M. 2014. 'Parkinson s Disease a Review'. *Frontiers in Bioscience* S6 (1): 65–74. https://doi.org/10.2741/S415.

Bellini, Gabriele, Vanessa D'Antongiovanni, Giovanni Palermo, et al. 2025. 'α-Synuclein in Parkinson's Disease: From Bench to Bedside'. *Medicinal Research Reviews* 45 (3): 909–46. https://doi.org/10.1002/med.22091.

Bellucci, Arianna, Laura Navarria, Elisa Falarti, et al. 2012. 'Correction: Redistribution of DAT/α-Synuclein Complexes Visualized by "In Situ" Proximity Ligation Assay in Transgenic Mice Modelling Early Parkinson's Disease'. *PLoS ONE* 7 (1). https://doi.org/10.1371/annotation/58679d17-c619-4f13-b11f-146dacfe7e92.

Bendor, Jacob T., Todd P. Logan, and Robert H. Edwards. 2013. 'The Function of α-Synuclein'. *Neuron* 79 (6): 1044–66. https://doi.org/10.1016/j.neuron.2013.09.004.

Benskey, Matthew J., Ruth G. Perez, and Fredric P. Manfredsson. 2016. 'The Contribution of Alpha Synuclein to Neuronal Survival and Function – Implications for Parkinson's Disease'. *Journal of Neurochemistry* 137 (3): 331–59. https://doi.org/10.1111/jnc.13570.

Blauwendraat, Cornelis, Mike A Nalls, and Andrew B Singleton. 2020. 'The Genetic Architecture of Parkinson's Disease'. *The Lancet Neurology* 19 (2): 170–78. https://doi.org/10.1016/S1474-4422(19)30287-X.

Braak, Heiko, and Kelly Del Tredici. 2017. 'Neuropathological Staging of Brain Pathology in Sporadic Parkinson's Disease: Separating the Wheat from the Chaff'. *Journal of Parkinson's Disease* 7 (s1): S71–85. https://doi.org/10.3233/JPD-179001.

Brakedal, Brage, Lilah Toker, Kristoffer Haugarvoll, and Charalampos Tzoulis. 2022. 'A Nationwide Study of the Incidence, Prevalence and Mortality of Parkinson's Disease in the Norwegian Population'. *Npj Parkinson's Disease* 8 (1): 19. https://doi.org/10.1038/s41531-022-00280-4.

Brodin, Lennart, Dragomir Milovanovic, Silvio O. Rizzoli, and Oleg Shupliakov. 2022. ‘α-Synuclein in the Synaptic Vesicle Liquid Phase: Active Player or Passive Bystander?’ *Frontiers in Molecular Biosciences* 9 (May): 891508. https://doi.org/10.3389/fmolb.2022.891508.

Burke, William J., Vijaya B. Kumar, Neeraj Pandey, et al. 2008. ‘Aggregation of α-Synuclein by DOPAL, the Monoamine Oxidase Metabolite of Dopamine’. *Acta Neuropathologica* 115 (2): 193–203. https://doi.org/10.1007/s00401-007-0303-9.

Burré, Jacqueline. 2015. ‘The Synaptic Function of α-Synuclein’. *Journal of Parkinson’s Disease* 5 (4): 699–713. https://doi.org/10.3233/JPD-150642.

Burré, Jacqueline, Manu Sharma, and Thomas C. Südhof. 2012. ‘Systematic Mutagenesis of α-Synuclein Reveals Distinct Sequence Requirements for Physiological and Pathological Activities’. *The Journal of Neuroscience* 32 (43): 15227–42. https://doi.org/10.1523/JNEUROSCI.3545-12.2012.

Burré, Jacqueline, Manu Sharma, and Thomas C. Südhof. 2018. ‘Cell Biology and Pathophysiology of α-Synuclein’. *Cold Spring Harbor Perspectives in Medicine* 8 (3): a024091. https://doi.org/10.1101/cshperspect.a024091.

Burré, Jacqueline, Manu Sharma, Theodoros Tsetsenis, Vladimir Buchman, Mark R. Etherton, and Thomas C. Südhof. 2010. ‘Alpha-Synuclein Promotes SNARE-Complex Assembly in Vivo and in Vitro’. *Science (New York, N.Y.)* 329 (5999): 1663–67. https://doi.org/10.1126/science.1195227.

Bussell, Robert, and David Eliezer. 2004. ‘Effects of Parkinson’s Disease-Linked Mutations on the Structure of Lipid-Associated α-Synuclein’. *Biochemistry* 43 (16): 4810–18. https://doi.org/10.1021/bi036135+.

Butler, Brittany, Kaustuv Saha, Tanu Rana, et al. 2015. ‘Dopamine Transporter Activity Is Modulated by α-Synuclein’. *Journal of Biological Chemistry* 290 (49): 29542–54. https://doi.org/10.1074/jbc.M115.691592.

Cevallos, Carlos A., Anna Leigh White, Brooke A. Fazio, et al. 2025. ‘Transcriptomic Analysis of CAD Cell Differentiation’. Preprint, Neuroscience, March 10. https://doi.org/10.1101/2025.03.09.642086.

Chacinska, Agnieszka, Carla M. Koehler, Dusanka Milenkovic, Trevor Lithgow, and Nikolaus Pfanner. 2009. ‘Importing Mitochondrial Proteins: Machineries and Mechanisms’. *Cell* 138 (4): 628–44. https://doi.org/10.1016/j.cell.2009.08.005.

Chandra, Sreeganga, Francesco Fornai, Hyung-Bae Kwon, et al. 2004. ‘Double-Knockout Mice for α- and β-Synucleins: Effect on Synaptic Functions’. *Proceedings of the National Academy of Sciences* 101 (41): 14966–71. https://doi.org/10.1073/pnas.0406283101.

Chandra, Sreeganga, Gilbert Gallardo, Rafael Fernández-Chacón, Oliver M. Schlüter, and Thomas C. Südhof. 2005. ‘α-Synuclein Cooperates with CSPα in Preventing Neurodegeneration’. *Cell* 123 (3): 383–96. https://doi.org/10.1016/j.cell.2005.09.028.

Chang, Diana, Mike A Nalls, Ingileif B Hallgrímsdóttir, et al. 2017. ‘A Meta-Analysis of Genome-Wide Association Studies Identifies 17 New Parkinson’s Disease Risk Loci’. *Nature Genetics* 49 (10): 1511–16. https://doi.org/10.1038/ng.3955.

Chen, Nian-Hang, Maarten E. A. Reith, and Michael W. Quick. 2004. ‘Synaptic Uptake and beyond: The Sodium- and Chloride-Dependent Neurotransmitter Transporter Family SLC6’. *Pfl□gers Archiv European Journal of Physiology* 447 (5): 519–31. https://doi.org/10.1007/s00424-003-1064-5.

Choi, Bong-Kyu, Mal-Gi Choi, Jae-Yeol Kim, et al. 2013. 'Large α-Synuclein Oligomers Inhibit Neuronal SNARE-Mediated Vesicle Docking'. *Proceedings of the National Academy of Sciences of the United States of America* 110 (10): 4087–92. https://doi.org/10.1073/pnas.1218424110.

Colby, D. W., and S. B. Prusiner. 2011. 'Prions'. *Cold Spring Harbor Perspectives in Biology* 3 (1): a006833–a006833. https://doi.org/10.1101/cshperspect.a006833.

Conway, Kelly A., Seung-Jae Lee, Jean-Christophe Rochet, Tomas T. Ding, Robin E. Williamson, and Peter T. Lansbury. 2000. 'Acceleration of Oligomerization, Not Fibrillization, Is a Shared Property of Both α-Synuclein Mutations Linked to Early-Onset Parkinson's Disease: Implications for Pathogenesis and Therapy'. *Proceedings of the National Academy of Sciences* 97 (2): 571–76. https://doi.org/10.1073/pnas.97.2.571.

Cuervo, Ana Maria, Leonidas Stefanis, Ross Fredenburg, Peter T. Lansbury, and David Sulzer. 2004. 'Impaired Degradation of Mutant α-Synuclein by Chaperone-Mediated Autophagy'. *Science* 305 (5688): 1292–95. https://doi.org/10.1126/science.1101738.

Davidson, W. Sean, Ana Jonas, David F. Clayton, and Julia M. George. 1998. 'Stabilization of α-Synuclein Secondary Structure upon Binding to Synthetic Membranes'. *Journal of Biological Chemistry* 273 (16): 9443–49. https://doi.org/10.1074/jbc.273.16.9443.

Di Maio, Roberto, Paul J. Barrett, Eric K. Hoffman, et al. 2016. 'α-Synuclein Binds to TOM20 and Inhibits Mitochondrial Protein Import in Parkinson's Disease'. *Science Translational Medicine* 8 (342). https://doi.org/10.1126/scitranslmed.aaf3634.

Dułak, Dawid, Małgorzata Gadzała, Mateusz Banach, Leszek Konieczny, and Irena Roterman. 2020. 'Alternative Structures of α-Synuclein'. *Molecules* 25 (3): 600. https://doi.org/10.3390/molecules25030600.

Dvorak, Vojtech, Tabea Wiedmer, Alvaro Ingles-Prieto, et al. 2021. 'An Overview of Cell-Based Assay Platforms for the Solute Carrier Family of Transporters'. *Frontiers in Pharmacology* 12 (August): 722889. https://doi.org/10.3389/fphar.2021.722889.

Elmorsy, Ekramy, Ayat Al-Ghafari, Huda Al Doghaither, et al. 2023. 'Differential Effects of Paraquat, Rotenone, and MPTP on Cellular Bioenergetics of Undifferentiated and Differentiated Human Neuroblastoma Cells'. *Brain Sciences* 13 (12): 1717. https://doi.org/10.3390/brainsci13121717.

Emamzadeh, FatemehNouri. 2016. 'Alpha-Synuclein Structure, Functions, and Interactions'. *Journal of Research in Medical Sciences* 21 (1): 29. https://doi.org/10.4103/1735-1995.181989.

Erreger, Kevin, Christof Grewer, Jonathan A. Javitch, and Aurelio Galli. 2008. 'Currents in Response to Rapid Concentration Jumps of Amphetamine Uncover Novel Aspects of Human Dopamine Transporter Function'. *The Journal of Neuroscience* 28 (4): 976–89. https://doi.org/10.1523/JNEUROSCI.2796-07.2008.

Farrell, Kaitlin F., Sesha Krishnamachari, Ernesto Villanueva, et al. 2014. 'Non-motor Parkinsonian Pathology in Aging A53T α-Synuclein Mice Is Associated with Progressive Synucleinopathy and Altered Enzymatic Function'. *Journal of Neurochemistry* 128 (4): 536–46. https://doi.org/10.1111/jnc.12481.

Flagmeier, Patrick, Georg Meisl, Michele Vendruscolo, et al. 2016. 'Mutations Associated with Familial Parkinson's Disease Alter the Initiation and Amplification Steps of α-Synuclein Aggregation'. *Proceedings of the National Academy of Sciences* 113 (37): 10328–33. https://doi.org/10.1073/pnas.1604645113.

Forrest, Lucy R., Yuan-Wei Zhang, Miriam T. Jacobs, et al. 2008. 'Mechanism for Alternating Access in Neurotransmitter Transporters'. *Proceedings of the National Academy of Sciences* 105 (30): 10338–43. https://doi.org/10.1073/pnas.0804659105.

Fortin, Doris L., Matthew D. Troyer, Ken Nakamura, Shin-ichiro Kubo, Malcolm D. Anthony, and Robert H. Edwards. 2004. 'Lipid Rafts Mediate the Synaptic Localization of α-Synuclein'. *The Journal of Neuroscience* 24 (30): 6715–23. https://doi.org/10.1523/JNEUROSCI.1594-04.2004.

Fujiwara, Hideo, Masato Hasegawa, Naoshi Dohmae, et al. 2002. 'α-Synuclein Is Phosphorylated in Synucleinopathy Lesions'. *Nature Cell Biology* 4 (2): 160–64. https://doi.org/10.1038/ncb748.

Gao, Hui-Ming, and Jau-Shyong Hong. 2011. 'Gene–Environment Interactions: Key to Unraveling the Mystery of Parkinson's Disease'. *Progress in Neurobiology* 94 (1): 1–19. https://doi.org/10.1016/j.pneurobio.2011.03.005.

Garcia Moreno, Sofia Ines, Fabian Limani, Iina Ludwig, et al. 2024. 'Viral Overexpression of Human Alpha-Synuclein in Mouse Substantia Nigra Dopamine Neurons Results in Hyperdopaminergia but No Neurodegeneration'. *Experimental Neurology* 382 (December): 114959. https://doi.org/10.1016/j.expneurol.2024.114959.

Giros, B., S. el Mestikawy, N. Godinot, et al. 1992. 'Cloning, Pharmacological Characterization, and Chromosome Assignment of the Human Dopamine Transporter'. *Molecular Pharmacology* 42 (3): 383–90.

Giros, Bruno, and Marc G. Caron. 1993. 'Molecular Characterization of the Dopamine Transporter'. *Trends in Pharmacological Sciences* 14 (2): 43–49. https://doi.org/10.1016/0165-6147(93)90029-J.

Greten-Harrison, Becket, Manuela Polydoro, Megumi Morimoto-Tomita, et al. 2010. 'Aβγ-Synuclein Triple Knockout Mice Reveal Age-Dependent Neuronal Dysfunction'. *Proceedings of the National Academy of Sciences of the United States of America* 107 (45): 19573–78. https://doi.org/10.1073/pnas.1005005107.

Guerrero-Ferreira, Ricardo, Nicholas Mi Taylor, Daniel Mona, et al. 2018. 'Cryo-EM Structure of Alpha-Synuclein Fibrils'. *eLife* 7 (July): e36402. https://doi.org/10.7554/eLife.36402.

Guo, Jun Tang, An Qi Chen, Qi Kong, Hua Zhu, Chun Mei Ma, and Chuan Qin. 2008. 'Inhibition of Vesicular Monoamine Transporter-2 Activity in α-Synuclein Stably Transfected SH-SY5Y Cells'. *Cellular and Molecular Neurobiology* 28 (1): 35–47. https://doi.org/10.1007/s10571-007-9227-0.

Hayes, Michael T. 2019. 'Parkinson's Disease and Parkinsonism'. *The American Journal of Medicine* 132 (7): 802–7. https://doi.org/10.1016/j.amjmed.2019.03.001.

Hellsberg, Eva, Gerhard F. Ecker, Anna Stary-Weinzinger, and Lucy R. Forrest. 2019. 'A Structural Model of the Human Serotonin Transporter in an Outward-Occluded State'. *PLOS ONE* 14 (6): e0217377. https://doi.org/10.1371/journal.pone.0217377.

Huang, Mingzhu, Bianbian Wang, Xiaopeng Li, Chongluo Fu, Changhe Wang, and Xinjiang Kang. 2019. 'α-Synuclein: A Multifunctional Player in Exocytosis, Endocytosis, and Vesicle Recycling'. *Frontiers in Neuroscience* 13 (January): 28. https://doi.org/10.3389/fnins.2019.00028.

International Parkinson's Disease Genomics Consortium (IPDGC), Parkinson's Study Group (PSG) Parkinson's Research: The Organized GENetics Initiative (PROGENI), 23andMe, et al. 2014. 'Large-Scale Meta-Analysis of Genome-Wide Association Data Identifies Six New Risk Loci for Parkinson's Disease'. *Nature Genetics* 46 (9): 989–93. https://doi.org/10.1038/ng.3043.

Jankovic, J. 2008. 'Parkinson's Disease: Clinical Features and Diagnosis'. *Journal of Neurology, Neurosurgery & Psychiatry* 79 (4): 368–76. https://doi.org/10.1136/jnnp.2007.131045.

Javitch, J A, R J D'Amato, S M Strittmatter, and S H Snyder. 1985. 'Parkinsonism-Inducing Neurotoxin, N-Methyl-4-Phenyl-1,2,3,6 -Tetrahydropyridine: Uptake of the Metabolite N-Methyl-4-Phenylpyridine by Dopamine Neurons Explains Selective Toxicity.' *Proceedings of the National Academy of Sciences* 82 (7): 2173–77. https://doi.org/10.1073/pnas.82.7.2173.

Jensen, Poul H., Morten S. Nielsen, Ross Jakes, Carlos G. Dotti, and Michel Goedert. 1998. 'Binding of α-Synuclein to Brain Vesicles Is Abolished by Familial Parkinson's Disease Mutation'. *Journal of Biological Chemistry* 273 (41): 26292–94. https://doi.org/10.1074/jbc.273.41.26292.

Jeschke, Gunnar. 2013. 'A Comparative Study of Structures and Structural Transitions of Secondary Transporters with the LeuT Fold'. *European Biophysics Journal* 42 (2–3): 181–97. https://doi.org/10.1007/s00249-012-0802-z.

Kalia, Lorraine V, and Anthony E Lang. 2015. 'Parkinson's Disease'. *The Lancet* 386 (9996): 896–912. https://doi.org/10.1016/S0140-6736(14)61393-3.

Kim, Changyoun, Dong-Hwan Ho, Ji-Eun Suk, et al. 2013. 'Neuron-Released Oligomeric α-Synuclein Is an Endogenous Agonist of TLR2 for Paracrine Activation of Microglia'. *Nature Communications* 4 (1): 1562. https://doi.org/10.1038/ncomms2534.

Koeglsperger, Thomas, Svenja-Lotta Rumpf, Patricia Schließer, et al. 2023. 'Neuropathology of Incidental Lewy Body & Prodromal Parkinson's Disease'. *Molecular Neurodegeneration* 18 (1): 32. https://doi.org/10.1186/s13024-023-00622-7.

Kristensen, Anders S., Jacob Andersen, Trine N. Jørgensen, et al. 2011. 'SLC6 Neurotransmitter Transporters: Structure, Function, and Regulation'. *Pharmacological Reviews* 63 (3): 585–640. https://doi.org/10.1124/pr.108.000869.

Krüger, Rejko, Wilfried Kuhn, Thomas Müller, et al. 1998. 'AlaSOPro Mutation in the Gene Encoding α-Synuclein in Parkinson's Disease'. *Nature Genetics* 18 (2): 106–8. https://doi.org/10.1038/ng0298-106.

Langston, J. William, Philip Ballard, James W. Tetrud, and Ian Irwin. 1983. 'Chronic Parkinsonism in Humans Due to a Product of Meperidine-Analog Synthesis'. *Science* 219 (4587): 979–80. https://doi.org/10.1126/science.6823561.

Lee, Byung Rho, and Tetsu Kamitani. 2011. 'Improved Immunodetection of Endogenous α-Synuclein'. *PloS One* 6 (8): e23939. https://doi.org/10.1371/journal.pone.0023939.

Lee, Frank J. S., Fang Liu, Zdenek B. Pristupa, and Hyman B. Niznik. 2001. 'Direct Binding and Functional Coupling of α-Synuclein to the Dopamine Transporters Accelerate Dopamine-Induced Apoptosis'. *The FASEB Journal* 15 (6): 916–26. https://doi.org/10.1096/fj.00-0334com.

Lee, Hye Mi, and Seong-Beom Koh. 2015. 'Many Faces of Parkinson's Disease: Non-Motor Symptoms of Parkinson's Disease'. *Journal of Movement Disorders* 8 (2): 92–97. https://doi.org/10.14802/jmd.15003.

Lee, Michael K., Wanda Stirling, Yanqun Xu, et al. 2002. 'Human α-Synuclein-Harboring Familial Parkinson's Disease-Linked Ala-53 → Thr Mutation Causes Neurodegenerative Disease with α-Synuclein Aggregation in Transgenic Mice'. *Proceedings of the National Academy of Sciences* 99 (13): 8968–73. https://doi.org/10.1073/pnas.132197599.

Lesage, Suzanne, Mathieu Anheim, Franck Letournel, et al. 2013. 'G51D A-synuclein Mutation Causes a Novel Parkinsonian–Pyramidal Syndrome'. *Annals of Neurology* 73 (4): 459–71. https://doi.org/10.1002/ana.23894.

Li, Amanda, Cyrus Rastegar, and Xiaobo Mao. 2022. 'α-Synuclein Conformational Plasticity: Physiologic States, Pathologic Strains, and Biotechnological Applications'. *Biomolecules* 12 (7): 994. https://doi.org/10.3390/biom12070994.

Li, Binsen, Peng Ge, Kevin A. Murray, et al. 2018. 'Cryo-EM of Full-Length α-Synuclein Reveals Fibril Polymorphs with a Common Structural Kernel'. *Nature Communications* 9 (1): 3609. https://doi.org/10.1038/s41467-018-05971-2.

Liu, Tsai-Wei, Chiung-Mei Chen, and Kuo-Hsuan Chang. 2022. 'Biomarker of Neuroinflammation in Parkinson's Disease'. *International Journal of Molecular Sciences* 23 (8): 4148. https://doi.org/10.3390/ijms23084148.

Logan, Todd, Jacob Bendor, Chantal Toupin, Kurt Thorn, and Robert H Edwards. 2017. 'α-Synuclein Promotes Dilation of the Exocytotic Fusion Pore'. *Nature Neuroscience* 20 (5): 681–89. https://doi.org/10.1038/nn.4529.

Longhena, Francesca, Gaia Faustini, Cristina Missale, Marina Pizzi, and Arianna Bellucci. 2018. 'Dopamine Transporter/α-Synuclein Complexes Are Altered in the Post Mortem Caudate Putamen of Parkinson's Disease: An In Situ Proximity Ligation Assay Study'. *International Journal of Molecular Sciences* 19 (6): 1611. https://doi.org/10.3390/ijms19061611.

Luk, Kelvin C., Victoria Kehm, Jenna Carroll, et al. 2012. 'Pathological α-Synuclein Transmission Initiates Parkinson-like Neurodegeneration in Nontransgenic Mice'. *Science* 338 (6109): 949–53. https://doi.org/10.1126/science.1227157.

Mat Taib, Che Norma, and Musa Mustapha. 2020. 'MPTP-Induced Mouse Model of Parkinson's Disease: A Promising Direction of Therapeutic Strategies'. *Bosnian Journal of Basic Medical Sciences*, ahead of print, December 14. https://doi.org/10.17305/bjbms.2020.5181.

Middleton, Elizabeth R., and Elizabeth Rhoades. 2010. 'Effects of Curvature and Composition on α-Synuclein Binding to Lipid Vesicles'. *Biophysical Journal* 99 (7): 2279–88. https://doi.org/10.1016/j.bpj.2010.07.056.

Miquel-Rio, Lluis, Diana Alarcón-Arís, María Torres-López, et al. 2022. 'Human α-Synuclein Overexpression in Mouse Serotonin Neurons Triggers a Depressive-like Phenotype. Rescue by Oligonucleotide Therapy'. *Translational Psychiatry* 12 (1): 79. https://doi.org/10.1038/s41398-022-01842-z.

Mosharov, Eugene V., Kristin E. Larsen, Ellen Kanter, et al. 2009. 'Interplay between Cytosolic Dopamine, Calcium, and α-Synuclein Causes Selective Death of Substantia Nigra Neurons'. *Neuron* 62 (2): 218–29. https://doi.org/10.1016/j.neuron.2009.01.033.

Moszczynska, Anna, Jumana Saleh, Hongyu Zhang, Brian Vukusic, Frank J. S. Lee, and Fang Liu. 2007. 'Parkin Disrupts the α-Synuclein/Dopamine Transporter Interaction: Consequences Toward Dopamine-Induced Toxicity'. *Journal of Molecular Neuroscience* 32 (3): 217–27. https://doi.org/10.1007/s12031-007-0037-0.

Muñoz, Ana, Andrea Lopez-Lopez, Carmen M. Labandeira, and Jose L. Labandeira-Garcia. 2020. 'Interactions Between the Serotonergic and Other Neurotransmitter Systems in the Basal Ganglia: Role in Parkinson's Disease and Adverse Effects of L-DOPA'. *Frontiers in Neuroanatomy* 14: 26. https://doi.org/10.3389/fnana.2020.00026.

Nellikka, Rohith K., Bhavya R. Bhaskar, Kinjal Sanghrajka, Swapnali S. Patil, and Debasis Das. 2021. 'α-Synuclein Kinetically Regulates the Nascent Fusion Pore Dynamics'.

Proceedings of the National Academy of Sciences 118 (34): e2021742118. https://doi.org/10.1073/pnas.2021742118.

Nemani, Venu M., Wei Lu, Victoria Berge, et al. 2010. 'Increased Expression of α-Synuclein Reduces Neurotransmitter Release by Inhibiting Synaptic Vesicle Reclustering after Endocytosis'. *Neuron* 65 (1): 66–79. https://doi.org/10.1016/j.neuron.2009.12.023.

Neupert, Walter, and Johannes M. Herrmann. 2007. 'Translocation of Proteins into Mitochondria'. *Annual Review of Biochemistry* 76 (1): 723–49. https://doi.org/10.1146/annurev.biochem.76.052705.163409.

Noyce, Alastair J., Jonathan P. Bestwick, Laura Silveira-Moriyama, et al. 2012. 'Meta-analysis of Early Nonmotor Features and Risk Factors for Parkinson Disease'. *Annals of Neurology* 72 (6): 893–901. https://doi.org/10.1002/ana.23687.

Nyola, Ajeeta, Nathan K Karpowich, Juan Zhen, Jennifer Marden, Maarten E Reith, and Da-Neng Wang. 2010. 'Substrate and Drug Binding Sites in LeuT'. *Current Opinion in Structural Biology* 20 (4): 415–22. https://doi.org/10.1016/j.sbi.2010.05.007.

Oaks, Adam W., and Anita Sidhu. 2011. 'Synuclein Modulation of Monoamine Transporters'. *FEBS Letters* 585 (7): 1001–6. https://doi.org/10.1016/j.febslet.2011.03.009.

Ostrerova, Natalie, Leonard Petrucelli, Matthew Farrer, et al. 1999. 'α-Synuclein Shares Physical and Functional Homology with 14-3-3 Proteins'. *The Journal of Neuroscience* 19 (14): 5782–91. https://doi.org/10.1523/JNEUROSCI.19-14-05782.1999.

Ostrerova-Golts, Natalie, Leonard Petrucelli, John Hardy, John M. Lee, Matthew Farer, and Benjamin Wolozin. 2000. 'The A53T α-Synuclein Mutation Increases Iron-Dependent Aggregation and Toxicity'. *The Journal of Neuroscience* 20 (16): 6048–54. https://doi.org/10.1523/JNEUROSCI.20-16-06048.2000.

Pagano, Gennaro, Flavia Niccolini, and Marios Politis. 2018. 'The Serotonergic System in Parkinson's Patients with Dyskinesia: Evidence from Imaging Studies'. *Journal of Neural Transmission* 125 (8): 1217–23. https://doi.org/10.1007/s00702-017-1823-7.

Peng, Xiangmin M., Roya Tehranian, Paula Dietrich, Leonidas Stefanis, and Ruth G. Perez. 2005. 'α-Synuclein Activation of Protein Phosphatase 2A Reduces Tyrosine Hydroxylase Phosphorylation in Dopaminergic Cells'. *Journal of Cell Science* 118 (15): 3523–30. https://doi.org/10.1242/jcs.02481.

Perez, Ruth G., Jack C. Waymire, Eva Lin, Jen J. Liu, Fengli Guo, and Michael J. Zigmond. 2002. 'A Role for α-Synuclein in the Regulation of Dopamine Biosynthesis'. *The Journal of Neuroscience* 22 (8): 3090–99. https://doi.org/10.1523/JNEUROSCI.22-08-03090.2002.

Pinho, Raquel, Isabel Paiva, Kristina Gotovac Jerčić, et al. 2019. 'Nuclear Localization and Phosphorylation Modulate Pathological Effects of Alpha-Synuclein'. *Human Molecular Genetics* 28 (1): 31–50. https://doi.org/10.1093/hmg/ddy326.

Politis, Marios, and Flavia Niccolini. 2015. 'Serotonin in Parkinson's Disease'. *Behavioural Brain Research* 277 (January): 136–45. https://doi.org/10.1016/j.bbr.2014.07.037.

Polymenidou, Magdalini, and Don W. Cleveland. 2012. 'Prion-like Spread of Protein Aggregates in Neurodegeneration'. *Journal of Experimental Medicine* 209 (5): 889–93. https://doi.org/10.1084/jem.20120741.

Polymeropoulos, Mihael H., Christian Lavedan, Elisabeth Leroy, et al. 1997. 'Mutation in the α-Synuclein Gene Identified in Families with Parkinson's Disease'. *Science* 276 (5321): 2045–47. https://doi.org/10.1126/science.276.5321.2045.

Postuma, Ronald B., Daniela Berg, Matthew Stern, et al. 2015. 'MDS Clinical Diagnostic Criteria for Parkinson's Disease: MDS-PD Clinical Diagnostic Criteria'. *Movement Disorders* 30 (12): 1591–601. https://doi.org/10.1002/mds.26424.

Priyadarshi, Anumeet, Sadik A. Khuder, Eric A. Schaub, and Snigdha S. Priyadarshi. 2001. 'Environmental Risk Factors and Parkinson's Disease: A Metaanalysis'. *Environmental Research* 86 (2): 122–27. https://doi.org/10.1006/enrs.2001.4264.

Prusiner, Stanley B. 1982. 'Novel Proteinaceous Infectious Particles Cause Scrapie'. *Science* 216 (4542): 136–44. https://doi.org/10.1126/science.6801762.

Prusiner, Stanley B. 1998. 'Prions'. *Proceedings of the National Academy of Sciences* 95 (23): 13363–83. https://doi.org/10.1073/pnas.95.23.13363.

Prusiner, Stanley B., Amanda L. Woerman, Daniel A. Mordes, et al. 2015. 'Evidence for α-Synuclein Prions Causing Multiple System Atrophy in Humans with Parkinsonism'. *Proceedings of the National Academy of Sciences* 112 (38). https://doi.org/10.1073/pnas.1514475112.

Ramamoorthy, Sammanda, Toni S. Shippenberg, and Lankupalle D. Jayanthi. 2011. 'Regulation of Monoamine Transporters: Role of Transporter Phosphorylation'. *Pharmacology & Therapeutics* 129 (2): 220–38. https://doi.org/10.1016/j.pharmthera.2010.09.009.

Richardson, Ben D., Kaustuv Saha, Danielle Krout, et al. 2016. 'Membrane Potential Shapes Regulation of Dopamine Transporter Trafficking at the Plasma Membrane'. *Nature Communications* 7 (1): 10423. https://doi.org/10.1038/ncomms10423.

Rocha, Emily M., Briana De Miranda, and Laurie H. Sanders. 2018. 'Alpha-Synuclein: Pathology, Mitochondrial Dysfunction and Neuroinflammation in Parkinson's Disease'. *Neurobiology of Disease* 109 (January): 249–57. https://doi.org/10.1016/j.nbd.2017.04.004.

Rodriguez, Jose A., Magdalena I. Ivanova, Michael R. Sawaya, et al. 2015. 'Structure of the Toxic Core of α-Synuclein from Invisible Crystals'. *Nature* 525 (7570): 486–90. https://doi.org/10.1038/nature15368.

Rudnick, Gary, and Janet Clark. 1993. 'From Synapse to Vesicle: The Reuptake and Storage of Biogenic Amine Neurotransmitters'. *Biochimica et Biophysica Acta (BBA) - Bioenergetics* 1144 (3): 249–63. https://doi.org/10.1016/0005-2728(93)90109-S.

Rudnick, Gary, and Pamlea J. Nelson. 1978. 'Platelet 5-Hydroxytryptamine Transport, an Electroneutral Mechanism Coupled to Potassium'. *Biochemistry* 17 (22): 4739–42. https://doi.org/10.1021/bi00615a021.

Saenz, Jacqueline, Oscar Yao, Elnaz Khezerlou, et al. 2023. 'Cocaine-Regulated Trafficking of Dopamine Transporters in Cultured Neurons Revealed by a pH Sensitive Reporter'. *iScience* 26 (1): 105782. https://doi.org/10.1016/j.isci.2022.105782.

Saunders, Christine, Jasmine V. Ferrer, Lei Shi, et al. 2000. 'Amphetamine-Induced Loss of Human Dopamine Transporter Activity: An Internalization-Dependent and Cocaine-Sensitive Mechanism'. *Proceedings of the National Academy of Sciences* 97 (12): 6850–55. https://doi.org/10.1073/pnas.110035297.

Segel, Irwin H. 1975. *Enzyme Kinetics: Behavior and Analysis of Rapid Equilibrium and Steady-State Enzyme Systems*. Wiley-Interscience.

Shahmoradian, Sarah H., Amanda J. Lewis, Christel Genoud, et al. 2019. 'Lewy Pathology in Parkinson's Disease Consists of Crowded Organelles and Lipid Membranes'. *Nature Neuroscience* 22 (7): 1099–109. https://doi.org/10.1038/s41593-019-0423-2.

Shin, Hae-Won, and Sun Ju Chung. 2012. 'Drug-Induced Parkinsonism'. *Journal of Clinical Neurology (Seoul, Korea)* 8 (1): 15–21. https://doi.org/10.3988/jcn.2012.8.1.15.

Shrimanker, Isha, Prasanna Tadi, Caroline Schoo, and Juan Carlos Sánchez-Manso. 2025. 'Parkinsonism'. In *StatPearls*. StatPearls Publishing. http://www.ncbi.nlm.nih.gov/books/NBK542224/.

Siderowf, Andrew, Luis Concha-Marambio, David-Erick Lafontant, et al. 2023. 'Assessment of Heterogeneity among Participants in the Parkinson's Progression Markers Initiative Cohort Using α-Synuclein Seed Amplification: A Cross-Sectional Study'. *The Lancet Neurology* 22 (5): 407–17. https://doi.org/10.1016/S1474-4422(23)00109-6.

Sidhu, Anita, Christophe Wersinger, and Philippe Vernier. 2004. 'α-Synuclein Regulation of the Dopaminergic Transporter: A Possible Role in the Pathogenesis of Parkinson's Disease'. *FEBS Letters* 565 (1–3): 1–5. https://doi.org/10.1016/j.febslet.2004.03.063.

Singleton, A. B., M. Farrer, J. Johnson, et al. 2003. 'α-Synuclein Locus Triplication Causes Parkinson's Disease'. *Science* 302 (5646): 841–841. https://doi.org/10.1126/science.1090278.

Spillantini, Maria Grazia, Marie Luise Schmidt, Virginia M.-Y. Lee, John Q. Trojanowski, Ross Jakes, and Michel Goedert. 1997. 'α-Synuclein in Lewy Bodies'. *Nature* 388 (6645): 839–40. https://doi.org/10.1038/42166.

Srivastava, Dushyant Kumar, Vikas Navratna, Dilip K. Tosh, et al. 2024. 'Structure of the Human Dopamine Transporter and Mechanisms of Inhibition'. *Nature* 632 (8025): 672–77. https://doi.org/10.1038/s41586-024-07739-9.

Strecker, Karl, Florian Wegner, Swen Hesse, et al. 2011. 'Preserved Serotonin Transporter Binding in de Novo Parkinson's Disease: Negative Correlation with the Dopamine Transporter'. *Journal of Neurology* 258 (1): 19–26. https://doi.org/10.1007/s00415-010-5666-5.

Stykel, Morgan G., Kayla M. Humphries, Evelyn Kamski-Hennekam, et al. 2021. 'α-Synuclein Mutation Impairs Processing of Endomembrane Compartments and Promotes Exocytosis and Seeding of α-Synuclein Pathology'. *Cell Reports* 35 (6): 109099. https://doi.org/10.1016/j.celrep.2021.109099.

Swant, Jarod, J. Shawn Goodwin, Ashley North, et al. 2011. 'α-Synuclein Stimulates a Dopamine Transporter-Dependent Chloride Current and Modulates the Activity of the Transporter'. *The Journal of Biological Chemistry* 286 (51): 43933–43. https://doi.org/10.1074/jbc.M111.241232.

Threlfell, Sarah, Amir Saeid Mohammadi, Brent J. Ryan, et al. 2021. 'Striatal Dopamine Transporter Function Is Facilitated by Converging Biology of α-Synuclein and Cholesterol'. *Frontiers in Cellular Neuroscience* 15 (April): 658244. https://doi.org/10.3389/fncel.2021.658244.

Tolosa, Eduardo, Alicia Garrido, Sonja W Scholz, and Werner Poewe. 2021. 'Challenges in the Diagnosis of Parkinson's Disease'. *The Lancet Neurology* 20 (5): 385–97. https://doi.org/10.1016/S1474-4422(21)00030-2.

Translational Neurogenetics Unit, Wallenberg Neuroscience Center, Lund University, Lund, Sweden, Itzia Jimenez-Ferrer, Maria Swanberg, and Translational Neurogenetics Unit, Wallenberg Neuroscience Center, Lund University, Lund, Sweden. 2018. 'Immunogenetics of Parkinson's Disease'. In *Parkinson's Disease: Pathogenesis and Clinical Aspects*, edited by John Van Geest Centre for Brain Repair, Department of Clinical Neurosciences, University of Cambridge, UK, Thomas B. Stoker, Julia C. Greenland, and John Van Geest Centre for Brain Repair, Department of Clinical Neurosciences, University of Cambridge, UK. Codon Publications. https://doi.org/10.15586/codonpublications.parkinsonsdisease.2018.ch2.

Ulmer, Tobias S., Ad Bax, Nelson B. Cole, and Robert L. Nussbaum. 2005. 'Structure and Dynamics of Micelle-Bound Human α-Synuclein'. *Journal of Biological Chemistry* 280 (10): 9595–603. https://doi.org/10.1074/jbc.M411805200.

Vasquez, Velmarini, Joy Mitra, Pavana M. Hegde, et al. 2017. 'Chromatin-Bound Oxidized α-Synuclein Causes Strand Breaks in Neuronal Genomes in in Vitro Models of Parkinson's Disease'. *Journal of Alzheimer's Disease* 60 (s1): S133–50. https://doi.org/10.3233/JAD-170342.

Vermilyea, Scott C., and Marina E. Emborg. 2015. 'α-Synuclein and Nonhuman Primate Models of Parkinson's Disease'. *Journal of Neuroscience Methods* 255 (November): 38–51. https://doi.org/10.1016/j.jneumeth.2015.07.025.

Volpicelli-Daley, Laura A., Kelvin C. Luk, Tapan P. Patel, et al. 2011. 'Exogenous α-Synuclein Fibrils Induce Lewy Body Pathology Leading to Synaptic Dysfunction and Neuron Death'. *Neuron* 72 (1): 57–71. https://doi.org/10.1016/j.neuron.2011.08.033.

Wang, Tai, Changhe Shi, Haiyang Luo, et al. 2022. 'Neuroinflammation in Parkinson's Disease: Triggers, Mechanisms, and Immunotherapies'. *The Neuroscientist* 28 (4): 364–81. https://doi.org/10.1177/1073858421991066.

Watanabe, Hirohisa, Johannes M. Dijkstra, and Toshiharu Nagatsu. 2024. 'Parkinson's Disease: Cells Succumbing to Lifelong Dopamine-Related Oxidative Stress and Other Bioenergetic Challenges'. *International Journal of Molecular Sciences* 25 (4): 2009. https://doi.org/10.3390/ijms25042009.

Wersinger, Christophe, Alexis Jeannotte, and Anita Sidhu. 2006. 'Attenuation of the Norepinephrine Transporter Activity and Trafficking via Interactions with A-synuclein'. *European Journal of Neuroscience* 24 (11): 3141–52. https://doi.org/10.1111/j.1460-9568.2006.05181.x.

Wersinger, Christophe, Milan Rusnak, and Anita Sidhu. 2006. 'Modulation of the Trafficking of the Human Serotonin Transporter by Human Alpha-synuclein'. *European Journal of Neuroscience* 24 (1): 55–64. https://doi.org/10.1111/j.1460-9568.2006.04900.x.

Wersinger, Christophe, and Anita Sidhu. 2003. 'Attenuation of Dopamine Transporter Activity by α-Synuclein'. *Neuroscience Letters* 340 (3): 189–92. https://doi.org/10.1016/S0304-3940(03)00097-1.

Wersinger, Christophe, and Anita Sidhu. 2005. 'Disruption of the Interaction of α-Synuclein with Microtubules Enhances Cell Surface Recruitment of the Dopamine Transporter'. *Biochemistry* 44 (41): 13612–24. https://doi.org/10.1021/bi050402p.

Wersinger, Christophe, and Anita Sidhu. 2009. 'Partial Regulation of Serotonin Transporter Function by Gamma-Synuclein'. *Neuroscience Letters* 453 (3): 157–61. https://doi.org/10.1016/j.neulet.2009.02.033.

Wersinger, Christophe, Philippe Vernier, and Anita Sidhu. 2004. 'Trypsin Disrupts the Trafficking of the Human Dopamine Transporter by α-Synuclein and Its A30P Mutant'. *Biochemistry* 43 (5): 1242–53. https://doi.org/10.1021/bi035308s.

Xilouri, Maria, Tereza Vogiatzi, Kostas Vekrellis, David Park, and Leonidas Stefanis. 2009. 'Abberant α-Synuclein Confers Toxicity to Neurons in Part through Inhibition of Chaperone-Mediated Autophagy'. *PLoS ONE* 4 (5): e5515. https://doi.org/10.1371/journal.pone.0005515.

Yaffe, Dana, Lucy R. Forrest, and Shimon Schuldiner. 2018. 'The Ins and Outs of Vesicular Monoamine Transporters'. *The Journal of General Physiology* 150 (5): 671–82. https://doi.org/10.1085/jgp.201711980.

Yamashita, Atsuko, Satinder K. Singh, Toshimitsu Kawate, Yan Jin, and Eric Gouaux. 2005. 'Crystal Structure of a Bacterial Homologue of Na+/Cl--Dependent Neurotransmitter Transporters'. *Nature* 437 (7056): 215–23. https://doi.org/10.1038/nature03978.

Yang, Ping-Chang, and Tahrin Mahmood. 2012. 'Western Blot: Technique, Theory, and Trouble Shooting'. *North American Journal of Medical Sciences* 4 (9): 429. https://doi.org/10.4103/1947-2714.100998.

Yoon, Tae-Young, and Mary Munson. 2018. 'SNARE Complex Assembly and Disassembly'. *Current Biology* 28 (8): R397–401. https://doi.org/10.1016/j.cub.2018.01.005.

Zahniser, Nancy R., and Alexander Sorkin. 2009. 'Trafficking of Dopamine Transporters in Psychostimulant Actions'. *Seminars in Cell & Developmental Biology* 20 (4): 411–17. https://doi.org/10.1016/j.semcdb.2009.01.004.

Zarranz, Juan J., Javier Alegre, Juan C. Gómez-Esteban, et al. 2004. 'The New Mutation, E46K, of A-synuclein Causes Parkinson and Lewy Body Dementia'. *Annals of Neurology* 55 (2): 164–73. https://doi.org/10.1002/ana.10795.

Zhang, Yuan-Wei, and Gary Rudnick. 2011. 'Myristoylation of cGMP-Dependent Protein Kinase Dictates Isoform Specificity for Serotonin Transporter Regulation'. *Journal of Biological Chemistry* 286 (4): 2461–68. https://doi.org/10.1074/jbc.M110.203935.

6 Appendix

Table 6 *Summary of kinetic parameters (V_{max} and K_m) for [^{3}H]5HT uptake in CAD SERT cells transfected with only SERT (1:0), 1:3 WT α-synuclein, or 1:3 A53T α-synuclein. Data represent mean ± SEM (n = 3).*

Group	V_{max} ± SEM [pmol/ mio/min]	K_m ± SEM [µM]	Vmax ± SEM [%]	Km ± SEM [%]
1:0	200.3 ± 96.9	1.289 ± 0.218	100 ± 0	100 ± 0
1:3 WT	500.1 ± 198.2	2.270 ± 0.297	292.93 ± 88.1	179.1 ± 8.9
1:3 A53T	481.5 ± 114.3	1.515 ± 0.105	349.7 ± 120.4	125.7 ± 24.5

Table 7 *Summary of statistical analysis of kinetic parameters of [^{3}H]5HT uptake in CAD SERT cells. Statistical significance was assessed using one-way ANOVA followed by Tukey's multiple comparisons test. Significant p-values ($p < 0.05$) are indicated in bold.*

Group	V_{max} [pmol/ mio/min] p-value	K_m [µM] p-value	V_{max} [%] p-value	K_m [%] p-value
1:0 vs. 1:3 WT	0.3647	**0.0459***	0.3222	**0.0233***
1:0 vs. 1:3 A53T	0.4050	0.7584	0.1813	0.4920
1:3 WT vs. 1:3 A53T	0.9953	0.1141	0.8894	0.1017

Table 8 *Numeric summary of the densitometric quantification of Western Blot image from the [³H]5HT CAD SERT uptake. AU = arbitrary units.*

Protein	Group	NET Protein/ NET Control ± SEM [AU]	Normalisation to 1:0 ± SEM [%]
ASYN	1:0	0.018 ± 0.012	100 ± 0
	1:3 WT	3.158 ± 2.970	225890 ± 20571
	1:3 A53T	7.912 ± 7.266	91097 ± 46541
SERT total	1:0	0.584 ± 0.117	100 ± 0
	1:3 WT	6.946 ± 6.157	898.1 ± 732.1
	1:3 A53T	9.497± 8.245	1242.7 ± 972.4
SERT mature	1:0	1.089 ± 0.161	100 ± 0
	1:3 WT	13.184 ± 11.976	967.3 ± 838.4
	1:3 A53T	18.103 ± 15.979	1344.2 ±1111.3
SERT core	1:0	0.385 ± 0.079	100 ± 0
	1:3 WT	5.838 ± 5.126	1140 ± 919
	1:3 A53T	8.442 ± 7.429	1660 ± 1325

Table 9 *Numeric summary of the statistical analysis for the densitometric quantification of the Western Blot image from the [³H]5HT CAD SERT uptake. The statistical analysis used was Kruska-Wallis test with Dunn's multiple comparison test. Significant p-values (p < 0.05) are indicated in bold.*

Protein	Group	NET Protein/ NET Control p-value	Normalisation to 1:0 p-value
ASYN	1:0 vs. 1:3 WT	0.5391	0.2861
	1:0 vs. 1:3 A53T	0.0760	**0.0458***
	1:3 WT vs. 1:3 A53T	>0.9999	>0.9999
SERT total	1:0 vs. 1:3 WT	0.4081	0.2065
	1:0 vs. 1:3 A53T	0.1107	0.0688
	1:3 WT vs. 1:3 A53T	>0.9999	>0.9999
SERT mature	1:0 vs. 1:3 WT	0.8902	0.2065
	1:0 vs. 1:3 A53T	0.3032	0.0688
	1:3 WT vs. 1:3 A53T	>0.9999	>0.9999
SERT core	1:0 vs. 1:3 WT	0.6991	0.2065
	1:0 vs. 1:3 A53T	0.1579	0.0688
	1:3 WT vs. 1:3 A53T	>0.9999	>0.9999

Table 10. *Summary of kinetic parameters (V_{max} and K_m) for [³H]5HT uptake in HEK- SERT cells transfected with only SERT (1:0), 1:3 WT α-synuclein, or 1:3 A53T α-synuclein. Data represent mean ± SEM (n = 3).*

Group	V_{max} ± SEM [pmol/ mio/min]	K_m ± SEM [µM]	Vmax ± SEM [%]	Km ± SEM [%]
1:0	71.25 ± 31.1	2.839 ± 0.616	100 ± 0	100 ± 0
1:3 WT	128.5 ± 58.9	2.759 ± 0.455	220.6 ± 86.9	101.3 ± 11.5
1:3 A53T	206.7 ± 58	4.633 ± 1.582	348.9 ± 68.1	155.0 ± 23.9

Table 11 *Summary of statistical analysis of kinetic parameters of [³H]5HT uptake in HEK SERT cells. Statistical significance was assessed using one-way ANOVA followed by Tukey's multiple comparisons test. Significant p-values (p < 0.05) are indicated in bold.*

Group	V_{max} [pmol/ mio/min] p-value	K_m [µM] p-value	V_{max} [%] p-value	K_m [%] p-value
1:0 vs. 1:3 WT	0.7199	0.9983	0.4270	0.9979
1:0 vs. 1:3 A53T	0.2248	0.4696	0.0732	0.0971
1:3 WT vs. 1:3 A53T	0.5570	0.4425	0.3880	0.1050

Table 12 *Numeric summary of the densitometric quantification of the Western Blot image from the [³H]5HT HEK SERT uptake.*

Protein	Group	NET Protein/ NET Control ± SEM [AU]	Normalisation to 1:0 ± SEM [%]
ASYN	1:0	0.093 ± 0.0122	100 ± 0
	1:3 WT	0.064 ± 0.008	70.0 ± 12.3
	1:3 A53T	0.151 ± 0.002	165.99 ± 16.4
SERT total	1:0	0.022 ± 0.012	100 ± 0
	1:3 WT	0.261 ± 0.131	1255 ± 179
	1:3 A53T	0.560 ± 0.113	2138 ± 355
SERT mature	1:0	0.880 ± 0.378	100 ± 0
	1:3 WT	1.118 ± 0.473	129.7 ± 3.4
	1:3 A53T	1.351 ± 0.469	210.9 ± 67.5
SERT core	1:0	0.875 ± 0.381	100 ± 0
	1:3 WT	1.090 ± 0.456	134.6 ± 11.7
	1:3 A53T	1.401 0.457	248.5 ± 101.5

Table 13 *Numeric summary of the statistical analysis for the densitometric quantification of the Western Blot image from the [³H]5HT HEK SERT uptake (one-way ANOVA with Tukey's multiple comparison test and Kruska-Wallis test with Dunn's multiple comparison test). Significant p-values (p < 0.05) are indicated in bold.*

Protein	Group	NET Protein/ NET Control p-value	Normalisation to 1:0 p-value
ASYN	1:0 vs. 1:3 WT	0.0888	0.2508
	1:0 vs. 1:3 A53T	**0.0055****	**0.0179***
	1:3 WT vs. 1:3 A53T	**0.0006*****	**0.0030****
SERT total	1:0 vs. 1:3 WT	0.2824	**0.0235***
	1:0 vs. 1:3 A53T	**0.0209***	**0.0030****
	1:3 WT vs. 1:3 A53T	0.1680	0.0735
SERT mature	1:0 vs. 1:3 WT	0.9247	0.3884
	1:0 vs. 1:3 A53T	0.7427	**0.0299***
	1:3 WT vs. 1:3 A53T	0.9265	0.8656
SERT core	1:0 vs. 1:3 WT	0.9353	0.3884
	1:0 vs. 1:3 A53T	0.6824	**0.0299***
	1:3 WT vs. 1:3 A53T	0.8693	0.8656

Table 14. *Summary of kinetic parameters (V_{max} and K_m) for [³H]DA uptake in HEK-DAT cells transfected with only SERT (1:0), 1:3 WT α-synuclein, or 1:3A53T α-synuclein. Data represent mean ± SEM (n = 3).*

Group	V_{max} ± SEM [pmol/ mio/min]	K_m ± SEM [µM]	Vmax ± SEM [%]	Km ± SEM [%]
1:0	30.82 ± 6.19	1.178 ± 0.266	100 ± 0	100 ± 0
1:3 WT	49.14 ± 10.88	1.138 ± 0.299	168.2 ± 26.3	103.1 ± 18.7
1:3 A53T	75.17 ± 2.85	2.704 ± 0.682	283.7 ± 68.4	238.9 ± 32.4

Table 15 *Summary of statistical analysis of kinetic parameters of [³H]DA uptake in HEK DAT cells. Statistical significance was assessed using one-way ANOVA followed by Tukey's multiple comparisons test. Significant p-values (p < 0.05) are indicated in bold.*

Group	V_{max} [pmol/ mio/min] p-value	K_m [µM] p-value	V_{max} [%] p-value	K_m [%] p-value
1:0 vs. 1:3 WT	0.2405	0.9979	0.5158	0.9942
1:0 vs. 1:3 A53T	**0.0056****	0.0970	**0.0325***	**0.0036****
1:3 WT vs. 1:3 A53T	0.0807	0.0882	0.1862	**0.0042****

Table 16 *Numeric summary of the densitometric quantification of the Western Blot image from the [³H]DA HEK DAT uptake.*

Protein	Group	NET Protein/ NET Control ± SEM [AU]	Normalisation to 1:0 ± SEM [%]
ASYN	1:0	0.099 ± 0.012	100 ± 0
	1:3 WT	0.118 ± 0.043	119.0 ± 37.07
	1:3 A53T	0.211 ± 0.007	227.6 ± 43.27
DAT total	1:0	0.827 ± 0.128	100 ± 0
	1:3 WT	1.351 ± 0.116	180.7 ± 38.3
	1:3 A53T	1.58 ± 0.052	208.3 ± 38.5
DAT mature	1:0	0.705 ± 0.116	100 ± 0
	1:3 WT	1.029 ± 0.121	165.079 ± 39.21
	1:3 A53T	1.228 ± 0.0769	194.9 ± 41.7
DAT core	1:0	1.030 ± 0.124	100 ± 0
	1:3 WT	1.757 ± 0.124	182.0 ± 32.6
	1:3 A53T	1.997 ± 0.0858	206.0 ± 34.9

Table 17 *Numeric summary of the statistical analysis for the densitometric quantification of the Western Blot image from the [^{3}H]DAT HEK DAT uptake (one-way ANOVA with Tukey's multiple comparison test and Kruska-Wallis test with Dunn's multiple comparison test).*

Protein	Group	NET Protein/ NET Control p-value	Normalisation to 1:0 p-value
ASYN	1:0 vs. 1:3 WT	0.8685	0.9133
	1:0 vs. 1:3 A53T	**0.0352***	0.0540
	1:3 WT vs. 1:3 A53T	0.0778	0.1016
DAT total	1:0 vs. 1:3 WT	**0.0153***	0.5832
	1:0 vs. 1:3 A53T	**0.0017****	0.0651
	1:3 WT vs. 1:3 A53T	0.3184	0.9546
DAT mature	1:0 vs. 1:3 WT	0.1350	0.4868
	1:0 vs. 1:3 A53T	**0.0175***	0.0843
	1:3 WT vs. 1:3 A53T	0.4196	>0.9999
DAT core	1:0 vs. 1:3 WT	**0.0035****	0.1442
	1:0 vs. 1:3 A53T	**0.0005*****	0.0561
	1:3 WT vs. 1:3 A53T	0.3315	0.8154

Table 18 *Numeric summary of the IC50 calculation from the AquaBluer cell viability assay.*

Group	$IC50_{rotenone}$ ± SEM [nM]	$IC50_{MPP+}$ ± SEM [µM]	$IC50_{rotenone}$ ± SEM [%]	$IC50_{MPP+}$ ± SEM [%]
1:0	1152.7 ± 549.8	25.9 ± 4.7	100 ± 0	100 ± 0
1:3 WT	293.3 ± 44.3	24.3 ± 3.5	43.3 ± 13.8	95.2 ± 4.5

Table 19 *Numeric summary of the statistical analysis for the IC50 calculation for the AquaBluer cell viability assay (unpaired, two-tailed student's t-test).*

Group	$IC50_{rotenone}$ [nM] p-values	$IC50_{MPP+}$ [µM] p-values	$IC50_{rotenone}$ [%] p-values	$IC50_{MPP+}$ [%] p-values
1:0 vs 1:3 WT	0.1503	0.7956	**0.0014****	0.1459

Table 20 Numeric summary of the RFUs from **Figure 29**.

Toxin	Group	Condition	RFU ± SEM [AU]
Rotenone	**NC**	1:0	1133555 ± 11605
		1:3 WT	1054323 ± 44130
	1. concentration	1:0	1254796 ± 50921
		1:3 WT	1145069 ± 41807
MPP+	**NC**	1:0	1180821 ± 27055
		1:3 WT	1108197 ± 54110
	1. concentration	1:0	960476 ± 20221
		1:3 WT	864430 ± 57938
Rotenone and MPP+	**NC w/ DMSO**	1:0	1133555 ± 11605
		1:3 WT	1054323 ± 44130
	NC w/o DMSO	1:0	1180821 ± 27055
		1:3 WT	1108197 ± 54110
Rotenone	**24h**	1:0	616822 ± 0
		1:3 WT	399354 ± 0
	48h	1:0	1109238 ± 6820
		1:3 WT	999807 ± 53984
	72h	1:0	1157872 ± 5959
		1:3 WT	1108839 ± 62056

Table 21 *Summary of statistical analysis of* ***Figure 29****. Two-way ANOVA with uncorrected Fisher's LSD. Significant values indicated in bold. (α <0.05)*

Figure	Comparison	p-value
30A	NC:1:0 vs. NC:1:3 WT	0.1774
	NC:1:0 vs. 1. concentration:1:0	**0.0449***
	NC:1:0 vs. 1. Concentration:1:3 WT	0.8411
	NC:1:3 WT vs. 1. Concentration:1:0	**0.0021****
	NC:1:3 WT vs. 1. Concentration:1:3 WT	0.1250
	1. concentration:1:0 vs. 1. Concentration:1:3 WT	0.0671
30B	NC:1:0 vs. NC:1:3 WT	0.2675
	NC:1:0 vs. 1. Concentration:1:0	**0.0068****
	NC:1:0 vs. 1. concentration:1:3 WT	**0.0008*****
	NC:1:3 WT vs. 1. Concentration:1:0	**0.0416***
	NC:1:3 WT vs. 1. concentration:1:3 WT	**0.0039****
	1. concentration:1:0 vs. 1. concentration:1:3 WT	0.1536
30C	NC w/ DMSO:1:0 vs. NC w/ DMSO:1:3 WT	0.0990
	NC w/ DMSO:1:0 vs. NC w/o DMSO:1:0	0.4039
	NC w/ DMSO:1:0 vs. NC w/o DMSO:1:3 WT	0.6513
	NC w/ DMSO:1:3 WT vs. NC w/o DMSO:1:0	**0.0371***
	NC w/ DMSO:1:3 WT vs. NC w/o DMSO:1:3 WT	0.3432
	NC w/o DMSO:1:0 vs. NC w/o DMSO:1:3 WT	0.2712
30D	24h:1:0 vs. 24h:1:3 WT	0.0642
	24h:1:0 vs. 48h:1:0	**0.0003*****
	24h:1:0 vs. 48h:1:3 WT	**0.0017****
	24h:1:0 vs. 72h:1:0	**0.0002*****
	24h:1:0 vs. 72h:1:3 WT	**0.0003*****
	24h:1:3 WT vs. 48h:1:0	**<0.0001******
	24h:1:3 WT vs. 48h:1:3 WT	**<0.0001******
	24h:1:3 WT vs. 72h:1:0	**<0.0001******
	24h:1:3 WT vs. 72h:1:3 WT	**<0.0001******
	48h:1:0 vs. 48h:1:3 WT	0.0984
	48h:1:0 vs. 72h:1:0	0.4300
	48h:1:0 vs. 72h:1:3 WT	0.9947
	48h:1:3 WT vs. 72h:1:0	**0.0270***
	48h:1:3 WT vs. 72h:1:3 WT	0.0994